CERN-TH-5980/91

Alternative Symmetry Breaking and Exotica*

CONVENORS: S. Dimopoulos[1,2,3], M. Lindner[1]

CONTRIBUTORS: E. Argyres[4], U. Baur[5†], R. Casalbuoni[6,7], P. Chiappetta[8], S. De Curtis[9], A. Dobado[1,10], J. Ellis[1], F. Feruglio[7,11], R. Gatto[7], M. Herrero[1,12], I. Josa[1], V.A. Khoze[1,13], B. Mele[1], C. Papadopoulos[4], F. Pauss[1], M. Perrottet[8], A. Ringwald[1], T. Rodrigo[1], F. Schrempp[14], M. Spira[15], J. Terron[12], S. Vlassopulos[16], C. Wetterich[14], P. Zerwas[15]

Contents

I. Electroweak Symmetry Breaking and the TeV Scale
II. V_LV_L Scattering : Chiral Lagrangian Approach
III. WZ Production from the BESS Model
IV. $W_L^{\pm}Z_L^0$ Production at the LHC from the Strongly Interacting Symmetry Sector - Experimental Aspects
V. Compositeness
VI. Signatures for Geometrical Flavour Interactions and $B+L$ Violation at LHC
VII. Summary

1) CERN, 1211 Geneva 23, Switzerland
2) permanent address: Stanford University, Stanford, CA 94305, USA
3) Boston University, Physics Dept., 590 Commonwealth Ave., Boston, MA 02215, USA
4) Institute of Nucl. Phys. NRCPS Democritos, GR-153 10 Athens Greece
5) University of Wisconsin, Physics Dept., 1150 Univ. Ave., Madison, WI 53706, USA
6) Dipartimento di Fisica and Sezione INFN, I-73100 Lecce, Italy
7) Dept. de Phys. Theor., Univ. de Geneve, 1211 Geneva 4, Switzerland
8) CPT CNRS LUMINY Case 907, 13288 Marseille, Cedex 9, France
9) I.N.F.N., Sezione di Firenze, I-50125 Firenze, Italy
10) Dep. de Fisica Teorica de la Univ. Complutense de Madrid, 28040 Madrid, Spain
11) Univ. of Padova, I-35100, Italy
12) Dep. de Fisica Teorica de la Univ. Autonoma de Madrid, 28049 Madrid, Spain
13) Leningrad Inst. for Nucl. Phys., 188350 Gatchina, USSR
14) DESY, Notkestraße 85, 2000 Hamburg 52, Germany
15) Rhein.-Westf. Tech. Hochschule, Physikzentrum, 5100 Aachen, Germany
16) Department of Physics, Nat. Tech. Univ., GR-157 73 Zografou, Athens, Greece

*To appear in the Proceedings of the Large Hadron Collider Workshop, Aachen, 4-9 October 1990
†SSC Fellow

One of the main motivations to build a machine like LHC is to try to get a deeper understanding of the mechanism of electroweak symmetry breaking. This question is so important to our understanding of what may lie ahead in particle physics that the aim of this working group was mostly to see how much we can expect to learn about this problem and how this can be done. In section I we recall the arguments which make the TeV scale special. These arguments are so central and stand behind the expectation that something essential can be learned about symmetry breaking that it is worth to give a short survey here. Sections II and III contain two contributions which model in different ways a strongly interacting Higgs sector corresponding to rather general dynamical symmetry breaking scenarios. Section IV deals with the experimental aspects of the detection of WZ production as expected by a strongly interacting Higgs sector. In section V we have some contributions on compositeness which do not fall under 'excited gauge bosons' which have been studied by a different working group. Section VI is a contribution discussing the possible implications of baryon number violating processes with possibly spectacular consequences for new experiments in the multi TeV area. Finally in section VII we summarize the main results of this working group.

I. ELECTROWEAK SYMMETRY BREAKING AND THE TeV SCALE

Contributors: S. Dimopoulos and M. Lindner

I.1. Introduction

So far the Standard Model (SM) with Spontaneous Symmetry Breaking (SSB) describes all data perfectly and no direct evidence of the Higgs sector or anything equivalent has been seen. We will illustrate why the $O(TeV)$ scale is under all circumstances special and that it is guaranteed that something connected inherently to electroweak symmetry breaking must show up before that scale. This could be a fundamental Higgs, a composite Higgs, a ρ-like state corresponding to Technicolor scenarios or something else which we did not even think of before depending on the mechanism of symmetry breaking. But it must show up and thus machines like the LHC are very important probes into the symmetry breaking mechanism.

Theoretically there are a number of reasons to believe that SSB with a fundamental scalar field may only be a technical step required by a consistent, renormalizable gauge invariant theory. In all but supersymmetric theories we have good reasons [1] not to like fundamental scalars and the way to avoid SSB with a fundamental Higgs particle is to replace it by a dynamical mechanism. Very attractive ideas in this direction were inspired by QCD when the longitudinal components of the W and Z bosons are identified with some sort of pions of a new interaction. This obviously requires a corresponding rescaling of all dimensionful quantities of QCD and would after rescaling automatically imply strong interactions in the TeV range. As a consequence W_L-W_L should (like pion-pion) be strongly coupled. If the Higgs particle of the SM is very heavy then the SM by itself also has rather strongly coupled $W's$ and $Z's$. But the result of a W_L-W_L scattering experiment will look different if a strongly coupled dynamical symmetry breaking mechanism with a nontrivial boundstate spectrum is at work. Therefore one of the key tasks of machines like the LHC will be to measure W_L-W_L scattering and to see if deviations from the SM pointing towards strongly coupled dynamical symmetry breaking in the TeV range can be found. Since QCD like confining gauge theories are just one out of many

thinkable alternative symmetry breaking mechanisms it is necessary to study the problem in a very general manner. Since individual scenarios have been discussed in detail (see e.g. [2] and references therein) we would like to recall the essence of the arguments which arise if one tries to avoid anything beyond the known fermions and the weak gauge bosons and we will see how this makes the TeV scale unavoidably special.

I.2. Substitutes for a Fundamental Higgs Particle

Looking at the Higgs mechanism one realizes immediately that it contains unavoidable essential elements and ugly features at the same time. If the SM Higgs field is split in a nonlinear way into Higgs modes η and Goldstone modes π_i then

$$\Phi = U \cdot \phi\,; \quad U = exp\left(\frac{i\pi_j\tau_i}{v}\right)\,; \quad \phi = \begin{pmatrix} 0 \\ v+\eta \end{pmatrix}\,; \quad v \simeq 175\ GeV \tag{1}$$

and we have $\Phi^+\Phi = \phi^2$ so that the Higgs potential does not depend on the Goldstone bosons in U:

$$V(\Phi^+\Phi) = V(\phi^2) = V(\eta) = \frac{m_H^2}{2}\eta^2 + \frac{m_H^2}{2v}\eta^3 + \frac{m_H^2}{8v^2}\eta^4 \tag{2}$$

The Goldstone degrees of freedom π_i reappear however with derivative couplings through the kinetic energy term

$$|\partial\Phi|^2 = |\partial\eta|^2 + \frac{v^2}{2}Tr(\partial_\mu U^+\partial^\mu U) + O(\eta\cdot\partial U, \partial\eta\partial U) \tag{3}$$

It is nicely seen that the Higgs mechanism needs only the 'rotational' π fields in order to work properly. In 'radial' direction a fixed, nonvanishing vacuum expectation value (VEV) is required and the oscillations η around this VEV are in some sense obsolete. This observation makes it very tempting to remove the η degrees of freedom from the theory by sending $m_H \to \infty$ (while v is fixed) and thus freezing out the physical Higgs field. The result is the nonlinear σ-model limit of the SM with two problems. First this limit corresponds to a nonrenormalizable theory. This means that (at least perturbatively) one cannot make much sense out of this model by itself beyond tree level while on the other hand some loop effects (radiative corrections) of the SM have already been seen [3]. If no miracles occur then the only way to cure the associated problems is to invent a cutoff Λ which controls the loop expressions. Physically such a cutoff would correspond to new physics at Λ which in this case is certainly not many orders of magnitude above M_W. Therefore we see that if we remove the Higgs modes η that we are forced to reinvent something new instead of it. This corresponds nicely to the second problem of the $m_H \to \infty$ limit of the SM. After η has been frozen out one finds that Goldstone boson scattering amplitudes grow like [4]

$$A(W^+W^- \to ZZ) \simeq \frac{-m_H^2}{v^2}(1 + \frac{m_H^2}{s-m_H^2}) \overset{m_H\to\infty}{\longrightarrow} \frac{s}{v^2} \tag{4}$$

and violate tree unitarity between 1 and 2 TeV [2]. Therefore some additional state must come in and dampen the amplitudes. Both problems of the $m_H \to \infty$ limit require that some Higgs substitute must cure the associated problems. If we are willing to accept a wealth of new states in the TeV area then the renormalizability of the SM or modifications does not mean much and we just need to restore tree unitarity so that only one problem is left over.

One obvious solution is going back to the starting point of a not too heavy fundamental Higgs scalar. But this is not desired due to the problems associated with fundamental scalars

[1]. A second solution to both problems could in principle lie in loop effects. This is because the limiting procedure $m_H \to \infty$ could give a different answer if performed in the fully renormalized theory with loop effects included. Large m_H with fixed v implies large λ and therefore strong loop effects might just cure the tree level unitarity problems so that the limiting procedure of the quantum theory could be better behaved. But this is not the case, as is well known from so–called "triviality" studies [5,6]. The underlying general consistency requirements show that for $m_H \gtrsim 200\ GeV$ even the renormalized SM cannot live without new physics at some scale $\Lambda \lesssim M_W \cdot exp[const \cdot M_W/(m_H - 200\ GeV)]$. If the Higgs mass is increased then Λ becomes significantly smaller until $\Lambda \simeq m_H \simeq O(TeV)$ requires immediately new additional physics beyond the SM. So one cannot send the Higgs mass to infinity in the renormalized SM and the old unitarity problem is recovered even after loop effects are included. Finally a whole class of solutions to the unitarity problem is given by dynamical symmetry breaking scenarios which anyway seem to be an attractive alternative to the static Higgs mechanism with fundamental scalars. The best known example is scaled QCD or Technicolor [7] where the π fields of eq. (1) are then the 'pions' of a new interaction and a new ρ meson solves the unitarity problems. Also a wealth of states ('Techni-mesons', 'Techni-baryons') would be expected to be found in the TeV area.

But note that for the mentioned problems minimally only one new state is required to cure the unitarity problems and that both the quantum numbers of this state(s) and the remaining part of the new spectrum are not fixed and entirely due to the assumed dynamics. If we scale QCD then we make a choice on the dynamics motivated by history and we expect a Techni-ρ meson and many other new states in the TeV area. But we should be openminded and think of all possible dynamical scenarios. As an example we will illustrate below that there are dynamical mechanisms which are in a certain sense the extreme opposite of QCD like dynamics. They predict only one composite scalar state in the TeV area and allow to put the remaining spectrum arbitrarily high in energy.

The fact that the tree amplitudes grow up to the point where a Higgs substitute shows up leads to the so–called 'no lose corollary' ([2] and references therein). The 'no lose corollary' says in short simply that the higher in energy the unitarization of amplitudes sets in the stronger it has to be to avoid unitarity problems. Within the SM this means that either the Higgs is light enough to be discovered directly or it will be so heavy that λ is so big as to imply strongly interacting $W_L - W_L$. For dynamical symmetry breaking schemes the statement is very similar and again either something new shows up directly or strong $W_L - W_L$ scattering is required. Therefore a certain success of machines like LHC seems guaranteed. But note that once unitarization is taken care of nothing else is required immediately. Especially there is no per se reason that the whole spectrum of a dynamical breaking scheme is settled in the TeV range as suggested by QCD-like scenarios. A perfect example of such a situation is given further down and has been called Minimal Dynamical Symmetry Breaking.

I.3. Simulation Methods for Alternative Symmetry Breaking

Two different approaches for simulations were used in this working group. The first method used in section II is based on Chiral Perturbation Theory and rests on the observation that in the limit $m_H \to \infty$ only the term

$$\frac{v^2}{2} Tr(\partial_\mu U^+ \partial^\mu U) \qquad (5)$$

is left over from the Higgs sector. From the previous chapter we know that this Higgs-less limit is not viable by itself and one must therefore add at least $O(p^4)$ terms. Unlike the leading $O(p^2)$ term of eq. (5) these new $O(p^4)$ terms are not fixed by the low energy symmetries. Therefore the most general terms with initially free new dimensionful couplings are added

$$\mathcal{L} = \frac{v^2}{2} Tr(\partial_\mu U^+ \partial^\mu U) + MTr(\partial_\mu U \partial^\mu U^+) \cdot Tr(\partial_\nu U \partial^\nu U^+) + NTr(\partial_\mu U \partial_\nu U^+) \cdot Tr(\partial^\mu U \partial^\nu U^+) \quad (6)$$

Since these new terms correspond to additional multi-pion dynamics it is possible to choose the dimensionful couplings M and N so that different dynamical situations are emulated as closely as possible. The addition of these new terms does not unitarize the amplitudes and in addition a unitarization procedure must be chosen Two different methods are used for comparison. The first is the K-matrix method which has a saturation behaviour and is not very abrupt. The other method is the Pade approximation which mimics in some approximation a resonance. Even though this general chiral approach allows to simulate many different dynamical scenarios as seen from low energies it is also clear that there are limitations. Especially the development of all new resonances can only be done approximately. Since e.g. a new ρ-like resonance turns out to be extremely important for the predictions it has been included explicitly in addition. This is especially important for scaled QCD or Technicolor scenarios where the ρ particle produces big effects via the $W - \rho$ mixing.

The second method used for simulations in section III is the so–called BESS approach. There some dynamics which develops a new ρ-like vector resonance is assumed and this new state is included by hand with the most general parameters. Also a possible direct $\rho - f\bar{f}$ coupling is included. This is of course inspired by and especially good for QCD-like electroweak symmetry breaking. Due to this analogy the most interesting situations arise when all details of QCD are scaled by F_π/f_π (scaled QCD) and additionally rescaled to an arbitrary number of colors by large N_C arguments (Technicolor).

I.4. Radiative Consistency and the TeV Scale

We discussed above that at least one extra state is needed (and guaranteed) in the $m_H \to \infty$ limit to solve the tree unitarity problems in the TeV area. Here we will show that more is required to show up at another scale if we ask for consistency beyond tree level. As already indicated above the fact that the SM is a well defined theory does not imply automatically that this remains so once radiative corrections are included. If one or more of the running effective coupling constants grows with energy scale then typically there is a scale Λ at which the couplings will begin to diverge into a Landau Singularity (LS). Such a blow–up is (if not an artifact of perturbation theory) inconsistent with the required functional form on pure dimensional grounds. A dimensionless coupling should (away from mass thresholds) run only logarithmically while a LS implies a power law. A theory is called "trivial" if the only way to avoid such problems is to restrict it to the non-interacting free case. For example for a single scalar with a quartic interaction term $\lambda\Phi^4$ triviality has been established rather reliably. Since there are hints that the problem is very common one should take every LS even in perturbation theory as a serious possible source of such inconsistencies. The way to avoid these problems in the SM is to anticipate a scale of new physics Λ and to demand that the parameters of the theory are chosen so that all couplings are well behaved (i.e. no blow–up) in the physical region up to Λ:

$$g(\mu),\ \ \lambda(\mu) < \infty \quad \text{for} \quad \mu \epsilon [m_H, \Lambda] \qquad (7)$$

In general the range of couplings is thus with a finite range of validity (i.e. up to Λ) in mind "restricted" as a function of Λ. If a theory is restricted to $\lambda \equiv 0$ in the limit $\Lambda \to \infty$, i.e. only the free version of the theory is consistent, then it is "trivial".

Another problem besides triviality is that the Higgs potential can become unstable under radiative corrections for large top masses and a moderate Higgs mass [8]. To one–loop precision the effective potential for the Standard Model single Higgs doublet is given by:

$$V(\phi) = -\mu^2\phi^2 + \frac{a}{16\pi^2 v^2}\phi^4 \ln(\phi^2/M^2)\ ; \quad a = 3\sum_V M_V^4 - 4m_t^4 + m_H^4 \tag{8}$$

where V runs over the vector bosons, $W^{\pm}, Z$ and the sum over fermions counts each quark color separately. Here μ and M are constants which are implicitly determined by specifying the Higgs particle mass and by demanding that the potential must have an absolute minimum at $\langle\phi\rangle/\sqrt{2} = 246$ GeV. The potential becomes unstable since the induced one loop radiative corrections to λ include a graph with a top loop proportional to $g_t^4 = m_t^4 \cdot v^4$. This contribution has a minus sign due to statistics and tends to drive λ negative. If the initial value of $\lambda = m_H^2/2v^2$ is small and $g_t = m_t/v$ is big then the sign of λ can change. If we look at eq. (8) then we see that the region of a stable potential is limited by a balance between the negative term from the top mass and a positive term from the Higgs mass. This can be crudely approximated to be

$$m_t \lesssim 90\ GeV + \frac{4}{7}\, m_H \tag{9}$$

though, for a more precise statement of the limits we refer to [9]. In the spirit of above we need only be concerned about such problems if the sign change occurs in the physical region up to Λ and therefore finite embedding scales were included in the analysis of ref. [9].

The limitations from both consistency requirements are summarized in Figs. 1) and 2) for different values of Λ. The strongest constraints for m_H and m_t arise for the highest values of Λ. So if LHC finds nothing than new lower limits on m_H and m_t then these limits will be so high that the highest values for Λ are excluded. When the window closes only the highest allowed Higgs masses are left over and imply the lowest scale of new physics which is of order TeV again. Therefore from this point of view it would be better if e.g. the Higgs particle or its equivalent were heavy since this implies that the Standard Model cannot be taken to be valid at arbitrarily high energies. If the Higgs mass were at its highest allowed value of order TeV then new physics *beyond* the SM is guaranteed to show up in the TeV range.

Note that these kind of statements come essentially from the fact that with higher Higgs and top mass λ and g_t get bigger and the stronger loop effects lead to instabilities in the running coupling constants. In short the bounds on Λ are stronger if the initial coupling is bigger and therefore the instability is reached faster. This statement has probably an equivalent of much more general scope. If we were to substitute the Higgs particle then very often a similar situation would be expected. If the state which ensures unitarity is of the order of 1 - 2 TeV then this is (since the unitarity problem is solved only shortly before one arrives at an inconsistency and strong effects are needed to avoid this) a sign of a strongly interacting Higgs sector. If we tried to take this model with a Higgs substitute serious by itself, then the strong couplings involved would tend to produce "accidents" in the running couplings when loop effects are included. These "accidents" could then in general be interpreted as the need for new physics beyond the SM. By this handwaving argument we expect that the heavier the unitarizing particle is the more likely it will be that physics beyond the SM must show up earlier.

I.5. Extreme Examples of Dynamical Symmetry Breaking

As indicated above tree unitarity guarantees that at least one state which is connected inherently to the breaking of the electroweak symmetry must show up in the few TeV area. If one thinks that dynamical symmetry breaking mechanisms are more attractive than static mechanisms with fundamental scalars then one immediately recalls the similarities between the pions of QCD and the W and Z bosons. This has led to the development of scaled QCD or Technicolor [7] theories based on new Techni-fermions which carry a new confining Technicolor. In its simplest version there is one Techni-doublet (U,D) in analogy to the existing quarks and leptons and the boundstates of this doublet give rise to a set of Goldstone bosons as desired. Bigger models use more fermions like full generations or even more generations. But most models which use more than a minimal doublet of Techni-quarks are nowadays barely acceptable since they would predict extra pseudo–Goldstone bosons with masses typically up to M_W or M_Z and most of the allowed range is already experimentally excluded. There are also limits on the number of new bososnic and fermionic fields in Technicolor scenarios from the analysis of precision data of radiative corrections to the SM [10]. Roughly speaking very big colour groups and very large numbers of fermions as well as technifermion mass splitings would lead to virtual effects that would already show up as deviations from the SM.

There is however one feature common to all Technicolor ideas. Since they are based on QCD scaled by F_π/f_π or additionally rescaled to any number of colors by large N_C arguments there is not much freedom in the spectrum. From radiative corrections [10] N_C is already restricted to be not too big and the Techni-meson to Techni-baryon mass ratios are only changed by N_C factors which implies that the Techni-baryons cannot be many orders of magnitude above the Techni-mesons. Therefore it seems as if a wealth of new states is unavoidably predicted in the multi TeV range. Another common feature of Technicolor scenarios is that the dampening of the amplitudes of the Higgs-less SM is always done by a Techni-rho.

To show that both the expectation of a wealth of states as well as the nature of the state that ensures unitarity are determined by the unknown dynamics we would like to contrast the Technicolor expectations with what has been called 'Minimal Dynamical Symmetry Breaking' [11]. There the fact that the top quark is very heavy is translated into a model where top quark condensation breaks the electroweak symmetry. One assumes that there is no fundamental Higgs field and that new four fermi interactions are added to the SM instead of it. The four fermi term is thought to be produced by new physics at Λ which has been integrated out so that one arrives at

$$\mathcal{L}_{(\mu=\Lambda)} = \mathcal{L}_{g,f} + \frac{g^2}{\Lambda^2}\,\bar{L}t_r\bar{t}_r L\ ; \quad L = (t_l, b_l) \tag{10}$$

where $\mathcal{L}_{g,f}$ refers to the part of the Lagrangian which contains only gauge fields, fermions and no scalars. If the coupling g is chosen suitable [11] to fulfil a gap equation like in BCS theory then the normal SM Higgs Lagrangian can be derived as an effective Lagrangian where the Higgs field is now a $\bar{t}t$ boundstate. The heaviness of the top quark would thus be linked to the non–fundamental nature of the Higgs field.

Besides reproducing *effectively* the Higgs field which was thrown out one obtains relations between m_t, m_H and M_W. In its simplest and most elegant form the preferred values for the Higgs and top mass are $m_H \simeq 250\ GeV$ and $m_t \simeq 225\ GeV$. This value of m_t is somewhat high when compared with the preferred range from the analysis of radiative corrections [3]. But even if the simplest version of this mechanism should not be acceptable on phenomenological grounds one can still start to build extensions which agree with experiment and have the same sort of dynamics. The important point is that the breaking of the electroweak symmetry by

top condensation can lead to situations very different from Technicolor ideas. The particle which ensures unitarity is a composite Higgs particle which is a $\bar{t}t$ boundstate with *exactly* the same properties as the fundamental Higgs field that was eliminated. Additionally unlike in Technicolor where mass ratios are rather inflexible here the ratio between the mass of this composite Higgs and the scale of new physics can be tuned to become *arbitrarily small.* Since the Higgs mass has to be somewhere in the TeV area this means that new physics besides this tight composite Higgs particle can be placed arbitrarily high. This would mean that we could find a Higgs particle where we are experimentally unable to tell if it is composite or fundamental since it is a very tight bound state and nothing else within reasonable energies accessible to any thinkable accelerator.

So even if the simplest version of top condensation turns out not to be realized it is still a good example which shows how dynamics determines the properties of the state which ensures unitarity and where the remaining spectrum is settled.

I.6. Cosmological Arguments for the TeV Scale: Dark Matter and Stable Particle Searches at LHC

The LHC and SSC are designed to unravel the mechanism of electroweak symmetry breaking. In this section we argue that these accelerators have a good chance to discovering much more. We point out that any perturbative new physics with cosmologically stable remnants has to occur below a few TeV. The single ingredient from which these conclusions follow is the cosmological requirement that the density of the universe does not exceed its critical value. This requirement implies that any perturbatively coupled cosmologically stable elemenatry particle must be lighter than the geometric mean of the Planck mass and the cosmic background radiation temperature of 2.7 K [12].

$$m \lesssim \sqrt{M_{Pl} \times 2.7\ K} \simeq few\ TeV \qquad (11)$$

By a remarkable coincidence this is of the order of a few TeV and thus implies that any stable electroweak particles must be energetically accessible to the LHC.

The list of theoretically motivated stable particles is long and distinguished.

(1) The Dark Matter of the Universe. Since it is most probably electrically neutral [13] and colorless it may be searched for via missing energy type experiments. They can also be searched for by looking for the decays of their heavy electroweak partners which, if any, are necessarily charged [14].

(2) Technibaryons. They typically weigh 2 TeV and carry fractional electric charge; they can be colorless or colorful depending on the theory [15].

(3) Lightest Superparticle (LSP). It is expected to be charge and color neutral; thus, it can be searched for by missing momentum measurements just like dark matter searches. In fact the LSP could eventually be true dark matter.

(4) Fractionally charged particles. These can occur in superstring theories [16]. They may be searched for by looking for sub (or super) -minimum ionizing particles. To measure their mass one needs time of flight experiments or/and magnetic fields.

References

[1] K. Wilson, unpublished; E. Gildener and S. Weinberg, Phys. Rev. **D13**(1976)3333; L. Susskind, Phys. Rev. **D20**(1979)2619.

[2] M. Chanowitz and M.K. Gaillard, Nucl. Phys. **B261**(1985)379.

[3] For a recent analyis see e.g. P. Langacker, Univ. of Pennsylvenia preprint UPR-0435T, Aug. 1990.

[4] M. Veltman, Acta Phys. Pol. **B8**(1977)475; B.W. Lee, C. Quigg and H. Thacker, Phys. Rev. **D16**(1977)1519.

[5] L.Maiani, G.Parisi and R. Petronzio, Nucl. Phys. **B136**(1978)115; N. Cabbibo et al., Nucl. Phys. **B158**(1979)295; R. Dashen and H. Neuberger, Phys. Rev. Lett. **50**(1983)1847.

[6] M. Lindner, Z. Phys. **C31**(1986)295.

[7] L. Susskind, Phys. Rev. **D20**(1979)2619; S. Dimopoulos and L. Susskind, Nucl. Phys. **B155**(1979)237; E. Eichten and K. Lane, Phys. Lett. **B90**(1980)125.

[8] P.Q. Hung, Phys. Rev. Lett. **42**(1979)873; H.D. Politzer and S. Wolfram, Phys. Lett. **B82**(1979)242.

[9] M. Lindner, M. Sher and H. Zaglauer, Phys. Lett. **B228**(1989)139.

[10] B. Lynn, M.E. Peskin and R.G. Stuart, CERN Yellow Book on Physics at LEP, ed. by J. Ellis and R. Peccei, CERN 86-02 report; M. Peskin and T. Takeuchi, Phys. Rev. Lett. **65**(1990)964.

[11] W. Bardeen, C. Hill and M. Lindner, Phys. Rev. **D41**(1990)1647.

[12] S. Dimopoulos, Phys. Lett. **B246**(1990)247 and references therein.

[13] S. Dimopoulos et al., Phys. Rev. **D41**(1990)2388; R.S. Chivukula et al., Phys. Rev. Lett. **65**(1990)957; G. Starkman et al., Phys. Rev. **D41**(1990)3594.

[14] S. Dimopoulos et al., "TeV Dark Matter", to be published in Nucl. Phys. **B**.

[15] R. Chivukula and T. Walker, Nucl. Phys. **B 329**(1990)445.

[16] G. Athanasiu et al., Phys. Lett. **B214**(1988)55.

Figure Captions

Fig. 1: Upper bounds on the top and Higgs mass from triviality and vacuum stability arguments for different values of Λ (taken from [6]).

Fig. 2: Lower limits on the Higgs mass from vacuum stability as a function of the top and Higgs mass and the scale of new physics (taken from [9]).

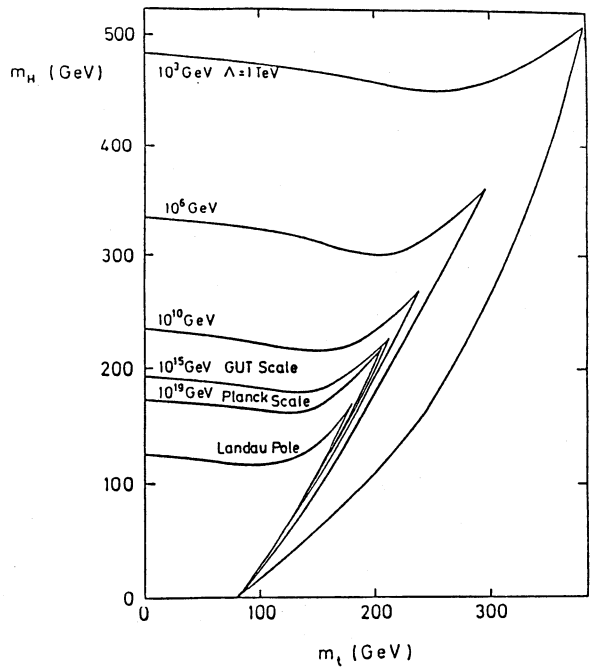

Fig. 1

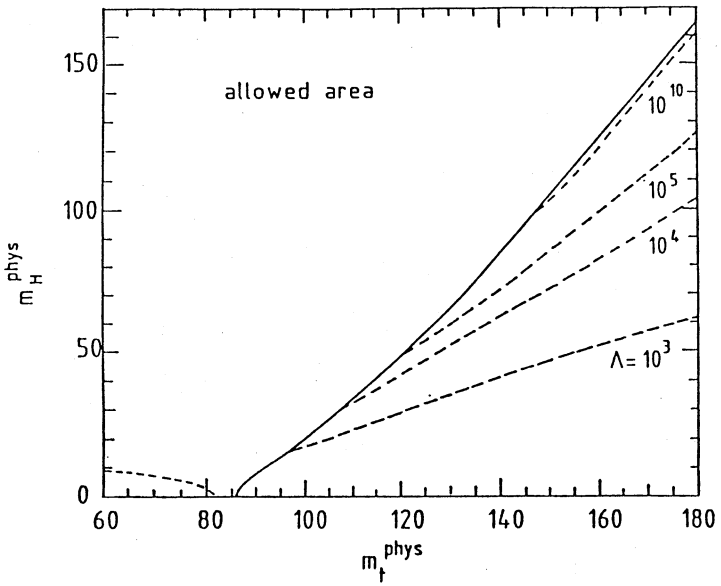

Fig. 2

II. V_LV_L SCATTERING : CHIRAL LAGRANGIAN APPROACH

Contributors: A. Dobado, M.J. Herrero and J. Terron

II.1. Introduction

One of the main goals of the LHC is to clarify the origin of the Symmetry Breaking Sector (SBS) of the Standard Model (SM). Either the Higgs particle will be found at LHC (or SSC) with a mass below 1 TeV or some manifestation of the strongly interacting system to which the longitudinal components of the gauge bosons, $W_L^{\pm}$ and Z_L, belong must show up in the TeV energy regime [1]. Generally speaking, the **Strongly Interacting Symmetry Breaking Sector (SISBS)** hypothesis simply means *the absence of any physical state belonging to the SBS well below 1 TeV other than the Longitudinal Weak Bosons (LWB) themselves.* In that case, the relative low masses of the gauge bosons as compared to the TeV energy domain, where the emerging resonances are expected to occur, may be understood on the basis of an approximate global symmetry of the SBS which is spontaneously broken and the LWB being the associated Nambu-Goldstone bosons. If experimentally achievable, the scattering of the LWB, V_LV_L ($V_L = W_L^{\pm}$ or Z_L), at the TeV energy scale [2] will provide the clue to fully understand the nature of the SBS. Why must this be so?

First of all, in the case of a SISBS the scattering of the longitudinal degrees of freedom at high energies (say for $\sqrt{s} >> M_W$) dominates over the scattering of the transverse components. Secondly, the Equivalence Theorem tells us that by measuring the $V_LV_L \to V_LV_L$ scattering at high energies ($\sqrt{s} >> M_W$) what is really being measured is the scattering of the corresponding Nambu-Goldstone bosons and, consequently, the strength of the interactions in the SBS. Thirdly, it is precisely the energy scale of about 1 TeV where perturbative unitarity in V_LV_L scattering is broken down. This has two important consequences. One is that the V_L's self-interactions cannot be treated perturbatively. The other and probably the most interesting consequence concerning the phenomenological implications at LHC is the fact that there must be a system that is responsible for restoring unitarity in the V_LV_L scattering at the TeV energy scale [3]. This system could be the Higgs particle itself as in the SM (H), a composite vector boson as for instance the technirho ($\rho_{TC}^{\pm}$ and ρ_{TC}^0) of Technicolor theories or the isotriplet ($V^{\pm}$ and V^0) of the BESS model, a composite scalar system resembling the Higgs particle , or it could even be a more exotic system with higher isospin and/or spin quantum numbers not even proposed yet.

The aim of this report is to set up the typical signatures of a SISBS at LHC and, for comparison, at SSC that come from different scenarios for the SBS as those just quoted above. In order to be able to deal with different physical situations for the SISBS on the same grounds and without loss of generality we choose the Chiral Lagrangian formalism and the Chiral Perturbation Theory (ChPT) techniques [4] that have been proven to be quite satisfactory in the context of low energy hadron physics.

The nicest feature of the Chiral Lagrangian approach when applied to the SISBS problem [5], besides being completely general, is that it relies just on three simple requirements: 1) The global symmetry pattern for the building-up of this Chiral Lagrangian must be compatible with the symmetries of the SM, $SU(2)_L \times U(1)_Y \to U(1)_{em}$, 2) The ρ parameter must be close to one, and, 3) The value of the dimensionful parameter that plays the role of f_π in low energy hadron physics is fixed here to $v = 246GeV$. These three requirements lead us to adopt the following

the following chiral symmetry breaking pattern: $SU(2)_L \times SU(2)_R \to SU(2)_V$ with $SU(2)_V$ being the so–called custodial symmetry, and $W_L^\pm$, Z_L being the three Nambu-Goldstone bosons associated to this global symmetry breaking. All what rests is provided by the machinery of ChPT and the V_LV_L scattering may, in fact, be described in formal analogy to $\pi\pi$ scattering. In the latter case the isospin symmetry plays the same role as the custodial symmetry does in the former case. More specifically, ChPT gives an expansion of the V_LV_L scattering amplitudes in powers of $s/(4\pi v)^2$ and it is valid in the energy range $M_W << \sqrt{s} << min(4\pi v, M_R)$, with M_R being the mass of the (unknown) lowest resonance belonging to the SISBS.

The V_LV_L scattering amplitudes computed by means of ChPT do not respect unitarity for energies larger than about 1.5 TeV [5]. The problem of getting unitary answers for the scattering amplitudes is treated here by supplementing the Chiral Lagrangian approach with a unitarization prescription (we call it **Unitarized-ChPT**) [6]. In particular we use the following procedures: the Padé approximant method and the K-matrix one.

In our search for typical signatures of a SISBS at LHC (and SSC) we have been systematic: 1) we have looked at the four different final states in pair boson production, W^+W^-, ZZ, $W^\pm Z$ and $W^\pm W^\pm$ and, 2) we have made predictions for three characteristic scenarios: Scaled-QCD, $SU(N_{TC})$ Technicolor and a Higgs-like scenario. Notice, however, that our study could be extended to more exotic scenarios as for instance those containing a system with isospin and electric charge equal to two that would resonate in the W^+W^+ or W^-W^- channels. For a more detailed description of the ChPT approach for V_LV_L scattering see refs. [5], [7] and [8]. Some of the results presented in this report are contained in [7].

II.2. Cross-sections for strongly interacting signals

In order to compute the cross-section for the process $pp \to (V_1^LV_2^L \to V_3^LV_4^L) + X$, we have used the effective W-approximation [9] that allows us to derive it in terms of the cross-section for the subprocess $V_1^LV_2^L \to V_3^LV_4^L$, where the initial longitudinal gauge bosons are taken to be real. More precisely, it is given by:

$$\sigma = \sum_{ij} \int\int d\tau d\eta f_i(x_1,Q^2) f_j(x_2,Q^2) \int\int d\hat{\tau} d\hat{\eta} \left(\frac{d^2\mathcal{L}}{d\hat{\tau} d\hat{\eta}}\right)_{V_1V_2} \times \int_{-1}^{1} dcos\theta \frac{d\hat{\sigma}}{dcos\theta} \qquad (1)$$

where, f_i and f_j are the distribution functions of the quarks i and j, respectively, inside the proton; the variables τ and η are related to the momentum fractions of the quarks by $x_{1,2} = \sqrt{\tau} e^{\pm\eta}$; the variables $\hat{\tau}$ and $\hat{\eta}$ are related to the momentum fractions of V_1, V_2 respect to q_i, q_j, $\hat{x_1}$ and $\hat{x_2}$, by $\hat{x}_{1,2} = \sqrt{\hat{\tau}} e^{\pm\hat{\eta}}$; $(\frac{d^2\mathcal{L}}{d\hat{\tau}d\hat{\eta}})$ is the luminosity function for the gauge boson pair $V_1^LV_2^L$ to be radiated from the quark pair q_iq_j; and $\frac{d\hat{\sigma}}{dcos\theta}$ is the differential cross-section for the subprocess $V_1^LV_2^L \to V_3^LV_4^L$ given by:

$$\frac{d\hat{\sigma}}{dcos\theta} = \frac{|T(V_1^LV_2^L \to V_3^LV_4^L)|^2}{32\pi M_{VV}^2}. \qquad (2)$$

For final states with identical particles an additional factor of 1/2 must be included.

The scattering amplitudes for the various signal subprocesses $T(V_1^LV_2^L \to V_3^LV_4^L)$ are given in ChPT to $O(p^4)$ by [5]:

$$T(W_L^+W_L^- \to W_L^+W_L^-) = A(s,t,u) + A(t,s,u)\ ,\ T(W_L^+W_L^- \to Z_L^0Z_L^0) = A(s,t,u)$$

$$T(Z_L^0Z_L^0 \to Z_L^0Z_L^0) = A(s,t,u) + A(t,s,u) + A(u,t,s)$$

$$T(W_L^\pm Z_L^0 \to W_L^\pm Z_L^0) = A(t,s,u)\ ,\ T(W_L^\pm W_L^\pm \to W_L^\pm W_L^\pm) = A(t,s,u) + A(u,t,s)$$

$$A(s,t,u) = \frac{s}{v^2} + \frac{4}{v^4}\left(2M_R(\nu)s^2 + N_R(\nu)(t^2+u^2)\right)$$

$$+\frac{1}{(4\pi)^2v^4}\left[-\frac{1}{12}(3t^2+u^2-s^2)\log\frac{-t}{\nu^2} - \frac{1}{12}(3u^2+t^2-s^2)\log\frac{-u}{\nu^2} - \frac{1}{2}s^2\log\frac{-s}{\nu^2}\right] \qquad (3)$$

and, $M_R(\nu)$, $N_R(\nu)$ are the two renormalized parameters appearing in the $O(p^4)$ terms of the Chiral Lagrangian. The values of M_R and N_R have to be chosen properly for each different scenario of the SISBS one is interested to mimic. The $O(p^2)$ terms in (3) are independent of the underlying dynamics and correspond to the well known Universal Low Energy Theorems results [10].

For the numerical computations we have introduced the above expressions into a parton level Monte Carlo program (VEGAS) that besides of calculating the total cross section it generates all the relevant distributions with the required cuts. The various background contributions were also computed by the same Monte Carlo program. The signal processes for the three scenarios considered here were also introduced into the PYTHIA Monte Carlo program and some of them were studied in parallel by another subgroup [11].

We have used the EHLQ structure functions set II [12] (the choice done for Q^2 will be discussed separately for each process), and the following parameters for LHC and SSC were assumed: $LHC, \sqrt{s} = 16TeV, L = 4\times10^{34}cm^{-2}sec^{-1}$ and $SSC, \sqrt{s} = 40TeV, L = 10^{33}cm^{-2}sec^{-1}$. Some comments will also be done for a lower luminosity at the LHC of $L = 10^{34}cm^{-2}sec^{-1}$ (unless it is said explicitly the highest luminosity with the factor 4 included will be assumed). All the numbers of events presented in this report correspond to a running time of 10^7sec.

Our starting "raw events" are those obtained after applying the following set of **minimal cuts**: $0.5TeV < M_{VV} < 10TeV$, $|p_{TV}| > 10GeV$, $|y| < 1.5$ *or* 2.5. Here M_{VV} is the invariant mass of the final gauge boson pair, p_{TV} is their transverse momentum and y is their rapidity. Notice that the lower cut on the invariant mass is necessary for the computation of the signal rates since we are using the Equivalence Theorem that assumes $M_{VV} >> M_V$. In order to improve the observability of the signal over the background processes we apply more stringent cuts than the minimal cuts. These are obtained from an optimization procedure that is based on making cuts simultaneously on M_{VV} and p_{TV}. Depending on the kind of the signal, we adopt one of the two following strategies:

(A) Whenever there is a wide resonance or there is an excess of events over the continuum we look for the cuts (we call them **optimal cuts**) that maximize the function

$$F((p_{TV})_c,(M_{VV})_c) = \frac{n_s(p_{TV} > (p_{TV})_c, M_{VV} > (M_{VV})_c)}{\sqrt{n_T(p_{TV} > (p_{TV})_c, M_{VV} > (M_{VV})_c)}} \qquad (4)$$

where $n_s(...)$ ($n_T(...)$) is the number of events in the signal (total = signal + background) that satisfy the cuts indicated. The notation used in the tables for the optimal cuts is: $((p_{TV})_c,(M_{VV})_c)$. Note that F measures the statistical significance of the signal.

(B) Whenever there is a narrow resonance we choose a window on the M_{VV} variable and search for the cut on p_{TV} that makes $F(p_{TV})$ maximal. The notation used in the tables for the optimal cuts is $((p_{TV})_c)$.

II.3. Scenarios for the SISBS

In order to study the phenomenological implications at LHC we have considered three scenarios [7]: Scaled-QCD, $SU(N_{TC})$ Technicolor and a Higgs-like scenario.

II.3.1. Scaled-QCD

This scenario is based on transferring the low energy phenomenology of QCD from the energy domain of several hundreds MeV to the region of several hundreds GeV. The LWB are really the pions of this Scaled- QCD scenario. In particular, the $V_L - V_L$ scattering is a replica of the $\pi - \pi$ scattering data (including the broad enhancement in the I=J=0 channel and the appearance of the ρ resonance in the I=J=1 channel) that have been scaled up in energy by a factor of $v/f_\pi = 2600$. We do this rescaling by means of Unitarized-ChPT.

The physical parameters of the ρ-like resonance of this Scaled-QCD scenario are the following: $M_{\rho_{QCD'}} = 2TeV$, $\Gamma_{\rho_{QCD'}} = 480GeV$.

II.3.2. $SU(N_{TC})$ Technicolor

In this scenario, $SU(N_{TC})$ Technicolor [13] , we assume there is a vector resonance I=J=1 in the spectrum. Using large N_{TC} arguments one expects that the mass of the vector resonance goes like [13] $M_{\rho_{TC}} \approx M_\rho \frac{v}{f_\pi}(\frac{3}{N_{TC}})^{\frac{1}{2}}$, where $M_\rho = 770MeV$. Increasing N_{TC} implies a lighter resonance as compared to the resonance in the QCD-like scenario that would correspond in this context to $N_{TC} = 3$. By assuming the KSFR relation [14] holds in $SU(N_{TC})$ theories as it (approximately) does in QCD, more specifically $\Gamma_{\rho_{TC}} = \frac{M^3_{\rho_{TC}}}{96\pi v^2}$, then the larger N_{TC} is, the narrower turns out to be the resonance. In this way one can study the experimental possibilities for detecting vector resonances over a wide range of mass values, based on some general assumptions. In particular, the existence of a ligther resonance increases considerably the production rates of $W^\pm Z^0$ pairs and, thus, the observability of these resonances. The way one has to choose M and N in order to reproduce the low energy behaviour of these $SU(N_{TC})$ scenarios is the following one:

$$M_R^{TC}(\frac{v}{f_\pi}(\frac{3}{N_{TC}})^{\frac{1}{2}}\nu) = \frac{N_{TC}}{3}M_R^{QCD}(\nu) \;\; ; \;\; N_R^{TC}(\frac{v}{f_\pi}(\frac{3}{N_{TC}})^{\frac{1}{2}}\nu) = \frac{N_{TC}}{3}N_R^{QCD}(\nu) \qquad (5)$$

where M_R^{QCD} and N_R^{QCD} are the parameters of the $O(p^4)$ terms in the chiral Lagrangian of low energy QCD.

In order to take into account properly the contribution of the I=J=1 resonance (the technirho) in the computations, we have chosen the Padé unitarization method. The reason is that it provides a resonant behaviour in the I=J=1 channel with the particularity of fulfilling automatically the KSFR relation. In particular, it is known to reproduce very well the $\pi - \pi$ scattering data in the three channels, I=J=0, I=J=1 and I=2,J=0 [15].

In order to study a wide range of signatures we have considered two technicolor scenarios: 1) $M_{\rho_{TC}} = 1.0TeV$, $\Gamma_{\rho_{TC}} = 55GeV$ and 2) $M_{\rho_{TC}} = 1.5TeV$, $\Gamma_{\rho_{TC}} = 185GeV$. They correspond to $N_{TC} = 12$, and $N_{TC} = 5$ respectively.

II.3.3. Higgs-like

We define the Higgs-like scenario in two steps. First, we choose the parameters of the effective Lagrangian to $O(p^4)$, M and N [5], so as to reproduce the LWB scattering amplitudes in the SM to one–loop order and in the limit $m_H^2 \gg s$ [16]. Thus, with this first step we are simulating the effect at low energies of a very heavy Higgs boson in the SM to one loop level. The way one has to choose the parameters M and N is the following: [2]

$$M_R(\nu) = \frac{1}{8}(c_1 - \frac{1}{2}c_2) + \frac{1}{12(4\pi)^2}log\frac{M_H}{\nu} \;\; ; \;\; N_R(\nu) = \frac{c_2}{8} + \frac{1}{6(4\pi)^2}log\frac{M_H}{\nu} \qquad (6)$$

where, $c_1 = \frac{1}{(4\pi)^2}(\frac{9\pi}{2\sqrt{3}} - \frac{76}{9})$, $c_2 = -\frac{4}{9}\frac{1}{(4\pi)^2}$ and M_H is the renormalized Higgs mass as defined in the first ref. of [16].

The second step involves the unitarization of the LWB scattering amplitudes obtained in the first step. We remind that, in their present form, they violate unitarity at about 1.5 TeV [5] and they should not be used without a unitarization prescription for the event rates computation at LHC or SSC [17]. The two unitarization methods used here give partial waves that verify $Im\, a_{IJ} = |a_{IJ}|^2$. Besides, they are characterized by:

** **K-matrix method:** It stops the increase with energy of the a_{IJ} partial waves (particularly the a_{00} partial wave in this Higgs-like scenario) and gives a saturation behaviour.

** **[1,1]-Padé-approximant method:** It also stops the increase with energy of the a_{IJ} partial waves but instead of saturating all of them it develops a resonant behaviour in the a_{00} channel. The scalar resonance S of the Higgs-like scenario shows up at a mass scale which is given by the position of the pole in the unphysical sheet of the $a_{00}^{[1,1]}(s)$ function [18]. More precisely, M_S is given by the solution to the equation:

$$M_S^2 = \frac{4v^2}{\frac{1}{3}(22c_1 + \frac{1}{4}c_2) + \frac{100}{9(4\pi)^2}log\frac{M_H}{M_S}}. \qquad (7)$$

We define the Higgs-like scenario in this case as the one having the scalar resonance at $M_S \sim 1\ TeV$. It is worth to mention that, as pointed out in [19], the features obtained by the Padé method when applied to the SM case (in particular the appearance of the so–called "*Higgs Remnant*" corresponding in our case to the scalar resonance S) are in qualitative agreement with the ones obtained by the large N expansion of the O(N) model [20].

II.4. Numerical Results

In view of the present controversy about the question of whether such a high luminosity as that planned for LHC and SSC will allow to disentangle SISBS signals by studying the hadronic decays of the weak bosons or not, we have considered in this report only their *LEPTONIC DECAYS*.

[2] Strictly speaking, there would be an additional contribution to M_R that comes from the tree level and is given by $M_{tree} = \frac{v^2}{8M_H^2}$ [8]. We thank G.Valencia for making us this remark. However, we do not consider this term here since it is completely negligible in the limit we are concerned with, $v^2 << s << M_H^2$.

II.4.1. W^+W^- Channel

This channel looks potentially very interesting in terms of signal rates and signal patterns as it would give resonant behaviour in all the three scenarios considered here. However, in view of the present lower bounds for the top quark mass, $m_t > 89\ GeV$ [21], already above the W-boson mass, it turns out that the dangerous background $pp \to t\bar{t}X$ with the top (anti-top) quarks decaying into real $W^{+\prime}s$ ($W^{-\prime}s$) overwhelms completely the signal. In view of that we have not considered this channel here.

II.4.2. ZZ Channel [7]

This channel offers a potential good probe for the Higgs-like scenario and in general for any scenario containing a scalar- isoscalar resonance. The reason is that it couples dominantly to the I=J=0 channel and therefore, in principle, it could produce either a bump or in the worst case an enhancement in the invariant mass distribution of the gold-plated events , $l^+l^-l^+l^-$ with $l = \mu$ or e, over the continuum background.

** **Leptonic branching ratio:** $BR(ZZ \to l^+l^-l^+l^-) = 0.4\%$

** **Signal processes:** The total rates for the signal correspond to the sum of the following separate contributions: 1) $W_L^+W_L^- \to Z_LZ_L$ and 2) $Z_LZ_L \to Z_LZ_L$. The Q^2 scale used in the distribution functions of the quarks is $Q^2 = M_W^2$.

** **Background processes:** The total background is the sum of the following separate contributions (in parenthesis it is written the percentage relative to the total background for both LHC and SSC and for top masses ranging from 100 GeV to 180 GeV): 1) $q\bar{q} \to Z^0Z^0$ (80%-70% at LHC) (65%-55% at SSC) and 2) $gg \to Z^0Z^0$ (20%-30% at LHC) (35%-45% at SSC). The Q^2 scale used in the distribution functions of quarks and gluons (and in $\alpha_s(Q^2)$) is $Q^2 = \hat{s}$. Here (and in the rest of the report) $\hat{s}$ is center-of-mass-energy squared of the parton-parton system.

** **Results and comments:** The results for the signal-to-background ratios, S/B, of the final leptonic $l^+l^-l^+l^-$ events ($l = \mu$ or e) after applying the optimal cuts are collected in table 1. We have chosen here two among the three scenarios: The Higgs-like and the Scaled-QCD scenarios.

Figs. 1a and 1b show the invariant mass distribution M_{ZZ} (no leptonic-BR has been included in the figs.) of the ZZ reconstructed events (it assumes 100% efficiency in the reconstruction). From these numerical results one can conclude that the search of SISBS signals in this channel seems difficult. The signal-to -background ratio is always less than one and there is no apparent bump in the M_{ZZ}-invariant mass distribution. The most favourable case is the Higgs-like scenario where the best S/B-ratio that can be got at LHC with the highest luminosity is 33/75. The S/B-ratio at SSC is slightly larger (8/11) but it is poor in statistics. The results with the K-matrix method (not shown in table 1) give comparable signal rates for the Scaled-QCD scenario and slightly smaller rates (about a factor 2/3) for the Higgs-like scenario.
The curves show a small enhancement in the high-M_{ZZ} region of the M_{ZZ}-invariant mass distribution over the continuum. This enhancement is clearly larger in the Higgs-like scenario than in the Scaled-QCD one and, in general, the corresponding total signal rates are in a ratio of 2 to 1 respectively. Finally, whether it will be possible to discern this small enhancement from the continuum or not is a question strongly dependent on the accuracy in the calibration of this continuum along the whole invariant mass range.

II.4.3. $W^\pm Z$ Channels [7]

These channels are a good probe for the Scaled- QCD and Technicolor scenarios and, in general, for any scenario containing a ρ-like vector resonance (for instance the $V^\pm$ resonances of the BESS model [22]). This resonance couples dominantly to the I=J=1 channel and therefore can give rise to a resonant behaviour in $W^\pm Z$ production at LHC and SSC. The final $l^\pm\nu l^+l^-$ leptonic events (with $l = \mu$ or e) produced from the decay chain $\rho^\pm \to W^\pm Z \to l^\pm\nu l^+l^-$ will present typical signatures and distributions characterized by the physical parameters (the mass and the width) of this resonance.

** **Leptonic branching ratio:** $BR(W^\pm Z \to l^\pm\nu l^+l^-) = 1.5\%$

** **Signal processes:** Here we distinguish the Higgs-like scenario from the other ones, i.e., the Scaled-QCD and the Technicolor scenarios.

Higgs-like: There is just one type of signal process: 1) $W_L^\pm Z_L \to W_L^\pm Z_L$.

Scaled-QCD and Technicolor: There are two kind of processes that contribute to the signal, that is to $W_L^\pm Z_L$ production: 1) $W_L^\pm Z_L \to W_L^\pm Z_L$, and 2) $q\bar{q}' \to W^\pm \to \rho_{TC} \to W_L^\pm Z_L$. The first mechanism is the so–called WZ fusion process and gives a generic SISBS signal since it is present in all the SISBS scenarios. The choice done for the Q^2 scale is $Q^2 = M_W^2$. The second mechanism where $q\bar{q}'$ annihilates into ρ_{TC} via $\rho_{TC} - W$ mixing is not present in the Higgs-like scenario but it is always present in any SISBS scenario containing a vector resonance with the quantum numbers of the W gauge boson. This is for instance the case of the Scaled-QCD scenario, Technicolor and the BESS model. For the two scenarios we are concerned with, we will assume as a reasonable working hypothesis that this second mechanism is well described in terms of Vector Meson Dominance (VMD) [23],[12]. The choice for the Q^2 scale here is $Q^2 = \hat{s}$.

** **Background processes:** We have taken into account the following background processes: 1) $q\bar{q}' \to W^\pm Z$. This is the main background. We have used the formulas of [12]; 2) $\gamma W^\pm \to W^\pm Z$. We have calculated the amplitudes for this process in the Standard Model and checked the expressions of [24]. The ratio of the production rates is $\gamma W_L^\pm \to W^\pm Z / \gamma W_T^\pm \to W^\pm Z = 0.04$ for both the LHC and the SSC; 3) $W^\pm Z \to W^\pm Z$ This background is defined as the contribution from all the polarization channels in WZ elastic scattering as predicted in the SM without the Higgs contribution and without the configuration $W_L^\pm Z_L \to W_L^\pm Z_L$. The latter is considered by us as the signal and is described by means of the effective chiral Lagrangian. We have obtained the following relations for the production rates: $W_T^\pm Z_T \to W^\pm Z : W_T^\pm Z_L + W_L^\pm Z_T \to W^\pm Z : W_L^\pm Z_L \to W^\pm Z = 1 : 0.1 : 0.003$ for both the LHC and the SSC for the 2.5 rapidity cut. The relative contributions respect to the total background are the following:

		LHC	*SSC*
$q\bar{q}'$	.....	65%	45%
$\gamma W^\pm$	.....	15%	20%
$W^\pm Z$	.....	20%	35%

The Q^2 scale used in each case is: $Q^2 = M_W^2$ for the WZ and γW processes and $Q^2 = \hat{s}$ for the $q\bar{q}'$ process.

There is an additional potentially dangerous background that we have not included here. It is the $t\bar{t}$ production with subsequent top decays into real W's. This process fakes our signal when both W's decay leptonically and one of the bottom quarks decays semileptonically. Although the rate for this process at the starting point is huge as compared to the signal, a careful study done by M.I.Josa, F.Pauss and T.Rodrigo [11] indicates that there exists a set of feasible cuts that diminishes this background to a level comparable to or even lower than the backgrounds considered here.

**** Results and comments:** The results for the signal-to-background ratios, S/B, of the final leptonic $l^{\pm}\nu l^{+}l^{-}$ events ($l = \mu$ or e) after applying the optimal cuts are collected in table 2. Predictions were made for the three scenarios: Scaled-QCD, Technicolor and the Higgs-like scenario. In looking for the optimal cuts we have used strategy A for the Higgs-like scenario and strategy B for the Scaled-QCD and Technicolor scenarios. We took: 950-1050 GeV, 1400-1550 GeV, 1500-2500 GeV as the windows in M_{WZ} for $M_\rho = 1.0, 1.5, 2.0 TeV$ respectively.

We have also computed the signal that would be produced in the Standard Model at tree level with a heavy Higgs boson of $m_H = 1TeV$ (SMH), in order to compare the results with our Higgs-like scenario results (HIGGS) that in contrast include the one loop corrections and a unitarization procedure. The analytic expressions in the SMH case were calculated for all possible configurations of polarizations (TT,TL,LT,LL, T for transverse and L for longitudinal). The formulae are too long to be included here and will be published elsewhere. As we have found some errors in the expressions for the $W_L^{\pm}Z_L \to W_L^{\pm}Z_L$ amplitudes published in the literature [25], the corrected formulae were included explicitly in [7] and incorporated into PYTHIA. In comparing the SMH and the Higgs- like scenario we find , as expected, comparable rates. The differences in S/B ratios of table 2 are due to the differences in the applied optimal cuts. As it is clear from the results in table 2, the S/B ratios are too low to be observable in either the Higgs-like scenario or in the SMH.

The situation is completely different in the Scaled-QCD and Technicolor scenarios were there are actual possibilities of observing the signal over the background with the total S/B ratios being always larger than one (see table 2). The contributions to the signal coming from the WZ fusion process and the $q\bar{q}'$ annihilation process via $\rho_{TC} - W$ mixing are presented separately in table 2. We would like to emphasize here that the S/B ratios obtained by considering just the WZ fusion contribution to the signal represent the most general and conservative expectations for the SISBS signals at LHC and SSC, and are already (for all the cases considered here) larger than one. The WZ fusion mechanism gives a generic SISBS signal and does not involve any assumption on the couplings between the fermionic sector and the SBS. The relative percentages of the WZ fusion contribution to the total signal are:

M_ρ	*rap.cut*	.....	$1.0TeV$	$1.5TeV$	$2.0TeV$
LHC	(2.5)	.....	9%	24%	45%
SSC	(2.5)	.....	22%	50%	72%

An increase in M_ρ results in a larger contribution from the WZ fusion process, which reveals itself as the most efficient mechanism in probing the SISBS for large enough values of M_ρ. This fact is clearly reflected in figures 2a and 2b. It is interesting to point out that the contribution of the fusion process is even more important at the SSC than at the LHC, due to the higher energy available at the subprocess level. The comparison of these mechanisms in technicolor theories was first discussed by Chivukula in [23] in the context of the SSC.

In figures 3a (LHC) and 3b (SSC) the M_{WZ} invariant mass distributions of the different background processes are displayed and for reference we have also included the spectrum of the WZ fusion signal process (with the optimal cuts).

As it is clearly manifested in figures 2 and 3 and in table 2 the results are encouraging for both LHC and SSC and for all the three values of M_ρ considered. Special mention must be given to the technicolor models where there is a large and clear signal in the M_{WZ} spectrum. In both cases, the Scaled-QCD and Technicolor scenarios, masses up to 2 TeV will be reachable at LHC. (See [11] for more details on this channel).

II.4.4. $W^{\pm}W^{\pm}$ Channels [26]

These channels are called exotic channels since they produce 2 like-sign leptons in the final state ($l^{\pm}\nu l^{\pm}\nu$ with $l = \mu$ or e) that are not easily produced by means of standard physics. Any potential signal in these channels will compete with a less prominent background than in the other channels. For instance, the important qq' background in W^+W^-, ZZ and $W^{\pm}Z$ channels is not present in $W^{\pm}W^{\pm}$ channels. Unfortunately, the latter are not good probes for any of the scenarios considered here in the sense that these do not contain any doubly charged resonance with I=2 that could resonate in the $W^{\pm}W^{\pm}$ channels. However, it is precisely its singular nature what makes this channel an interesting landmark especially adequated to probe new unexpected resonances. For the scenarios we are concerned with, the expected SISBS signal will be an enhancement in the large invariant mass M_{WW} that, unfortunately, is hard to translate into physical leptonic variables. These channels will serve at best as a test-confirmation of compatibility with whatever is seen in the ZZ and/or $W^{\pm}Z$ channels.

**** Leptonic branching ratio:** $BR(W^{\pm}W^{\pm} \to l^{\pm}\nu l^{\pm}\nu) = 5\%$

**** Signal processes:** $W_L^{\pm}W_L^{\pm} \to W_L^{\pm}W_L^{\pm}$. The Q^2 scale chosen here was $Q^2 = \hat{s}$.

**** Background processes:** These have been studied in detail by Barger et al. in [26]. The numerical results used in this report for the various background processes were taken from that reference. The main background processes in the W^+W^+ case are the following:
1) $qq' \to qq'W^+W^+$ (weak): This takes place through electroweak interactions and produces mainly $W_T^+W_T^+$ pairs. The exact calculation was presented in [26]. We will refer to this background as $W_T^+W_T^+$. 2) $qq' \to qq'W^+W^+$ (semi-weak): This takes place through gluon exchange. It will be referred to as gluon exchange. 3) $q\bar{q} \to W^+t\bar{t}$: This process fakes the leptonic signal when the quark top decays into a real W^+ , both W^+'s decay semileptonically and the remaining bottom and anti-top quarks decay hadronically. Its contribution depends crucially on the top mass value. The values $m_t = 100GeV$ and $200GeV$ were chosen here. 4) W^+W^+ + 3-jets-QCD: One contributing process is for instance, $qq' \to qq'W^+W^+g$. It will be called 3 jets QCD.
The relative contributions of the various backgrounds respect to the total for $M_{WW} > 0.8TeV$ and $|y_W| < 1.5$ are as follows:

Process		*LHC*	*LHC*	*SSC*	*SSC*
$(m_t =)$		$100GeV$	$200GeV$	$100GeV$	$200GeV$
$W_T^+W_T^+$	.....	31%	36%	43%	46%
gluon exchange	.....	14%	15%	19%	19%
3 *jets QCD*	.....	12%	13%	17%	16%
$W^+t\bar{t}$	.....	43%	36%	21%	19%

It has also been checked (by explicit computation) in [26] that a cut on the W-boson variables given by $M_{WW} > 0.8TeV$ and $|y_W| < 1.5$ is approximately equivalent to the following cuts on the leptonic variables (this is for both the total signal and the total background): $m_{ll} > 0.5TeV$, $|y_l| < 2.0$ and $p_T(l) > 25GeV$.

**** Results and comments:** The results for the signal-to-background ratios, S/B, of the final $l^+\nu l^+\nu$ events ($l = \mu$ or e), for various choices of the invariant mass cut are shown in table 3. The corresponding rates for the $l^-\nu l^-\nu$ events (not shown in the table) are approximately 1/3 of those in table 3. The results from a tree level calculation in the SM with a Higgs boson of $M_H = 1TeV$ (SMH) are also included for comparison with our Higgs-like scenario (HIGGS). From these numerical results one can conclude that the search of SISBS signals coming from the kind of scenarios considered in this report will be very hard in these channels. The S/B ratio is always less than one and the M_{WW} distribution of the signal shows no singular behaviour.

From figs. 4a and 4b it is clear that for the energy range of interest the total background is well above the signal. In ref.[26] it is claimed that by using central jet vetoing techniques one can notably improve the S/B ratios. Since the signal in this report is computed by means of the Effective W approximation, that assumes zero transverse momentum for the WW system and the remaining jet-jet system, these jet vetoing techniques cannot be implemented properly here. We leave this work for a Monte Carlo level simulation.

II.4.5. Multiple V_L Production

Another probe to test the nature of the Symmetry Breaking Sector is the multiple production of LWB [27]. In the case of a SISBS, the multiple production of LWB is not suppressed by powers of the weak coupling constant as it occurs in weakly interacting SBS. We consider here the production of four LWB, $V_LV_L \to V_LV_LV_LV_L$, in the context of the effective Chiral Lagrangian approach [3]. We first calculate the amplitude for this process at the tree level, that is to $O(p^2)$ in ChPT. Thus, as long as these results are universal (fixed just by the scale v) they constitute a conservative estimate of the rates and they serve to test the nature of the SBS, but not the underlying dynamics.

As these amplitudes increase with the energy, it is necessary to study the question of unitarity. In fact, the $2 \to 4$ amplitudes are expected to violate unitarity at the same scale as the $2 \to 2$ channels, namely O(1-2 TeV). This implies that the effects of higher order corrections must be taken into account in order to restore unitarity. As we have already seen for the case of pair production, one way of incorporating these effects is through the use of a unitarization procedure. In order to obtain conservative estimates, we consider the K-matrix method (a more detailed presentation of these computations will be given in [28]). Comparing the non-unitarized amplitudes with the unitarized ones, it results that they begin to differ from each other by about 20% (in units of (amplitude)^2) for $M_{VV} \sim$ 1.5-2 TeV. As we have skipped the Chiral expansion via a unitarization procedure we have no information about the scale that controls the range of validity of the unitarized amplitudes. It is expected the unitarized amplitudes to be reliable up to, at least, 2 TeV, although their validity is doubtful beyond $4\pi v \sim 3TeV$ (the scale that controls the original chiral expansion).

In table 4 the results after unitarization and for various upper cuts on M_{VV} (the invariant mass of the initial pair) of 2 TeV, 3 TeV and no cut, are presented. They include in addition the following cuts: a lower cut on M_{VV} of M_{VV} >1 TeV, cuts on the rapidity and transverse momentum of each final state bosons, $|y| < 2.5$, $p_T > 10$ GeV , and in the separation of the final state boson ,$\Delta R_{VV} > 0.7$. The results without unitarizing and without applying any upper cut on M_{VV} are also given (in parenthesis) for comparison. As it is clearly seen, the effects of unitarization are very important in the total number of events, meaning that one should only trust the results obtained after unitarization. In particular, the two first numbers of table 4, corresponding to a cut of $M_{VV} < 2TeV$ and 3TeV respectively, give the most realistic lower bound to the total number of expected events.

On the other hand, in order to have a detectable experimental signal with acceptable rates it is necessary to consider the hadronic decay channels of the LWB, and consequently the background from QCD needs to be computed. A large suppression of the QCD background relative to the signal is expected when a very stringent cut on the transverse momentum of the jets is applied. The jets coming from the signal have a very large p_T of $p_T \sim$ 0.5-1 TeV for the

[3]Notice that processes like $V_LV_L \to V_LV_LV_L$ are not allowed due to the symmetry breaking pattern assumed here, $SU(2)_L \times SU(2)_R \to SU(2)_V$.

LHC(SSC).

From this preliminary study we conclude that if there is a SISBS, about a total number of 100 $V_LV_LV_LV_L$ events will be produced at LHC. They will provide events with multiple jets with the particularity of having very high p_T. However, given the fact that this kind of SISBS probe relies on the spectroscopy of jets, it is still premature to conclude anything more precise until a more detailed analysis including the QCD background is done [28].

II.5. Conclusions

We have studied the V_LV_L scattering at LHC and SSC in the Chiral Lagrangian formalism that incorporates all the facts that are known about the symmetry breaking sector of the SM and has the appealing feature of treating the SISBS problem within a general framework (a feature always desirable given the controversial nature of the subject). It allows the simulation of different possible scenarios for the SISBS. We have studied in this report the phenomenological implications of three of them: Scaled-QCD, Technicolor and a Higgs-like scenario. This study was done in a systematic way for the three relevant channels: ZZ, $W^\pm Z$ and $W^\pm W^\pm$, and, in order to be conservative, we have considered just the leptonic decays of the gauge bosons.

Our main conclusions can be summarized as follows:
1.- If the SBS behaves at the TeV energy scale as the Higgs-like scenario or as the Standard Model with a heavy Higgs boson of $M_H = 1TeV$, it will be difficult to disentangle any signal from the background at LHC (and SSC). The most favourable channel is ZZ where a small enhancement in the O(1TeV) M_{ZZ} region of the spectrum of the gold plated events is found. The S/B ratios are always less than one and there is lack of statistics in the signal. The best ratio found is S/B = 33/75 and it corresponds to the highest integrated luminosity option for LHC of $L = 4 \times 10^5 pb^{-1}$.
2.- If the SBS behaves at the TeV energy scale as the Scaled-QCD or Technicolor scenarios, characterized by the existence of a ρ-like vector resonance, there are actual possibilities of observing the signal over the background in the $W^\pm Z$ channels. A clear resonance shape will show up in the M_{WZ} and p_T^Z spectra. If the highest luminosity option for LHC is achieved, masses up to $M_\rho \sim 2TeV$ will be tested. The WZ fusion mechanism contributes about 50% (70%) to the total signal at LHC (SSC) for $M_\rho = 2TeV$. It will provide by itself generic SISBS signals that involve just the interactions in the SBS and not the interactions of the SBS with the fermionic sector.

For ρ-like particles lighter than $2TeV$ ($1.5TeV$) the qq' annihilation mechanism where qq' annihilates into ρ via $\rho - W$ mixing starts being the dominant signal contribution at LHC (SSC). The rates computed with the VMD assumption show that there will be sizeable S/B ratios with also sizeable statistical significance (see table 2).
3.- No clear SISBS signal is found in the $W^\pm W^\pm$ channels for any of the three scenarios studied here. However, this channel offers itself as an ideal laboratory to search for new exotic resonances. Will LHC show up new unexpected physics in the Symmetry Breaking Sector of the SM?

Acknowledgments: We would like to thank S.Dimopoulos for encouragement and stimulating discussions. A.D and M.J.H thank T.Truong for providing them information about the unitarization procedures and for interesting discussions. M.J.H thanks M.K.Gaillard for reading a preliminary version of this work and for stimulating her interest for this subject.

References

[1] D.A.Dicus, V.Marthur, Phys.Rev. **D7**(1973)3111; J.M. Cornwall,D. N. Levin and G. Tiktopoulos, Phys. Rev. **D10** (1974)1145; B. W. Lee, C. Quigg and H. Thacker, Phys. Rev. **D16**(1977)1519; M. Veltman, Acta Phys. Pol. **B8**(1977)475; M. S. Chanowitz and M. K. Gaillard, Nucl. Phys. **B261**(1985)379.

[2] R.N.Cahn and S.Dawson, Phys.Lett.**136B**(1984)196; **138B**(E)(1984)464.

[3] For a recent review of the field and many further references see M. S. Chanowitz, Ann. Rev. Nucl. Part. Sci. **38**(1988)323.

[4] S. Weinberg, Physica **96 A**(1979)327;
J. Gasser and H. Leutwyler, Ann. of Phys. **158**(1984)142.

[5] A.Dobado and M.J. Herrero, Phys.Lett.**B228**(1989)495; **B233**(1989)505; J.F.Donoghue and C.Ramirez, Phys.Lett.**B234**(1990)361.

[6] T.N.Truong, Phys.Rev.Lett. **61**(1988)2526; A.Dobado, M.J.Herrero and T.N.Truong, Phys.Lett.**B235** (1990)129, and 134.

[7] A. Dobado, M.J. Herrero, J. Terron, CERN preprint CERN-TH.5670/90 to appear in Z.fur Phys. C (1990); A. Dobado, M.J. Herrero, J. Terron, CERN preprint CERN-TH.5813/90. Submitted to Z.fur Phys.C.

[8] G.Valencia and S.Dawson, preprint BNL-45194, to appear in Nucl.Phys.B(1990).

[9] S. Dawson, Nucl. Phys. **B249**(1985)42.

[10] M. Chanowitz, M. Golden and H. Georgi, Phys. Rev. **D36**(1987)1490.

[11] M.I.Josa, F.Pauss, T.Rodrigo. Contribution to these proceedings.

[12] E.Eichten et al., Rev.Mod.Phys.**56**(1984)579.

[13] E.Farhi and L.Susskind, Phys.Rep.**74**(1981)277; S.Dimopoulos, L.Susskind, Nucl.Phys. **B155**(1979)237.

[14] K.Kawarabayashy and M.Suzuki, Phys.Rev.**16B**(1966)225; Riazuddin and Fayazuddin, Phys.Rev.**147**(1966)1071.

[15] A. Dobado, M.J. Herrero, T.N. Truong, Phys.Lett. **B235** (1990) 129.

[16] S.Dawson, S.Willenbrock, Phys.Rev.**D40**(1989)2880; M.Veltman, F.J.Yndurain,Nucl. Phys.**B325** (1989) 1. A one loop computation of the logarithmic terms was previously done in an effective Lagrangian approach in: O.Cheyette, M.K.Gaillard, Phys.Lett. **B197** (1987) 205.

[17] The problem of unitarization in LWB scattering has been discussed recently by a number of authors: O.Cheyette, M.K.Galliard in [16]. D.A.Dicus and W.Repko, Phys. Lett. **B228** (1989) 503; S. Dawson, S. Willenbrock, Phys. Rev. Lett. **62** (1989) 1232; A.Dobado et al in [5], [6] and [7]; A.Dobado, Phys.Lett. **B237** (1990) 457; D.A. Dicus, W.W. Repko, preprint MSUTH 89/06; R.Rosenfeld, preprint EFI-89-54.

[18] A.Dobado et al. in [6].

[19] A.Dobado in [17]; S.Willenbrock, preprint BNL-44955 (1990).

[20] M.B. Einhorn, Nucl.Phys.**B246** (1984)75; R. Casalbuoni, R. Dominici, R. Gatto, Phys. Lett. **147B**(1984)419. See also, Lee et al. in [1].

[21] CDF collaboration, F.Abe et al., Phys.Rev.Lett.**64**(1990)142.

[22] R.Casalbuoni et al. Contribution to these proceedings.

[23] J.J. Sakurai, *Currents and Mesons*, University of Chicago Press,1969; R. Rosenfeld, J.L. Rosner Phys. Rev.**D38** (1988)1530; R.S. Chivukula, preprint BUHEP-88-16.

[24] B.Mele, Proceedings of the Workshop on Physics at Future Accelerators, La Thuile, CERN report 87-07, Vol.2, p.13 (1987).

[25] M.C. Bento, C.H. Llewellyn Smith, Nucl. Phys. **B289** (1987)36.

[26] V.Barger et al., preprint MAD-PH-556(1990); J.Terron, Doctoral Thesis (Univ. Autonoma de Madrid), unpublished.

[27] M.S.Chanowitz, M.K.Gaillard, Phys.Lett.**B142** (1984)85.

[28] A. Dobado, M.J. Herrero and J. Terron, in preparation.

Figure Captions

Fig. 1: ZZ-events distribution with respect to the invariant mass M_{ZZ} for SISBS signals at LHC. No leptonic BR has been included. The top mass value chosen is $m_t = 100GeV$. The LWB scattering amplitudes were unitarized with the Padé method. Solid histograms are the total rates, signal plus background. Dashed histograms are the background contribution alone. (a) Predictions for the Higgs-like scenario. (b) Predictions for the Scaled-QCD scenario.

Fig. 2: (a) WZ invariant mass distribution of the signal and background processes with the optimal cuts for the LHC (the 2.5 rapidity cut has been chosen). No leptonic BR has been included. The results for the Scaled-QCD and Technicolor scenarios are displayed: lower solid histogram represents WZ fusion signal process and dotted histogram represents qq' annihilation signal process. The total background is the dashed histogram and the total background plus total signal is the upper solid histogram. (b) Same for the SSC.

Fig. 3: (a) WZ invariant mass distribution for the WZ fusion signal process (solid histogram) and for the background processes (dashed histogram for qq', dotted histogram for γ W fusion and dash-dotted histogram for WZ fusion background process) of the Scaled-QCD scenario for the LHC (the 2.5 rapidity cut has been chosen). No leptonic BR has been included. (b) Same for the SSC.

Fig. 4: Like-sign WW invariant mass distribution for the various SISBS scenarios and for the total background. Rates are for $W^+W^+ + W^-W^-$. No leptonic BR has been included. The short-dashed line is for the Scaled-QCD scenario and the lower solid

line is for the Higgs-like scenario. The upper solid curve corresponds to the unitarized Low Energy Theorems results taken from [26]. The SM rates for $M_H = 1TeV$ (SMH) are also shown for comparison (dot-dashed line). The long dashed lines are the results for the total background taken from [26]. The upper line is for $m_t = 100GeV$. The lower line is for $m_t = 200GeV$.

Table Captions

Table 1: ZZ channel: Number of $l^+l^-l^+l^-$ events for SISBS signals in two scenarios, and for the total background. Rates are presented in the form of S/B-ratios for both LHC and SSC. Two different rapidity cuts and two values of the top quark mass were chosen. The numbers in parenthesis are the optimal cuts.

Table 2: WZ channel: Number of $l^+\nu l^+l^- + l^-\nu l^+l^-$ events for the total SISBS signal in various scenarios and for the total background at LHC and SSC. Rates are presented in the form of S/B-ratios. The rates for both processes contributing to the signal in Scaled-QCD and Technicolor scenarios: WZ-fusion (WZ) and qq' annihilation (qq') are also shown separately for comparison. The optimal cuts are shown in parenthesis.

Table 3: W^+W^+ channel: Number of $l^+\nu l^+\nu$ events for SISBS signals in various scenarios at LHC and SSC. Rates are presented in the form of S/B-ratios.

Table 4: $V_LV_LV_LV_L$ channels: Partial and total SISBS signal rates. The results are after unitarization and for $M_{VV} < 2TeV, 3TeV$ and *no* M_{VV} cut respectively. In parenthesis the non-unitarized results without any upper cut on M_{VV} are shown for comparison.

Table 1:

Scenario	LHC (1.5) $m_t = 100GeV$	LHC (2.5) $m_t = 100GeV$	SSC (1.5) $m_t = 100GeV$	SSC (2.5) $m_t = 100GeV$
HIGGS	27/48 (300,750)	33/75 (300,750)	5/6 (240,750)	8/11 (240,750)
QCD	9/36 (360,750)	15/90 (300,700)	2/3 (360,800)	3/6 (360,800)
	LHC (1.5) $m_t = 180GeV$	LHC (2.5) $m_t = 180GeV$	SSC (1.5) $m_t = 180GeV$	SSC (2.5) $m_t = 180GeV$
HIGGS	25/57 (300,750)	39/111 (240,750)	5/8 (240,750)	8/14 (240,750)
QCD	12/69 (300,700)	15/102 (300,700)	2/6 (300,800)	3/12 (300,750)

Table 2:

Scenario	LHC (1.5)	LHC (2.5)	SSC (1.5)	SSC (2.5)
TECHN 1.0	1713/71 161 (WZ) 1552 $(q\bar{q}')$ (10)	2628/213 318 (WZ) 2310 $(q\bar{q}')$ (180)	142/7 26 (WZ) 116 $(q\bar{q}')$ (10)	263/24 59 (WZ) 204 $(q\bar{q}')$ (180)
TECHN 1.5	136/16 33 (WZ) 103 $(q\bar{q}')$ (360)	197/43 59 (WZ) 138 $(q\bar{q}')$ (300)	18/2 8 (WZ) 10 $(q\bar{q}')$ (300)	33/6 17 (WZ) 16 $(q\bar{q}')$ (300)
QCD 2.0	53/25 23 (WZ) 30 $(q\bar{q}')$ (480)	65/31 29 (WZ) 36 $(q\bar{q}')$ (540)	11/4 7 (WZ) 4 $(q\bar{q}')$ (480)	21/12 15 (WZ) 6 $(q\bar{q}')$ (420)
HIGGS	20/434 (300,500)	27/786 (300,500)	3/17 (420,500)	5/34 (420,500)
SMH	29/907 (240,500)	39/1744 (240,500)	5/87 (240,500)	7/196 (240,500)

Table 3:

$m_t = 100GeV$	LHC (1.5)			SSC (1.5)		
Scenario	$M_{WW} > 0.8TeV$	1.0TeV	1.2TeV	$M_{WW} > 0.8TeV$	1.0TeV	1.2TeV
QCD	32/212	20/96	12/150	8/26	5/14	4/8
HIGGS	22/212	13/96	7/50	5/26	3/14	2/8
SMH	30/212	16/96	9/50	6/26	4/14	2/8
$m_t = 200GeV$	LHC (1.5)			SSC (1.5)		
Scenario	$M_{WW} > 0.8TeV$	1.0TeV	1.2TeV	$M_{WW} > 0.8TeV$	1.0TeV	1.2TeV
QCD	32/154	20/71	12/38	8/21	5/11	4/7
HIGGS	22/154	13/71	7/38	5/21	3/11	2/7
SMH	30/154	16/71	9/38	6/21	4/11	2/7

Table 4:

Channel	LHC	SSC
$W^+W^- \to W^+W^-W^+W^-$	7-17-25 (54)	3-9-78 (331)
$W^+W^- \to W^+W^-Z^0Z^0$	6-9-12 (56)	3-14-24 (347)
$W^+W^- \to Z^0Z^0Z^0Z^0$	5-7-7 (59)	2-3-3 (366)
$Z^0Z^0 \to W^+W^-W^+W^-$	6-8-8 (69)	2-3-4 (430)
$Z^0Z^0 \to W^+W^-Z^0Z^0$	2-4-5 (18)	1-2-6 (111)
$Z^0Z^0 \to Z^0Z^0Z^0Z^0$	2-4-6 (0)	1-2-6 (0)
$W^+Z^0 \to W^+Z^0W^+W^-$	7-16-22 (57)	2-6-27 (356)
$W^-Z^0 \to W^-Z^0W^+W^-$	3-7-9 (19)	1-3-12 (116)
$W^+Z^0 \to W^+Z^0Z^0Z^0$	5-11-15 (37)	2-6-17 (229)
$W^-Z^0 \to W^-Z^0Z^0Z^0$	2-4-6 (13)	1-2-7 (79)
$W^+W^+ \to W^+W^+W^+W^-$	11-25-34 (108)	3-9-27 (665)
$W^-W^- \to W^-W^-W^+W^-$	2-4-5 (12)	1-2-4 (78)
$W^+W^+ \to W^+W^+Z^0Z^0$	3-7-9 (27)	1-2-12 (168)
$W^-W^- \to W^-W^-Z^0Z^0$	1-1-1 (3)	0-0-2 (19)
Total	62-124-164 (532)	23-63-229 (3295)

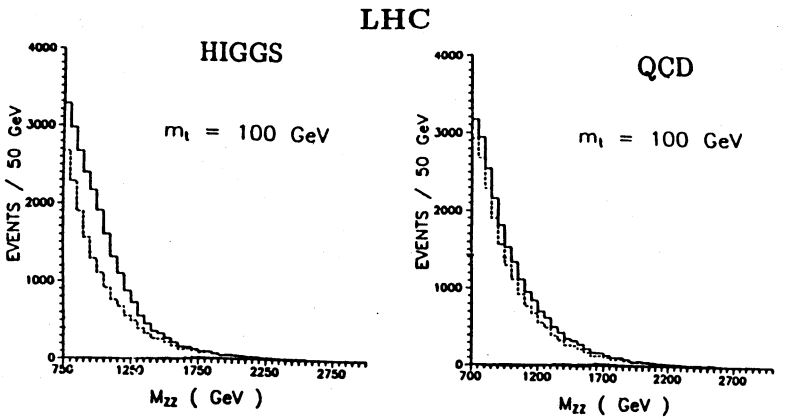

Figure 1

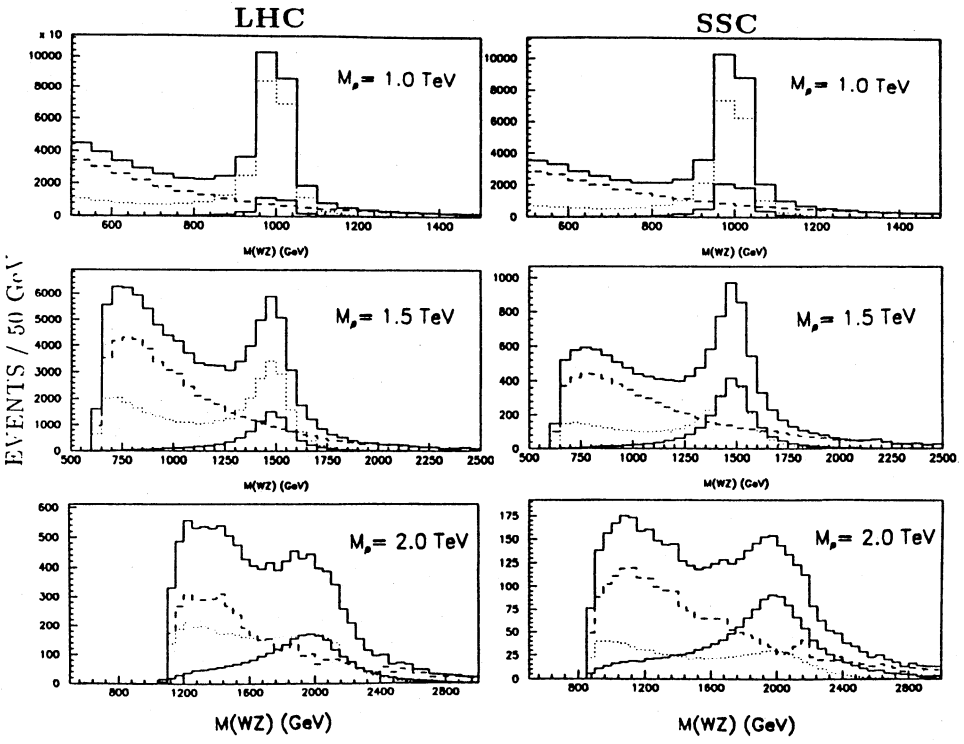

Figure 2

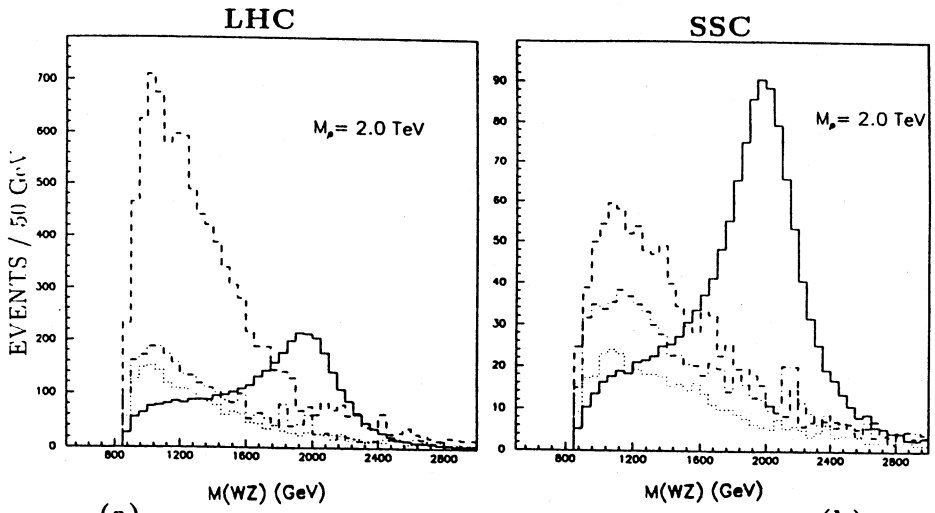

Figure 3

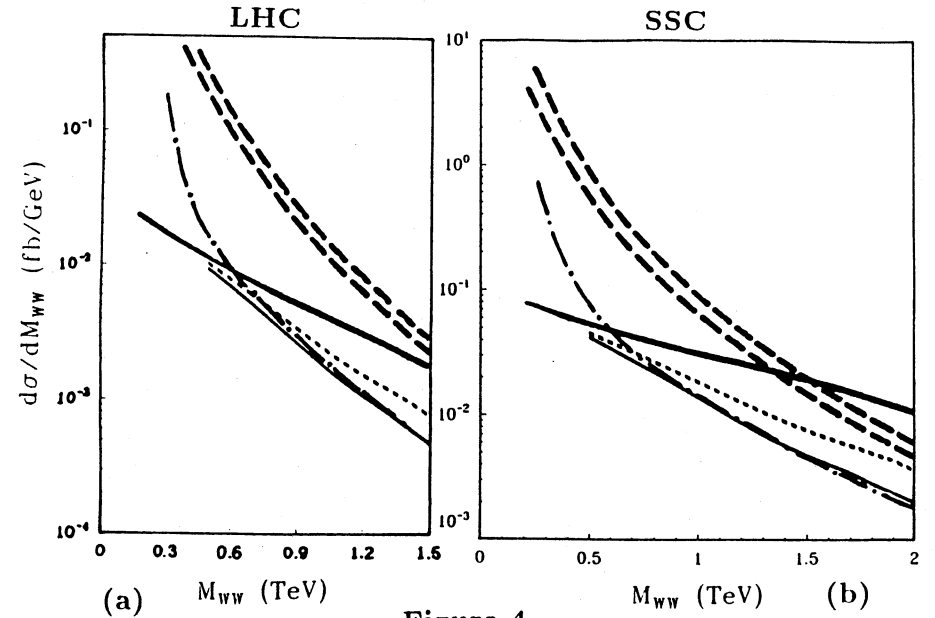

Figure 4

III. WZ PRODUCTION FROM THE BESS MODEL

Contributors: R.Casalbuoni, P.Chiappetta, S.De Curtis, F.Feruglio, R.Gatto, B.Mele and J.Terron

III.1. Introduction

In this report we shall examine the capability of LHC [1] to explore a possible strong sector responsible for electroweak symmetry breaking. A comparison with SSC [2] will also be made.

Our analysis will be carried out within the BESS model (BESS standing for Breaking Electroweak Symmetry Strongly) [3]. The BESS model is at the same time very simple and it hopefully contains the most relevant elements of a possible strong electroweak breaking. The model has no Higgs particle. In addition to W and Z it contains a triplet of new massive vector bosons V. In BESS the electroweak symmetry breaking is described in a non-linear way. A local "hidden" $SU(2)$ symmetry is implicit in the description and the bosons V are indeed the associated gauge bosons. It is explicitly assumed that they constitute effective dynamical degrees of freedom. The bosons V mix with W and Z. The existing data of CDF/UA2 [4] and of LEP [5] already imply certain restrictions on BESS parameters. To remain on the safe, we shall take into account not only these restrictions, but also possible stronger restrictions from future LEP data, assuming no deviations will be observed from the standard model within the foreseen experimental precision [6].

III.2. The BESS model

The vector resonances of the BESS model are bound states of a strongly interacting sector. In this sense they are similar to ordinary ρ vector mesons, or to the techni-ρ particle of technicolor theories [7]. Due to their composite nature, the V particles are then expected to mix with the photon and with the W and Z vector bosons. From this, a non trivial behaviour under the electromagnetic gauge group $U(1)_{em}$ is expected (see ref. [8]). Using this fact and the requirement that the electroweak ρ-parameter be equal to 1 at tree level, one can easily construct the most general mixing term of the V-particles with the ordinary vector bosons. By defining

$$\mathcal{V}_\mu = \sum_{i=1}^{3} ig'' \frac{\tau^i}{2} \tilde{V}^i_\mu, \quad \mathcal{W}_\mu = \sum_{i=1}^{3} ig \frac{\tau_i}{2} \tilde{W}^i_\mu, \quad \mathcal{B}_\mu = ig' \frac{\tau_3}{2} \tilde{B}_\mu \tag{1}$$

one has

$$\mathcal{L}_M = -\frac{v^2}{4} \left[\mathrm{tr}(\mathcal{W} - \mathcal{B})^2 + \alpha \mathrm{tr}(\mathcal{W} + \mathcal{B} - 2\mathcal{V})^2 \right] \tag{2}$$

where v and α are free parameters. The first term is nothing but the usual mass term for the Weinberg-Salam fields, whereas the second one is the only mixing term compatible with the properties we have just discussed. The Lagrangian (2) must then be supplemented by kinetic Yang-Mills terms for all the three vector boson fields, with a gauge coupling g'' for the field $\vec{V}$. As far as the interactions with fermions are concerned, one must specify the current $\vec{J}$ to which the new triplet of states $\vec{V}$ couples. If we assume $\vec{J} = \vec{J}_L$ (see ref. [3] for a more general discussion), the $U(1)_{em}$ gauge invariance requires the interaction Lagrangian to be

$$\mathcal{L} = \frac{g}{1+b} \vec{W} \cdot \vec{J}_L + g' \tilde{B} J_Y + \frac{1}{2} \frac{b}{1+b} g'' \vec{V} \cdot \vec{J}_L \tag{3}$$

The parameter b specifies a possible direct coupling of the fermions to the new gauge vector bosons. However, it must be stressed that also when $b = 0$ a coupling of the physical V-particles to fermions is present due to their mixing with the physical Weinberg-Salam vector bosons. At the zeroth order in the weak couplings the V mesons are degenerate in mass and

$$M_V^2 = \frac{1}{4} v^2 \alpha g''^2 \tag{4}$$

The complete list of couplings to fermions can be found in refs. [3,6]. Here we will only be concerned with the couplings to the charged currents:

$$(h_W W_\mu^i + h_V V_\mu^i) T_L^i, \quad i = 1,2 \tag{5}$$

where the coupling of $V^\pm$ is given by

$$h_V = \frac{1}{1+b}\left(g \sin\varphi + \frac{1}{2} g'' b \cos\varphi\right) \tag{6}$$

The parameter space of the model is given by (g, g', v, M_V, g'', b). We trade off (g, g', v) for (α_{em}, G_F, M_Z) and therefore we remain with (M_V, g'', b). In turn, the parameter v can be reexpressed in terms of M_W, and the expressions of (g, g', M_W) in terms of (α_{em}, G_F, M_Z) can be found in ref. [6]. In order to get the physical region for the parameters (M_V, g'', b) we have considered the envelope of the 90% C.L. curves obtained from the observables related to the Z-line shape measured at LEP1, and from the ratio M_W/M_Z measured at CDF and UA2. The most restrictive observables turn out to be Γ_{had}, Γ_Z and M_W/M_Z. The experimental values we have used come from the LEP1 combined data [5], $\Gamma_h(MeV) = 1764 \pm 16$, $\Gamma_Z(MeV) = 2496 \pm 16$, and from the CDF and UA2 combined data [4], $(M_W/M_Z)^2 = 0.773 \pm 0.006$. As an example we give in Fig. 1 the allowed region in the plane $(b, g/g'')$ for $M_V = 1500\ GeV$. We have taken $m_{top} = 150\ GeV$ and $\alpha_s = 0.12$. For increasing m_{top} and/or M_V the area of the allowed region has only a small increase. Notice that the origin of the plane (standard model limit) lies inside the allowed region.

III.3. Gauge boson pair production in the BESS model

At hadron colliders, as far as detection of a signal from a strongly interacting symmetry breaking sector is concerned, vector boson pair production is particularly relevant. In the BESS model there are two main mechanisms which compete for the production of a pair of ordinary gauge vector bosons at a pp collider: $q\bar{q}$ annihilation, and WW (WZ, ZZ) fusion.

In the first mechanism a quark-antiquark pair annihilates into a V vector boson, which in turn decays into a pair of ordinary gauge vector bosons. We stress the fact that this process is always operating in BESS independently of the existence of a direct coupling of V to fermions. In fact, the mixing of V with W and Z always induces a well determined coupling of order g/g'' between the mass eigenstates V and the fermions, even if the original, unmixed, states $\tilde{V}$ were not coupled to matter. We further observe that, at least in the range of masses for V we are interested in (few TeVs), the decay of V's is dominated by the WW, WZ channels, due to the large coupling, (of order $\alpha g''$), for $V^0 W_L^+ W_L^-$ and $V^\pm W_L^\mp Z_L$ (L stands for the longitudinal components). On this basis we expect (and we shall verify quantitatively) that, even in the case $b = 0$, the $q\bar{q}$ mechanism remains efficient in producing a W/Z pair. We have evaluated the $q\bar{q}$ contribution in the context of the parton model along the lines described in ref. [6], and the relevant expressions are given in ref. [9].

Another mechanism to produce W/Z pairs is the rescattering of a pair of ordinary gauge vector bosons, each being initially emitted from a quark or antiquark leg. In the so–called effective-W approximation the initial W/Z's are assumed to be real and the cross section for producing a W/Z pair is obtained by a double convolution of the cross section for the rescattering (or fusion) process with the luminosities of the initial W/Z's inside the quarks and the structure functions of the quarks inside the proton [10]. The relevance of this mechanism is then related to the strength of the fusion process. In the standard model of electroweak interactions such a fusion process is expected to be weak. The potentially large amplitudes, those among the longitudinally polarized W/Z's, are in fact asymptotically constant (for large energy), once the whole set of lowest order diagrams is taken into account. However such a constant depends on the Higgs mass m_H and for a sufficiently large value of m_H the asymptotic value of the amplitude violates the perturbative unitarity requirement. The speculations on a possible strongly interacting regime for the standard model [11,3] are based on this observation. In BESS the rescattering process is naturally strong. In fact the scattering of two longitudinally polarized W/Z's proceeds via the exchange of a V vector boson with large couplings (of order $\alpha g''$) at each vertex. If some W/Z's is taken to be transverse, the corresponding amplitude is strongly depressed and will be neglected in our analysis. We have computed the scattering amplitudes among longitudinal W/Z's in BESS, by making use of the equivalence theorem [12]. Such amplitudes approach the ones among the corresponding Goldstone bosons as the value of the energy increases, the difference being of order $(M/\sqrt{s})$ ($M = M_W$ or M_Z), or, in other words, they verify the low-energy theorems [13]. The full expressions for the corresponding amplitudes can be found in ref. [9]. Here we will give only the expression for the width of the V particle

$$\Gamma_V = \frac{G_F^2}{24\pi} \frac{M_V^5}{g''^2} \tag{7}$$

which is valid in the limit $M_V \gg M_W, M_Z$, and where we have neglected the fermionic decays.

III.4. Discussion of the results

In hadronic collisions the $pp \to W^\pm Z + X$ reaction appears to be the most interesting one in the framework of the BESS model. The process $pp \to W^+W^- + X$ is expected to suffer from a very severe background coming from $pp \to t\bar{t} + X$, with t and $\bar{t}$ both decaying into W, which should be the dominant mode for $m_{top} > M_W$. Final leptonic configurations from $t\bar{t}$ production might also simulate configurations from $W^\pm Z$, but the Z mass reconstruction should protect the signal from such a background. The ZZ mode has not been considered because it does not proceed via an s-channel contribution in BESS.

Comparing the two channels W^+Z and W^-Z, we find that W^-Z is roughly one half of the W^+Z. Finally we remark that the final states observed at LHC and SSC will be demanded to contain leptons. Our results will be given in terms of numbers of produced $W^\pm Z$ pairs. For both bosons decaying leptonically one has to multiply by the branching factor $B(Z \to \ell^+\ell^-) \cdot B(W^\pm \to \ell^\pm \bar{\nu}_\ell) \approx 1.5\%$, for $(\ell = e, \mu)$.

The relevant backgrounds are the standard model production of $W^\pm Z$ through quark-antiquark annihilation [14], $\gamma W^\pm$ fusion [15], and $W_T^\pm Z_T$ fusion. In our calculation we have

made use of the DFLM structure functions [16], for $\Lambda_{QCD} = 260\ MeV$. We have also run the computer programs by using the EHLQ1 structure functions [17] obtaining very similar results (actually the DFLM structure functions give a number of events which is about 6-8% lower than for EHLQ1). In the case of the fusion process, we have used a value of Q^2 inside the structure functions equal to the square of the invariant mass of the produced gauge boson pair. The K-factor coming from soft gluon resummation is not known for all the processes considered here, and we have decided not to introduce it. As a consequence the number of events we have evaluated is probably underestimated by about 20-30% (in fact, where the K-factor is known, as in the case of the V-production through $q\bar{q}$ [18], it has a value of about 1.3).

Our results were obtained through a Monte Carlo simulation which allowed to study the details of the various final state distributions. They are summarized in Tables 1-2. Tables 1 and 2 refer to the process $W^+Z + W^-Z$ at LHC and at SSC respectively. The assumed energy parameters for LHC and SSC are 16 TeV and 40 TeV respectively. The luminosities we have assumed are $10^{34}\ cm^{-2}\ sec^{-1}$ for LHC, and $10^{33}\ cm^{-2}\ sec^{-1}$ for SSC, and all the numbers refer to one effective year $= 10^7\ sec$ of running of the colliders. In the Tables we have considered a very extensive choice of parameters. A first cut on the rapidity $y_{W,Z}$ of the final W and Z, $|y_{W,Z}| \leq 2.5$ was applied to all cases. Then we applied a lower cut in M_{WZ} (the invariant mass of the WZ-pair), approximately corresponding to the beginning of the resonance at the left of the peak. An upper cut has been fixed once for all at $M_{WZ} = 3\ TeV$, where in all the practical cases considered here the resonance tail is already extinguished. Finally a cut in p_T (the transverse momentum of the Z) has been obtained from the requirement of maximizing the statistical significance of the signal, $S/(S+B)^{1/2}$, S being the signal and B the background, which in our case includes the continuum standard WZ-pair production both from $q\bar{q}$ annihilation and γW fusion.

For a better understanding of the results we have exhibited in Tables 1 and 2 the different contributions, fusion and $q\bar{q}$ annihilation, to the signal. We have also given the number of events from the background and the total number of events. The range of M_V values we have explored runs from 1 TeV up to 2.5 TeV. The last value can be probably considered as a limiting value for discovery at both machines. About this point notice that in order to have a decent number of events at LHC, say more than 10 leptonic events/year and a good statistical significance $S/\sqrt{B}$, for $M_V = 2500\ GeV$, one have to run LHC at a luminosity of about $3.5 \times 10^{34}\ cm^{-2}\ sec^{-1}$ at least, for $b \approx 0$.

The values chosen for g'' and b are well inside the region allowed from LEP1, and CDF/UA2 data (see Fig. 1). Furthermore (see ref. [6]) they will be inside the allowed region also after precision measurements of forward-backward asymmetry and of tau-polarization will be made at LEP1, if we make the hypothesis that no deviation from the SM is observed within the expected experimental precision. For instance, from ref. [6] in the more restrictive case of $M_V = 250\ GeV$ one gets $g/g'' < 0.1$ at $b = 0$ both from A_{FB} and from A_τ. For the values of g'' that we have considered, one has a width for the V (see eq. (7)) of 11 GeV for $M_V = 1000\ GeV$, 84 GeV for $M_V = 1500\ GeV$, whereas we have $\Gamma_V = 353\ GeV$ for $M_V = 2000\ GeV$ (notice that this case corresponds almost exactly to a techni-ρ obtained by scaling from QCD), and $\Gamma_V = 455\ GeV$ for $M_V = 2500\ GeV$. For smaller g'' the resonance becomes broader. In the computation of Γ_V we have ignored the contribution from the fermionic channels because it turns out to be completely negligible. Notice that the $b = 0$ case corresponds, in practice, to the most pessimistic situation, since in general allowing for a direct coupling ($b \neq 0$) a much larger signal from production via $q\bar{q}$ annihilation is predicted. Direct couplings of techni-ρ to fermions emerge in extended technicolor theories (for calculations at SSC energies see ref. [19]).

Table 1 : Events per year in $pp \to (W^+Z + W^-Z) + X$ at LHC from BESS.

(M_V, g'', b)	$(p_T)_c$	$(M_{WZ})_c$	Fusion	$q\bar{q}$	Signal	Backgr.	Total
(1000,13,0)	360	850	858	10089	10947	4786	15733
(1500,13,0)	480	1250	498	1929	2427	1121	3548
(2000,13,.02)	540	1400	339	3863	4202	608	4810
(2000,13,0)	600	1600	241	443	684	310	994
(2000,13,-.01)	540	1400	339	4186	4525	608	5133
(2500,20,0)	600	1400	212	57	269	430	699
(2500,20,-.01)	600	1800	141	1807	1498	211	2159

Table 2 : Events per year in $pp \to (W^+Z + W^-Z) + X$ at SSC from BESS.

(M_V, g'', b)	$(p_T)_c$	$(M_{WZ})_c$	Fusion	$q\bar{q}$	Signal	Backgr.	Total
(1000,13,0)	300	800	1280	3969	5249	3963	9212
(1500,13,0)	420	1250	895	1030	1925	1063	2988
(2000,13,.02)	480	1600	671	2814	3485	462	3947
(2000,13,0)	480	1600	671	339	1010	462	1472
(2000,13,-.01)	480	1400	772	3119	3891	636	4527
(2500,20,0)	540	1500	486	54	540	428	968
(2500,20,-.01)	600	1800	360	1721	2081	211	2292

From the Tables we see that the fusion signal increases going from LHC to SSC, whereas the signal from $q\bar{q}$ decreases (of course the decreasing in the luminosity by a factor 10 has to be considered). This is expected on the basis of the different ratio of LHC and SSC values for $q\bar{q}$ and W_LW_L luminosities [20]. In particular, for $b = 0$, at LHC the $q\bar{q}$ annihilation dominates for low V masses up to $M_V = 2\ TeV$, whereas at SSC the two mechanisms are already comparable at $M_V = 1500\ GeV$. However for $b < 0$ the situation changes and, increasing $|b|$, the $q\bar{q}$ annihilation will overcome again the fusion contribution.

We have also made an extensive study of the $(p_T)_Z$ and M_{WZ} distributions. Here we give examples in Figs. 2-9 of the two distributions both at LHC (Figs. 2, 3, 4 and 5) and SSC (Figs. 6, 7, 8 and 9) in the case of $M_V = 1500\ GeV$, $g'' = 13$, $b = 0$ and $M_V = 2000\ GeV$, $g'' = 13$, $b = 0$ (for a case with $b \neq 0$, see ref. [21] in this volume).

The figures show that, even after multiplying by the branching factor corresponding to selecting only leptonic decays of W and Z, one is left with a statistically significant signal having quite well distinguished features both in M_{WZ} and $(p_T)_Z$ distributions. The vertical lines in the graphs indicate where the lower cuts in M_{WZ} and p_T have been put for the illustrated cases (see corresponding entries in Tables 1-2). We emphasize that the statistical significance of the signal versus the background is very good practically in all the cases we have considered in this note.

III.5. Conclusions

We have studied WZ pair production at LHC and SSC within the BESS model, which is simple and probably contains the dominant features of a strong electroweak breaking. To extrapolate to

possible future scenarios, we have restricted the BESS parameters below the expected limitations from future LEP data, assuming these turn out not to deviate, within the expected precision, from the standard model prediction. The new conclusion of our work is the generally dominant role, particularly at LHC, of production through $q\bar{q}$ annihilation, as compared to the extensively studied boson pair fusion mechanism. The increase of gauge boson pairs, resulting from the $q\bar{q}$ mechanism, as expected in the BESS model, together with its distinguished features in the p_T and invariant mass distributions, suggests an important role of LHC and SSC in the exploration of a possible strong electroweak symmetry breaking sector.

Figure Captions

Fig. 1 - Allowed region (90% C.L.) in the $(b, g/g'')$ plane for $M_V = 1500\ GeV$, $m_{top} = 150\ GeV$ and $\alpha_s = 0.12$, from M_W/M_Z (continuous line), Γ_Z (dashed line) and Γ_{had} (dashed-dotted line). The origin (corresponding to the standard model limit) is inside the allowed region.

Fig. 2 - Invariant mass distribution of the $W^+Z + W^-Z$ pairs produced per year (1 year = $10^7\ sec$) at LHC for $M_V = 1500\ GeV$, $g'' = 13$ and $b = 0$, with a luminosity of $10^{34}\ cm^{-2}\ sec^{-1}$. The applied cuts are: $|y_{W,Z}| < 2.5$, $(p_T)_Z > 480\ GeV$ and $M_{WZ} > 1250\ GeV$. The lower, intermediate and higher histograms refer to the background, background plus fusion signal and background plus fusion signal plus $q\bar{q}$ annihilation signal, respectively.

Fig. 3 - $(p_T)_Z$ distribution from the $W^+Z + W^-Z$ pairs produced per year at LHC for $M_V = 1500\ GeV$, $g'' = 13$ and $b = 0$, for a luminosity of $10^{34}\ cm^{-2}\ sec^{-1}$. The applied cuts are: $|y_{W,Z}| < 2.5$, $(p_T)_Z > 480\ GeV$ and $M_{WZ} > 1250\ GeV$. The lower, intermediate and higher histograms refer to the background, background plus fusion signal and background plus fusion signal plus $q\bar{q}$ annihilation signal, respectively.

Fig. 4 - Invariant mass distribution of the $W^+Z + W^-Z$ pairs produced per year at SSC for $M_V = 1500\ GeV$, $g'' = 13$ and $b = 0$, for a luminosity of $10^{33}\ cm^{-2}\ sec^{-1}$. The applied cuts are: $|y_{W,Z}| < 2.5$, $(p_T)_Z > 420\ GeV$ and $M_{WZ} > 1250\ GeV$. The lower, intermediate and higher histograms refer to the background, background plus fusion signal and background plus fusion signal plus $q\bar{q}$ annihilation signal, respectively.

Fig. 5 - $(p_T)_Z$ distribution from the $W^+Z + W^-Z$ pairs produced per year at SSC for $M_V = 1500\ GeV$, $g'' = 13$ and $b = 0$, for a luminosity of $10^{33}\ cm^{-2}\ sec^{-1}$. The applied cuts are: $|y_{W,Z}| < 2.5$, $(p_T)_Z > 420\ GeV$ and $M_{WZ} > 1250\ GeV$. The lower, intermediate and higher histograms refer to the background, background plus fusion signal and background plus fusion signal plus $q\bar{q}$ annihilation signal, respectively.

Fig. 6 - Invariant mass distribution of the $W^+Z + W^-Z$ pairs produced per year at LHC for $M_V = 2000\ GeV$, $g'' = 13$ and $b = 0$, with a luminosity of $10^{34}\ cm^{-2}\ sec^{-1}$. The applied cuts are: $|y_{W,Z}| < 2.5$, $(p_T)_Z > 600\ GeV$ and $M_{WZ} > 1600\ GeV$. The lower, intermediate and higher histograms refer to the background, background plus fusion signal and background plus fusion signal plus $q\bar{q}$ annihilation signal, respectively.

Fig. 7 - $(p_T)_Z$ distribution from the $W^+Z + W^-Z$ pairs produced per year at LHC for $M_V = 2000\ GeV$, $g'' = 13$ and $b = 0$, for a luminosity of $10^{34}\ cm^{-2}\ sec^{-1}$. The applied cuts are: $|y_{W,Z}| < 2.5$, $(p_T)_Z > 600\ GeV$ and $M_{WZ} > 1600\ GeV$. The lower, intermediate and higher histograms refer to the background, background plus fusion signal and background plus fusion signal plus $q\bar{q}$ annihilation signal, respectively.

Fig. 8 - Invariant mass distribution of the $W^+Z + W^-Z$ pairs produced per year at SSC for $M_V = 2000\ GeV$, $g'' = 13$ and $b = 0$, for a luminosity of $10^{33}\ cm^{-2}\ sec^{-1}$. The applied cuts are:

$|y_{W,Z}| < 2.5$, $(p_T)_Z > 480\ GeV$ and $M_{WZ} > 1600\ GeV$. The lower, intermediate and higher histograms refer to the background, background plus fusion signal and background plus fusion signal plus $q\bar{q}$ annihilation signal, respectively.

Fig. 9 - $(p_T)_Z$ distribution from the $W^+Z + W^-Z$ pairs produced per year at SSC for $M_V = 2000\ GeV$, $g'' = 13$ and $b = 0$, for a luminosity of $10^{33}\ cm^{-2}\ sec^{-1}$. The applied cuts are: $|y_{W,Z}| < 2.5$, $(p_T)_Z > 480\ GeV$ and $M_{WZ} > 1600\ GeV$. The lower, intermediate and higher histograms refer to the background, background plus fusion signal and background plus fusion signal plus $q\bar{q}$ annihilation signal, respectively.

References

[1] C. Rubbia, seminar given at CERN on November 2, 1989; "Large Hadron Collider in the LEP Tunnel", ed. G. Brianti et al., CERN 84/10.

[2] "Superconducting Super Collider Conceptual Design", Central Design Group, SSC Report SR-2020, March 1986.

[3] R. Casalbuoni, S. De Curtis, D. Dominici and R. Gatto, Phys. Lett. **B155** (1985) 95; Nucl. Phys. **B282** (1987) 235.

[4] L. Pondrom, Summary Talk presented at the Singapore Conference, Singapore, August 1990.

[5] F. Dydak, Summary Talk presented at the Singapore Conference, Singapore, August 1990.

[6] R. Casalbuoni, P. Chiappetta, D. Dominici, F. Feruglio and R. Gatto, Nucl. Phys. **B310** (1988) 181.

[7] S. Weinberg, Phys. Rev. **D 13** (1976) 974; **D 20** (1979) 1277; L. Susskind, Phys. Rev. **D 20** (1979) 2619; for extended technicolor, see: S. Dimopoulos and L. Susskind, Nucl. Phys. **B155** (1979) 237. See also the review by E. Fahri and L. Susskind, Phys. Rep. **74** (1981) 277.

[8] G. Altarelli, R. Casalbuoni, D. Dominici, F. Feruglio and R. Gatto, Nucl. Phys. **B342** (1990) 15.

[9] R. Casalbuoni, P. Chiappetta, S. De Curtis, F. Feruglio, R. Gatto, B. Mele and J. Terron, Phys. Lett. **B249** (1990) 130.

[10] S. Dawson, Nucl. Phys. **B249** (1985) 42. G.L. Kane, W.W. Repko and W.B. Rolnick, Phys. Lett. **148B** (1985) 367; M.S. Chanowitz and M.K. Gaillard, Phys. Lett. **142B** (1984) 85.

[11] M. Veltman, Acta Phys. Polon. **B8** (1977) 475; B.W. Lee, C. Quigg and H.B. Thacker, Phys. Rev. **D 16** (1977) 1519; see also the review by M.S. Chanowitz, Ann. Rev. Nucl. Part. Sc. **38** (1988) 363.

[12] J.M. Cornwall, D.N. Levin and G. Tiktopoulos, Phys. Rev. **D 10** (1974) 1145. C.G. Vayonakis, Lett. N. Cimento **17** (1976) 17; M.S. Chanowitz and M.K. Gaillard, Nucl. Phys. **B261** (1985) 379; G.J. Gounaris, R. Kögerler and H. Neufeld, Phys. Rev. **D 34** (1986) 3257.

13] S. Weinberg, Physica **96A** (1979) 327; M.S. Chanowitz, M. Golden and H. Georgi, Phys. Rev. **D 36** (1987) 1490; Phys. Rev. Lett. **57** (1986) 2344.

[14] R.W. Brown, D. Sahdev and K.O. Mikaelian, Phys. Rev. **D 20** (1979) 1164; K.O. Mikaelian, M.A. Samuel and D. Sahdev, Phys. Rev. Lett. **43** (1979) 746.

[15] B. Mele, Proceedings of the Workshop on Physics at Future Accelerators, La Thuile and Geneva, ed. J.H. Mulvay, CERN report 87-07, vol. 2, p. 13, Geneva (1987)

[16] M. Diemoz, F. Ferroni, E. Longo and G. Martinelli, Z. Phys **C39** (1988) 21.

[17] E. Eichten, I. Hinchliffe, K. Lane and C. Quigg, Rev. Mod. Phys. **56** (1984).

[18] P. Chiappetta, T. Grandou, M. Le Bellac and J.L. Meunier, Nucl. Phys. **B207** (1982) 251.

[19] R.S. Chivukula, Proc. of the 12th Johns Hopkins Workshop, Baltimore June 1988, eds. G. Domokos and S. Kövesi-Domokos, World Scientific, Singapore (1988).

[20] Z. Kunszt, Proceedings of the Workshop on Physics at Future Accelerators, La Thuile and Geneva, ed. J.H. Mulvay, CERN report 87-07, vol. 1, p. 123, Geneva (1987).

[21] R. Casalbuoni, P. Chiappetta, M.C. Cousinou, S. De Curtis, F. Feruglio and R. Gatto, preprint CPT-90/P.2429 and UGVA/DPT 1990-08-690.

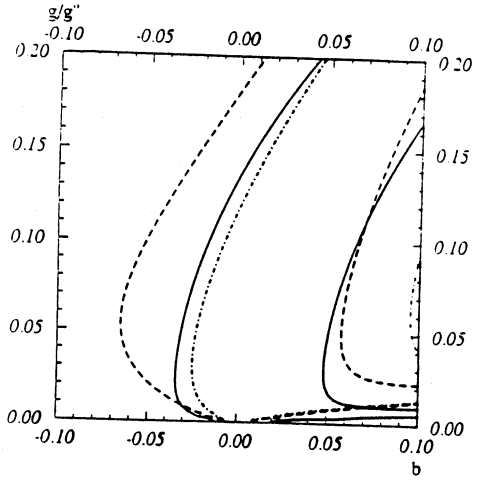

Fig. 1

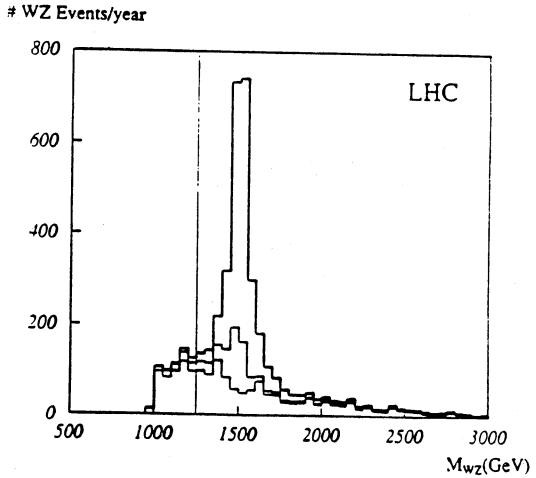

Fig. 2

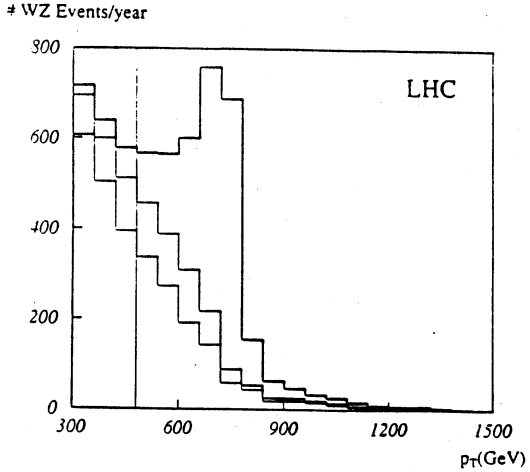

Fig. 3

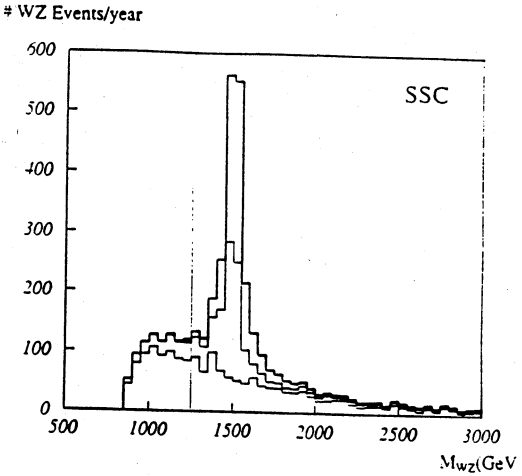

Fig. 4

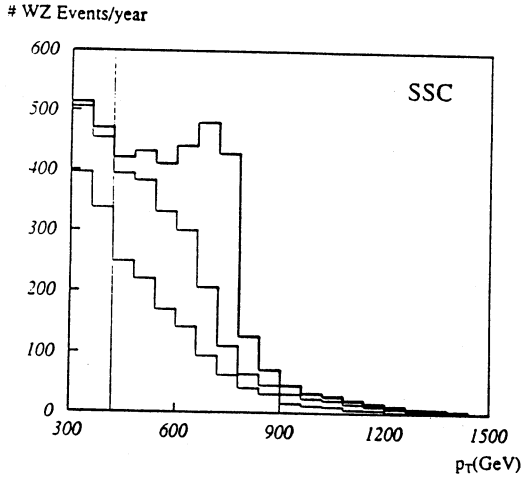

Fig. 5

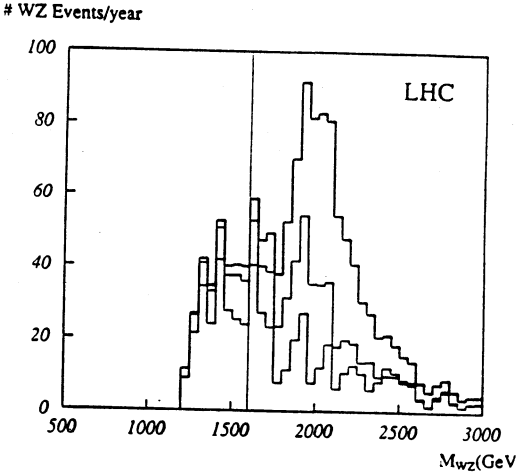

Fig. 6

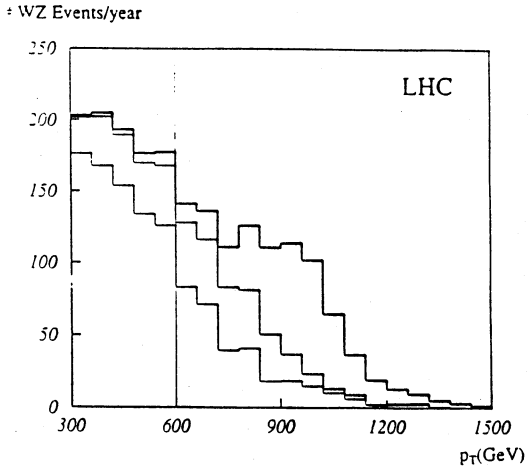

Fig. 7

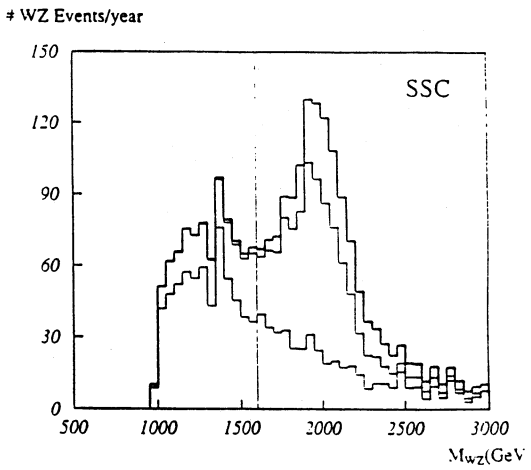

Fig. 8

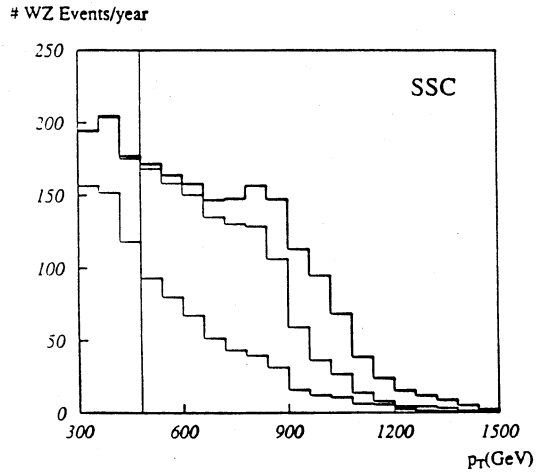

Fig. 9

IV. $W_L^{\pm}Z_L^0$ PRODUCTION AT THE LHC FROM THE STRONGLY INTERACTING SYMMETRY BREAKING SECTOR – EXPERIMENTAL ASPECTS

Contributors: Isabel Josa, Felicitas Pauss and Teresa Rodrigo

IV.1. Introduction

We study the $W_L^{\pm}Z_L^0$ production at $\sqrt{s}$ = 16 TeV in the presence of a strongly interacting symmetry breaking sector (SISBS) using two different approaches: the DHT model [1] (DHT stands for Dobado, Herrero and Terron) and the BESS model [2] (BESS stands for Breaking Electroweak Symmetry Strongly).

In the DHT model the SISBS is treated within a chiral perturbation theory, supplemented by a unitarization procedure [1]. Within this general approach to V_LV_L scattering three different scenarios have been considered: a) a unitarized Standard Model with heavy Higgs boson to one-loop (Higgs-like scenario); b) a scenario based on scaling the low-energy phenomenology of QCD to the TeV region (QCD-like scenario); in this case one expects the appearance of a vector resonance in analogy with the existence of the ρ resonance in QCD; and c) a SU(N) gauge theory in the spirit of Technicolor with the possibility of changing the number of Technicolors N_{TC}, thus allowing the study of the vector resonance production over a wide range of mass values:

$$m_{\rho_{TC}} \sim 2 \times (3/N_{TC})^{1/2} \text{ TeV} \quad \text{and} \quad \Gamma_{\rho_{TC}} \sim 480 \times (3/N_{TC})^{3/2} \text{ GeV}.$$

In the case of $N_{TC} = 3$, $\rho_{TC} \equiv \rho_{QCD}$, and for example, for $m_{\rho_{QCD}} = 2$ TeV one expects a width of $\Gamma_{\rho_{QCD}} \sim 480$ GeV. The different scenarios can be simulated by choosing the parameters of the effective Lagrangian accordingly. In the SU(N) Technicolor case it is possible to incorporate the additional mechanism for $W_L^{\pm}Z_L^0$ production via $q\bar{q}$ annihilation: $q\bar{q} \rightarrow W^{\pm} \rightarrow W_L^{\pm}Z_L^0$, where $W-\rho_{TC}$ mixing is assumed to be described in terms of Vector Meson Dominance.

In the BESS model [2] the electroweak symmetry breaking is described in a non-linear way. The model has no Higgs particles and contains a triplet of new massive vector bosons, $V^{\pm}$, V^0, which are bound states of a strongly interacting sector. They are similar to the ordinary ρ vector mesons, or the Techni-ρ particle of Technicolor theories. The V bosons are produced through $q\bar{q}$ annihilation and intermediate vector boson (IVB) fusion. The process $q\bar{q} \rightarrow V$ depends on the direct coupling of the V to fermions, but is still present even in the absence of this direct coupling. The fusion process, where two longitudinally polarized IVB's are rescattered, proceeds through the exchange of a V boson. The decay of V is dominated by $V \rightarrow WW$ or WZ.

The relation to Technicolor theories is obtained for a limited set of values of the parameter space of the BESS model: $\alpha = 2$, $g'' > 5.4$ ($N_{TC} \leq 14$) and $b = 0$. The parameter b specifies a possible direct coupling of the fermions to the new gauge vector bosons, g'' is the additional gauge coupling and α is a free parameter.

Signals from W_LZ_L production at the Large Hadron Collider (LHC) are discussed in Ref.[3] for the DHT model and in Ref.[4] for the BESS model. In order to understand the experimental requirements for observing a possible signal above background in the WZ channel, a Monte Carlo simulation is performed on the particle level. The signal is evaluated using the PYTHIA Monte Carlo program [5], where the $q\bar{q}$ annihilation and the WZ fusion process have been included. The parameters of the models are chosen such that the result of the simulation can

be applied to both model predictions discussed above. We have generated 15000 events for two different mass values of the ρ_{TC} vector resonance: $m_\rho = 1$ TeV, $\Gamma_\rho \simeq 55$ GeV and $m_\rho = 2$ TeV, $\Gamma_\rho \simeq 480$ GeV. The first case corresponds to N_{TC}= 12 and the second one to $N_{TC} = 3$ in SU(N) Technicolor. In the context of the BESS model the corresponding set of values are $\alpha = 2$, $g'' = 5.9$ and $\alpha = 2$, $g'' = 11.7$. No direct coupling to fermions has been assumed, i.e. $b = 0$, which leads to a more conservative rate estimate.

PYTHIA allows the two different production mechanisms involved in $W_L^\pm Z_L^0$ production to be studied separately: W_LZ_L fusion (taken from the DHT model) and $q\bar{q}$ annihilation (taken from the BESS model). Expected event rates are evaluated for an integrated luminosity of 4×10^5 pb^{-1}, i.e. one year of running at a high luminosity of L = 4×10^{34} cm^{-2} s^{-1}.

IV.2. $W_L^\pm Z_L^0$ production properties and background evaluation

A signal in the W_LZ_L channel is studied considering only the leptonic decays of W and Z. Using the PYTHIA Monte Carlo we predict the following cross-sections:

a) for $m_\rho = m_V = 1$ TeV, $\Gamma \simeq 55$ GeV the cross-section $\sigma(pp \rightarrow W_LZ_L)\times$ BR(W$\rightarrow \ell\nu)\times$ BR(Z$\rightarrow \ell\ell$) = 1.321×10^{-2} pb, where $q\bar{q}$ annihilation contributes 84% and the fusion process contributes 16% to the total cross-section.

b) for $m_\rho = m_V = 2$ TeV, $\Gamma \simeq 480$ GeV the cross-section $\sigma(pp \rightarrow W_LZ_L)\times$ BR(W$\rightarrow \ell\nu)\times$ BR(Z$\rightarrow \ell\ell$) = 0.809×10^{-3} pb; here the dominant contribution (78%) comes from the fusion process, while $q\bar{q}$ annihilation contributes 22% to the total cross-section.

The transverse momentum spectrum of the final-state leptons are shown in Fig. 1a for the new vector resonance of 1 TeV mass. Leptons produced via the $q\bar{q}$ annihilation mechanism have a harder spectrum than those coming from VV fusion. Figure 1b shows the lepton acceptance for both production mechanisms as a function of the lepton p_T. A cut on $p_T^\ell > 20$ GeV results in an acceptance of $\geq 85\%$ for VV fusion and $q\bar{q}$ annihilation. Rapidity distribution and acceptance as a function of the rapidity coverage are shown in Figs. 2a and b respectively. More than 95% of the leptons are contained in $|\eta| < 3$. With these cuts on p_T and η full acceptance efficiency is obtained for both kinds of production mechanism, and will be used in this analysis.

The backgrounds from the Standard Model to pp $\rightarrow W_L^\pm Z_L^0 \rightarrow$ 3 leptons include the production of WZ through quark-antiquark annihilation, γW fusion, and W_TZ_T fusion as well as $t\bar{t}$ production. We have used the ISAJET Monte Carlo program [6] to generate the dominant background contributions expected from WZ production through quark-antiquark annihilation and $t\bar{t}$ production. A top mass of 200 GeV has been used in the simulation. A total of about 15000 background events have been generated.

The cross-sections of Table 1 are obtained with ISAJET after requiring $|\eta^\ell| < 3$ and $p_T^\ell > 20$ GeV : σ(pp$\rightarrow t\bar{t} \rightarrow$ 3 leptons + X) = 7.25 pb and σ(pp $\rightarrow$ WZ $\rightarrow$ 3 leptons) = 0.077 pb.

IV.3. Discussion of results

For an integrated luminosity of 4×10^5 pb^{-1} and requiring the leptons to have $p_T > 20$ GeV and $|\eta| < 3$, one expects a total of 4829 (277) events from a signal pp $\rightarrow W_LZ_L \rightarrow$ 3 leptons for $m_\rho = m_V = 1$ TeV (2 TeV) respectively. The background from $t\bar{t}$ production amounts to 2.9×10^6 events and 3.1×10^4 events are expected from Standard Model WZ production.

$\Delta p/p$ [%]	W_LZ_L [%]	$t\bar{t}$ ($m_t = 200$ GeV) [%]
2	78	15
5	91	39
10	96	64

Table 1: Z^0 selection efficiency as a function of lepton resolution for signal and $t\bar{t}$ background, using ($m_Z \pm 3\sigma$).

In order to reduce the background coming from $t\bar{t}$ production we first require a Z^0 mass constraint, considering all possible two-lepton combinations (no charge requirement is used). The dilepton mass spectrum obtained for signal and background is shown in Fig. 3, assuming a lepton resolution of $\Delta p/p = 5\%$. Retaining events with $m_Z \pm 3\sigma$ (with $\Delta p/p = 5\%$) results in a reduction factor for top events of ~ 2.3 and the selection efficiency for events containing a real Z^0 is $\sim 91\%$. The dependence on the reduction of the background as a function of lepton resolution is given in Table 1. A gain of a factor ~ 4 in background rejection is possible if one uses a resolution of $\Delta p/p = 2\%$ instead of $\Delta p/p = 10\%$. Charge information would further improve the background rejection for $t\bar{t}$ events.

In order to further reduce the background from $t\bar{t}$ and WZ production, the differences in the topology of signal and background events can be exploited. The signal is expected to have a much harder p_T^Z distribution than that of the background processes. Figures 4a and b show the transverse momentum distribution of the reconstructed Z^0 boson for $m_\rho = m_V = 1$ TeV and 2 TeV respectively, together with the total background prediction. These distributions were obtained by imposing a constraint on the lepton-pair mass, $m_{\ell\ell} = m_Z \pm 3\sigma$, using a lepton resolution of $\Delta p/p = 5\%$ and requiring that $p_T^\ell > 20$ GeV and $|\eta_\ell| < 3$. A clear signal is observed for $m_\rho = m_V = 1$ TeV, coming mostly from $q\bar{q}$ annihilation. Requiring $p_T^Z > 400$ GeV results in a signal of 2579 ± 671 events for 4×10^5 pb^{-1}, where the fusion process only contributes 6% to the signal. For a 2 TeV vector resonance, no clear signal is visible. For $p_T^Z > 400$ GeV one expects 113 ± 29 events, where 56% of the signal comes from the fusion process. The total background, shown in Figs. 4a and b, is dominated by $t\bar{t}$ production. For $p_T^Z > 400$ GeV the total background contribution amounts to 590 ± 230 events, where 524 ± 250 events come from $t\bar{t}$, whereas Standard Model WZ production has been reduced to 66 ± 20 events after imposing the above cuts.

The $t\bar{t}$ background can be further reduced by imposing an isolation cut on all three leptons. The signal is expected to have three isolated leptons, whereas in the $t\bar{t}$ case the third lepton has to come from b- or c-quark decay and is therefore not expected to be isolated. Figure 5 shows the lepton isolation distribution, where $\sum E_T$ in $\Delta R = 0.2$ ($\Delta R = \sqrt{\Delta\eta^2 + \Delta\phi^2}$) around the lepton is plotted for the signal and both backgounds. As expected, leptons from $t\bar{t}$ are less isolated. The efficiency of reducing the $t\bar{t}$ background via isolation requirements increases with increasing lepton p_T. Figure 6 shows the average p_T of the leptons from $t\bar{t}$ production as a function of the reconstructed p_T^Z. For $p_T^Z > 400$ GeV one expects $< p_T^\ell > \simeq 200$ GeV. The isolation of leptons coming from b-jets was studied separately using a high statistics Monte Carlo sample of $b\bar{b}$ events. A rejection factor from lepton isolation as a function of lepton transverse momentum was calculated, requiring that leptons of $p_T = 10$ to 15 GeV yield a rejection factor of about 10, achieved at present Collider experiments. Figure 7 shows the thus obtained rejection factor as a function of p_T for leptons comming from b-jets. However, applying an isolation cut on all three

leptons in $t\bar{t}$ events did not leave enough Monte Carlo statistics to obtain a reliable estimate for the $t\bar{t}$ background contribution – a well-known problem when dealing with cut efficiencies $\ll$ 1%. Therefore a conservative $t\bar{t}$ background reduction of a factor of 50 was used after requiring $p_T^Z > 400$ GeV, based on Figs. 6 and 7. For the signal and for the WZ background only about 5% of the events are removed if lepton isolation is required.

The result, after imposing a cut of $p_T^Z > 400$ GeV and applying the reduction factor from lepton isolation, is shown in Figs. 8a and b for $m_\rho = m_V = 1$ TeV and 2 TeV as well as for the total background. For an integrated luminosity of 4×10^5 pb^{-1}, one expects a signal of 2450 $\pm$ 637 (107 $\pm$ 27) events for $m_\rho = m_V = 1$ TeV (2 TeV). The total background amounts to 74 $\pm$ 30 events (64 events from WZ and 10 events from $t\bar{t}$). For the 2 TeV vector resonance, an improvement in signal-to-background ratio is obtained by applying a harder p_T^Z cut. For $p_T^Z >$ 600 GeV a signal of 67 $\pm$ 17 events is expected over a total background of 15 $\pm$ 3 events (13 events from WZ and 2 events from $t\bar{t}$). Thus the background can be reduced sufficiently to observe a signal from new vector resonances with masses up to 2 TeV, provided the integrated luminosity exceeds 10^5 pb^{-1}. It should be noted that the stringent cuts on p_T^Z are imposed to obtain the final signal-to-background ratios. However, the full p_T^Z range has to be measured experimentally, in order to see a clear Jacobian peak (see Fig. 4a) or an excess at high p_T^Z (see Fig. 4b) over the Standard Model background.

We have not studied the effect of pile-up due to multiple interactions present at high-luminosity ($L > 10^{34}$ cm^{-2}s^{-1}) running, which should however be taken into account for a 2 TeV mass reach. The effect of pile-up on electron identification has been studied, for example in Ref.[7].

The possibility of forward jet ($|\eta^{jet}| > 3$) tagging, perhaps possible at the LHC [8], could allow further separation of the fusion process from background. This additional background rejection could be important for large masses of the new vector resonance, where the fusion process becomes the dominant production mechanism.

IV.4. Conclusions

We have studied the feasibility of detecting a signal above background in the $W_L^\pm Z_L^0 \to \ell^\pm\nu\ell^+\ell^-$ channel if the underlying dynamics contains a new vector resonance as present in the BESS model or in SU(N) Technicolor theories. A clear signal for a 1 TeV vector resonance can be expected in the Jacobian peak of the p_T^Z distribution. To reach a 2 TeV mass scale, a luminosity of $L > 10^{34}$ cm^{-2}s^{-1} is required in order to observe the expected enhancement at a high transverse momentum of the p_T^Z spectrum. In this case a good lepton-detection capability is crucial. Electrons and muons have to be detected up to $|\eta| = 3$, with a resolution of ~ 5 to 10%, and lepton-isolation requirements are necessary in order to reduce the large $t\bar{t}$ background.

With the high-luminosity option at the LHC we can explore a possible strongly interacting symmetry breaking sector if the underlying dynamics contains a vector resonance up to a mass of about 2 TeV.

Acknowledgement: We like to thank T. Sjöstrand for many discussions and his help in using the PYTHIA Monte Carlo program.

References

1. A. Dobado and M.J. Herrero, Phys. Lett. **228B** (1989) 495 and **233B** (1989) 505.

   A. Dobado, M.J. Herrero and J. Terrón, preprints CERN TH 5670/90 to appear in Z. für Physik C, and CERN TH 5813/90.

2. R. Casalbuoni, S. de Curtis, D. Dominici and R. Gatto, Phys. Lett. **155B** (1985) 95, Nucl. Phys. **B282** (1987) 235.

   R. Casalbuoni, P. Chiappetta, D. Dominici, F. Feruglio and R. Gatto, Nucl. Phys. **B310** (1988) 181.

   R. Casalbuoni, P. Chiappetta, S. De Curtis, F. Feruglio, R. Gatto, B. Mele and J. Terrón, preprint CERN TH 5814/90.

3. A. Dobado, M.J. Herrero and J. Terrón, these proceedings.

4. R. Casalbuoni, P. Chiappetta, S. De Curtis, F. Feruglio, R. Gatto, B. Mele and J. Terrón, these proceedings.

5. T. Sjöstrand, Int. J. Mod. Phys. **A3** (1988) 75, and on-line documentation of PYTHIA, version 5.4.

6. F. Paige and S.D. Protopopescu, BNL 38034 (1986), ISAJET Monte Carlo, version 6.36.

7. C. Albajar, C. Fuglesang, S. Hellman, F. Pauss and G. Polesello, these proceedings.

8. M. Seymour and D. Froidevaux, these proceedings.

Figure Captions

Fig. 1 a) Transverse momentum distribution of final-state leptons from $pp \to W_L^\pm Z_L^0 \to 3$ leptons ($m_\rho = m_V = 1$ TeV) for the fusion mechanism (full line) and the $q\bar{q}$ annihilation mechanism (dotted line). The upper full line represents the total $W_L^\pm Z_L^0$ production (fusion + $q\bar{q}$ annihilation); b) acceptance as a function of the p_T^ℓ threshold for the fusion mechanism (open circles) and for the total $W_L^\pm Z_L^0$ production (full circles).

Fig. 2 a) Rapidity distribution of final-state leptons and b) acceptance as a function of $|\eta|$ coverage from $pp \to W_L^\pm Z_L^0 \to 3$ leptons ($m_\rho = m_V = 1$ TeV). Same notation as in Fig.1.

Fig. 3 Dilepton mass spectrum for $p_T^\ell > 20$ GeV and $|\eta^\ell| < 3$. From top to bottom, the histograms show the backgrounds from $t\bar{t}$ and WZ, and the signals from the decay chain $pp \to V/\rho_T \to W_L Z_L \to \ell\nu\ell\ell$, for masses of 1 and 2 TeV.

Fig. 4 Transverse momentum distribution of the reconstructed Z^0 boson for a signal from $pp \to V/\rho_T \to W_L Z_L \to \ell\nu\ell\ell$, for a) $m_\rho = m_V = 1$ TeV and b) $m_\rho = m_V = 2$ TeV. The solid histogram represents the total signal, the dashed histogram shows the contribution from WZ fusion only. The stars show the total background from $t\bar{t}$ and WZ production.

Fig. 5 Lepton isolation ($\sum E_T$ in $\Delta R = 0.2$) for $W_L^{\pm}Z_L^0$ events (shaded histogram), $t\bar{t}$ events (full line), and $W^{\pm}Z^0$ background events (dotted line).

Fig. 6 Average p_T of leptons from $t\bar{t}$ production as a function of the reconstructed p_T^Z.

Fig. 7 Reduction factor for leptons from b-jets after isolation requirement.

Fig. 8 The same distributions as in Fig. 4, but after the final selection cuts have been applied.

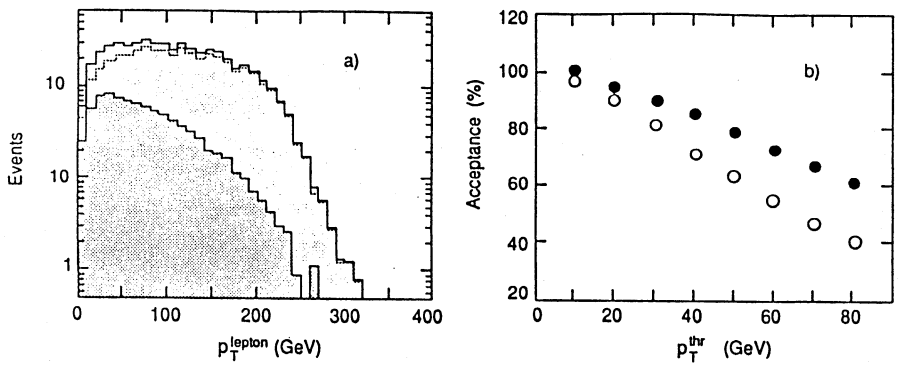

FIG. 1

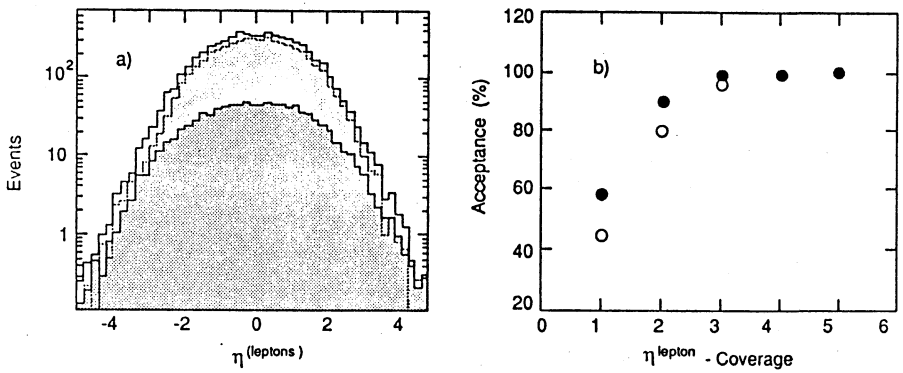

FIG. 2

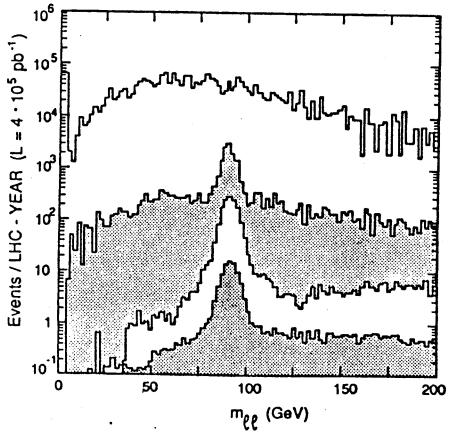

FIG. 3

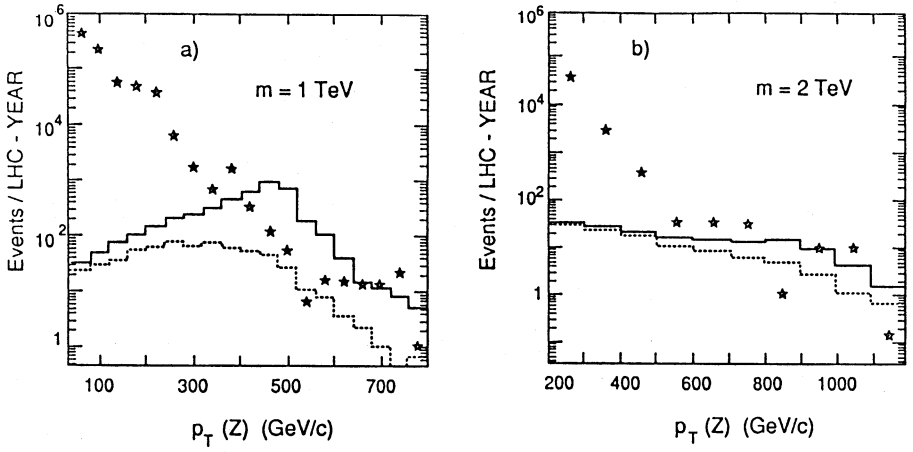

FIG. 4

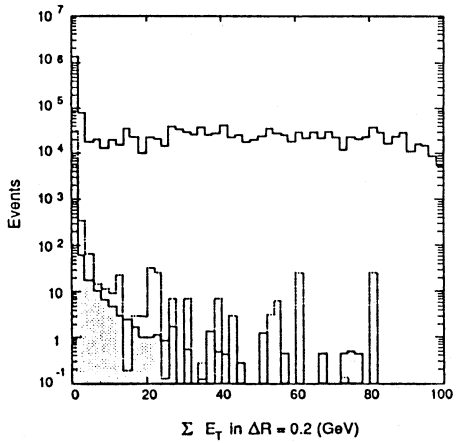

FIG. 5

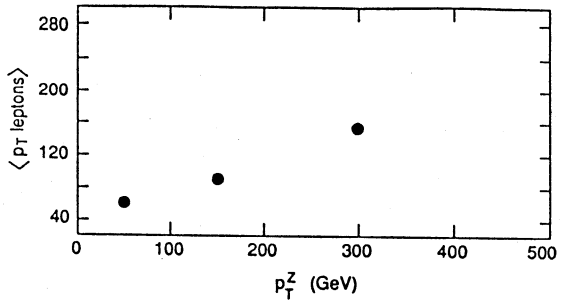

FIG. 6

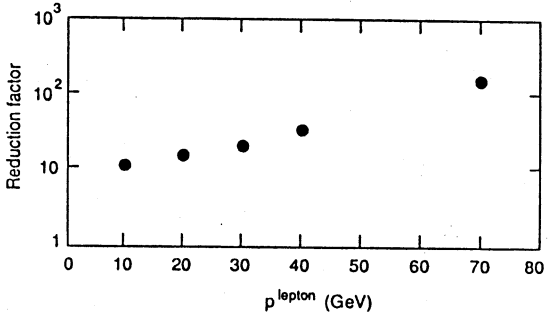

FIG. 7

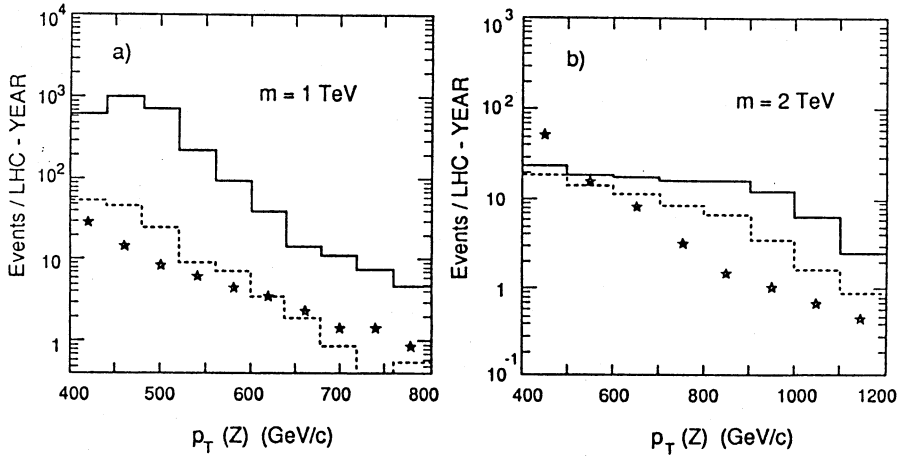

FIG. 8

V. COMPOSITENESS

Contributors: E.N. Argyres, U. Baur, P. Chiappetta, C.G. Papadopoulos, M. Perrottet M. Spira, S.D.P. Vlassopulos, P. Zerwas

V.1. Introduction

The proliferation of quarks and leptons and their mysterious deep relations among each other are suggestive indications for substructures of these particles [1]. No satisfactory theoretical model has been developed so far, in which the light masses of quarks and leptons could be reconciled with their small radii $< \mathcal{O}(10^{-16}$ cm) corresponding to a compositeness scale of 1 TeV and beyond. However, the quark model of hadrons has taught us very clearly in the past that theorists' puzzles cannot force Nature not to realize physically novel concepts. The compositeness scale may be anywhere between the $\mathcal{O}(1$ TeV) range and the Planck scale. A high–energy collider like the LHC will be able to either discover preonic substructures or to improve the limits on quark radii down to $\mathcal{O}(10^{-17}$ cm) in a model independent way, an order of magnitude more than accessible now.

(i) Quark radii can be measured or bounded by studying jet production at large transverse momenta [2]. A surplus of scattering events over the predictions from standard QCD would be observed at transverse momenta $p_\perp \sim \mathcal{O}(R^{-1})$ where the cross section would begin to be dominated by the non–pointlike quark radius R.

(ii) A unique signal for the substructure of quarks and leptons would be the discovery of excited states [3] towering over the lepton and quark ground states: $\ell, \ell^*, \ell^{**}, \ldots$ and $q, q^*, q^{**}, \ldots$ The masses m^* of excited fermions are generally expected to be of the order of the compositeness scale Λ.

We will not discuss a specific model in the following, but we will elaborate the experimental consequences of these two rather general physical points for the LHC. The main results of this study may be summarized in limits of ~ 20 TeV for the compositeness scale probed in quark–quark scattering, and mass limits of 5 to 10 TeV for the production of excited leptons and quarks.

Other signatures of compositeness — strongly produced multi–lepton final states, lepto-quarks, colored leptons and other novel particle types — have been discussed frequently in the literature, see e.g. [1].

Compositeness of gauge bosons and Higgs particles can stabilize the Higgs mass. The natural scale of this sector is the Fermi scale ~ 250 GeV. Substructures of these particles would manifest themselves through excited W^* and Z^* bosons and isoscalar partners which have been described elsewhere in this report. Anomalous production of gauge boson pairs due to non–standard trilinear self–couplings is another signal of substructures at distances of $\mathcal{O}(10^{-16}$ cm).

V.2. Bounds on Quark and Lepton Radii

Contributors: P. Chiappetta and M. Perrottet

The aim of this report is to study some effects of contact terms due to composite quarks and leptons on inclusive jet production and on massive dilepton production [4].

V.2.1. Inclusive jet production.

We first compute the effect of the 4 quark contact term of dimension 6 [5]

$$\mathcal{L}_{qqqq} = \frac{\eta g^2}{2\Lambda_q^2} \bar{\psi}_q^L \gamma^\mu \psi_q^L \bar{\psi}_q^L \gamma_\mu \psi_q^L \tag{1}$$

on the inclusive one jet production at $\sqrt{s} = 16$ TeV (LHC) and $\sqrt{s} = 40$ TeV (SSC). Here η is a sign $(\pm 1), g$ a strong interaction coupling constant such that $g^2 = 4\pi$ and Λ_q is the compositeness scale associated with the effective 4 quark operator of eq. (1). ψ_q^L is the usual $SU(2)_L$ doublet made out of up- and down-type quarks. Note that the current in the current-current interaction (1) is a color- and isospin-singlet. More precisely, we study the deviations due to (1), with respect to the lowest order QCD predictions, on the differential cross section

$$\frac{d^2\sigma}{dp_T dy}\Big|_{y=0} \tag{2}$$

where p_T is the jet transverse momentum and y is rapidity. The contact term (1) modifies the various elementary two-body quark cross sections. Because we disagree with some of the results published by other authors [5,7], we give below a list of our own formulas

$$q_i\bar{q}_j \to q_i\bar{q}_j : |\mathcal{M}|^2 = \frac{4}{9}\frac{\hat{u}^2+\hat{s}^2}{\hat{t}^2} + \hat{u}^2C^2 \tag{3}$$

$$q_iq_j \to q_iq_j : |\mathcal{M}|^2 = \frac{4}{9}\frac{\hat{u}^2+\hat{s}^2}{\hat{t}^2} + \hat{s}^2C^2 \tag{4}$$

$$q_i\bar{q}_i \to q_j\bar{q}_j : |\mathcal{M}|^2 = \frac{4}{9}\frac{\hat{u}^2+\hat{t}^2}{\hat{s}^2} + \hat{u}^2C^2 \tag{5}$$

$$\bar{q}_i\bar{q}_j \to \bar{q}_i\bar{q}_j : |\mathcal{M}|^2 = \frac{4}{9}\frac{\hat{u}^2+\hat{s}^2}{\hat{t}^2} + \hat{s}^2C^2 \tag{6}$$

$$q_iq_i \to q_iq_i : |\mathcal{M}|^2 = \frac{4}{9}\left\{\frac{\hat{s}^2+\hat{u}^2}{\hat{t}^2} + \frac{\hat{s}^2+\hat{t}^2}{\hat{u}^2} - \frac{2}{3}\frac{\hat{s}^2}{\hat{u}\hat{t}}\right\} + \frac{8}{9}\hat{s}^2\left(\frac{1}{\hat{t}}+\frac{1}{\hat{u}}\right)C + \frac{8}{3}\hat{s}^2C^2 \tag{7}$$

$$q_i\bar{q}_i \to q_i\bar{q}_i : |\mathcal{M}|^2 = \frac{4}{9}\left\{\frac{\hat{u}^2+\hat{s}^2}{\hat{t}^2} + \frac{\hat{u}^2+\hat{t}^2}{\hat{s}^2} - \frac{2}{3}\frac{\hat{u}^2}{\hat{s}\hat{t}}\right\} + \frac{8}{9}\hat{u}^2\left(\frac{1}{\hat{t}}+\frac{1}{\hat{s}}\right)C + \frac{8}{3}\hat{u}^2C^2 \tag{8}$$

$$\bar{q}_i\bar{q}_i \to \bar{q}_i\bar{q}_i : |\mathcal{M}|^2 = \frac{4}{9}\left\{\frac{\hat{s}^2+\hat{u}^2}{\hat{t}^2} + \frac{\hat{s}^2+\hat{t}^2}{\hat{u}^2} - \frac{2}{3}\frac{\hat{s}^2}{\hat{u}\hat{t}}\right\} + \frac{8}{9}\hat{s}^2\left(\frac{1}{\hat{t}}+\frac{1}{\hat{u}}\right)C + \frac{8}{3}\hat{s}^2C^2 \qquad (9)$$

The indices i and j refer to quark flavors. $\hat{s},\hat{t}$ and $\hat{u}$ are the usual Mandelstam variables. C is directly related to the compositeness scale Λ_q through

$$C = \frac{\eta}{\alpha_s(Q^2)\Lambda_q^2} \qquad . \qquad (10)$$

Finally, the differential cross sections $d\sigma/d\hat{t}$ which enter into the computation of eq. (2) are given by

$$\frac{d\sigma}{d\hat{t}} = \frac{\pi}{\hat{s}^2}\alpha_s^2(Q^2)|\mathcal{M}|^2 \qquad (11)$$

where the argument Q^2 of the effective QCD coupling constant is p_T^2. In order to obtain results which are little sensitive to the choice of structure functions and mass scales, we have studied the ratio

$$D = \frac{\frac{d^2\sigma}{dp_Tdy}\Big|_{y=0}(\text{QCD}+\text{CT}) - \frac{d^2\sigma}{dp_Tdy}\Big|_{y=0}(\text{QCD})}{\frac{d^2\sigma}{dp_Tdy}\Big|_{y=0}(\text{QCD})} \qquad (12)$$

where CT means contact term. The discovery limits for the compositeness scale Λ_q that we will give below correspond to a deviation from the QCD prediction larger than 100%, namely $D \geq 1$ (theoretical uncertainties including higher order corrections are of the order of 40% [8]). With $\Delta p_T = 100\text{GeV/c}$, we would like to have at least ten events per year in the standard model. Considering the expected luminosities $\mathcal{L}_{\text{LHC}} = 10^{34}cm^{-2}s^{-1}$ and $\mathcal{L}_{\text{SSC}} = 10^{33}cm^{-2}s^{-1}$, one can reach for the cross section (2) $x_T \equiv \frac{2p_T}{\sqrt{s}} \cong 0.5$ for LHC, and $x_T \cong 0.3$ for SSC.These discovery limits are displayed in table 1 for LHC and SSC, using two sets of distribution functions, DFLM set of ref. [9] with $\Lambda_{QCD} = 160$ MeV, and set 1 of Duke-Owens [10]. As expected, there is little sensitivity to the choice of structure functions, typically a few percent. It should be noted that the difference in luminosities compensates to a large extent the gap in energy between LHC and SSC. We have checked that another choice of the mass scale ($Q^2 = p_T^2/4$) changes the discovery limits by a few percent only.

Table 1

	qqqq CT		qqgg CT	
	$\eta = +1$	$\eta = -1$	Vector	Axial
LHC Duke–Owens	20 TeV	28 TeV	4.6 TeV	4.6 TeV
LHC Diemoz et al.	20 TeV	27 TeV	4.3 TeV	4.4 TeV
SSC Duke–Owens	27 TeV	33 TeV	7.6 TeV	7.7 TeV
SSC Diemoz et al.	27 TeV	32 TeV	7.4 TeV	7.5 TeV

Obviously discovery limits depend on luminosity and the value of required deviation from QCD prediction. As an example if we assume $\mathcal{L}_{LHC} = 10^{33}cm^{-2}sec^{-1}$ and a deviation larger than 200 % we get a discovery limit of 13 TeV for $\eta = +1$. We have also computed the effect

of a contact term between transverse gluons considered as true gauge particles and composite quarks. Several CP- and chirality-conserving operators can be written [11] but for the present study we have selected the one of the lowest dimension. It is called N_{TT}^2 in ref. [11] and can be written as [12]

$$\mathcal{L}_{qqgg} = i\frac{\alpha_s}{\Lambda_g^4}\bar{\psi}_q\{(\gamma^\mu\partial_\rho + \gamma_\rho\partial^\mu)(C_V - C_A\gamma_5)\psi_q\}\,G_{\mu\nu}G^{\nu\rho} \qquad (13)$$

where Λ_g is the compositeness scale associated with the dimension 8 operator, $C_V(C_A)$ the vector (axial) part of the lagrangian. For completeness, we give below the contribution of (13) to the relevant processes [6]

$$q_i\bar{q}_i \to gg : |\mathcal{M}|^2 = \frac{8}{3}\left(\hat{u}^2+\hat{t}^2\right)\left\{\frac{4}{9\hat{u}\hat{t}} - \frac{1}{\hat{s}^2}\right\} + \frac{4}{3}\frac{\hat{u}^2+\hat{t}^2}{\Lambda_g^4}\left\{\frac{2}{3}C_V + \frac{\hat{u}\hat{t}}{\Lambda_g^4}\left(C_V^2+C_A^2\right)\right\} \qquad (14)$$

$$q_ig \to q_ig : |\mathcal{M}|^2 = -\left(\hat{u}^2+\hat{s}^2\right)\left\{\frac{4}{9\hat{u}\hat{s}} - \frac{1}{\hat{t}^2}\right\} - \frac{1}{2}\frac{\hat{u}^2+\hat{s}^2}{\Lambda_g^4}\left\{\frac{2}{3}C_V + \frac{\hat{u}\hat{s}}{\Lambda_g^4}\left(C_V^2+C_A^2\right)\right\} \qquad (15)$$

$$gg \to q_i\bar{q}_i : |\mathcal{M}|^2 = \frac{3}{8}\left(\hat{u}^2+\hat{t}^2\right)\left\{\frac{4}{9\hat{u}\hat{t}} - \frac{1}{\hat{s}^2}\right\} + \frac{3}{16}\frac{\hat{u}^2+\hat{t}^2}{\Lambda_g^4}\left\{\frac{2}{3}C_V + \frac{\hat{u}\hat{t}}{\Lambda_g^4}\left(C_V^2+C_A^2\right)\right\} \qquad . \qquad (16)$$

We have assumed that the color structure in the contact term is the same as that of the QCD amplitude. The differential cross section $d\sigma/d\hat{t}$ is still given by eq. (11). Since QCD is a vector theory, the interference term between QCD and the contact interaction (13) is simply proportional to the vector coupling C_V. To set discovery limits for the compositeness scale Λ_g, we used the same approach as for interaction (1). These limits are given in Table 1. There is little difference between the vector case ($C_V = 1, C_A = 0$) and the axial one ($C_V = 0, C_A = 1$). Of course, the operator (13) being of higher dimension than (1), the discovery limits are much lower and will be completely hidden by the presence of the contact term (1) if one assumes that Λ_q is of the order of Λ_g.

V.2.2. Massive lepton pair production

Finally, we have similarly analyzed the influence of a contact term between quarks and leptons on massive dilepton production through the Drell-Yan mechanism. The effective contact interaction is similar to (1)

$$\mathcal{L}_{qqll} = \frac{\eta g^2}{4\Lambda_{lq}^2}\bar{\psi}_l\gamma^\mu(1-\eta_l\gamma_5)\psi_l\bar{\psi}_q\gamma_\mu(1-\eta_q\gamma_5)\psi_q \qquad (17)$$

with $\eta = \pm 1, \eta_l = \pm 1, \eta_q = \pm 1, g^2 = 4\pi$ and Λ_{lq} is the compositeness scale associated to the dimension 6 operator of eq. (17). We will use the same criteria as described previously to define the discovery limits, namely deviations with respect to the QCD predictions larger than 100%.

We will concentrate on the differential cross section $\frac{d\sigma}{dM_{l^+l^-}}$ where $M_{l^+l^-}$ is the invariant mass of the lepton pair. Then the deviation to study is

$$\tilde{D} = \frac{\frac{d\sigma}{dM_{l^+l}}(\text{QCD} + \text{CT}) - \frac{d\sigma}{dM_{l^+l^-}}(\text{QCD})}{\frac{d\sigma}{dM_{l^+l^-}}(\text{QCD})} \tag{18}$$

where CT is now the contribution from the interaction (17). Keeping in mind a rate of at least 10 events per year from the standard model with $\Delta M = 100$GeV, a direct computation shows that one can reach $M_{l^+l^-} \cong 2.05$TeV at LHC and $M_{l^+l^-} \cong 2.15$TeV at SSC. For illustration, we have considered the two extreme chirality cases $\eta_l = \eta_q = 1$ (left-left, or LL) and $\eta_l = \eta_q = -1$ (right-right or RR). The corresponding discovery limits are displayed in Table 2 for LHC and SSC with the structure functions of ref. [9]. One can see that the difference in luminosity between LHC and SSC compensates exactly the difference in energy. We can also notice that for a given overall sign of the contact interaction (17), the discovery limits depend very little on the choice of chirality (LL or RR).

Table 2

	$\eta = +1$		$\eta = -1$	
	LL	RR	LL	RR
LHC	15 TeV	16 TeV	25 TeV	25 TeV
SSC	15 TeV	16 TeV	24 TeV	24 TeV

V.2.3. Conclusion

To conclude, it is interesting to make a comparison between our results and the corresponding limits at Hera and at the Tevatron. For Hera, the LL 2quark- 2lepton contact term (17) leads to a discovery limit of about 5 TeV [13], to be compared with the 15 TeV limit of Table 2. Concerning the 4 quark contact term (1), LHC and SSC will improve the expected Tevatron limit (2 to 3 TeV) [14] by roughly one order of magnitude.

V.3. Testing Contact Interactions of Quarks and Gluons at Future pp Colliders

Contributors: E.N.Argyres, C.G.Papadopoulos and S.D.P.Vlassopulos

New interactions at an energy scale Λ of the order of a few TeV will manifest themselves at energies below this scale, through deviations from the Standard Model (SM), described by an effective non-renormalizable $SU(3) \otimes SU(2) \otimes U(1)$ invariant lagrangian. Such interactions may arise either as low-energy tails of heavy exotic particle exchange (e.g. non-minimal Higgses, E_6-diquarks, extra neutral currents, etc) or as a manifestation of quark and gluon substructure. It is therefore, interesting to search for deviations from the SM predictions at future accelerators, like LHC and SSC, which will provide us with the highest available center of mass energies, $\sqrt{s}$ =16TeV and 40TeV, respectively.

In this work we calculate the effect of qq,qg,gg contact interactions, described by [15]

$$\mathcal{L}_{eff} = g_1 f_{ABC} G^{A\nu}_{\mu} G^{B\lambda}_{\nu} G^{C\mu}_{\lambda} \tag{19a}$$

$$+ i g_2 \bar{q} \lambda^A \gamma_\mu D_\nu q G^{A\mu\nu} \tag{19b}$$

$$+ i g_3 \bar{q} \gamma_\mu q \bar{q} \gamma^\mu q \tag{19c}$$

$$+ i g_4 \bar{q} \lambda^A \gamma_\mu q \bar{q} \lambda^A \gamma^\mu q \tag{19d}$$

in the 2- and 3-jet cross sections. The dimensionful coupling constants, g_i, are given by $g_i = \eta_i \frac{4\pi}{\Lambda^2}$, where $\eta_i = \pm 1$ and we have assumed a common scale Λ. More explicitly we calculate

$$\sigma(pp \to \text{n jets} + \text{X}) = \int \sum_{a,b} dx_a dx_b \mathcal{F}_a(x_a, Q) \mathcal{F}_b(x_b, Q) \mid \mathcal{M}_{ab} \mid^2 d\mathcal{L}ips^{(n)} \tag{20}$$

where $\mathcal{F}_a$ are the quark and gluon distributions and $\mathcal{M}_{ab}$ the helicity amplitudes, calculated using the "E-product" [16] formulation of the well known spinor-product technique [17]. Notice that in the case $n = 2$ the full lagrangian (19) has been used, whereas in the case $n = 3$ only the operator (19c) has been employed[4]. In both cases we use $\eta_i = +1$.

In order to compare the theoretical predictions with experimental data we have to impose appropriate cuts on the momenta of the produced jets, quarks and gluons, which, neglecting all hadronization effects, are simply

$$\mid \eta_{\text{jet}} \mid \leq 2.5 \tag{21a}$$

$$\cos(\theta_{ij}) \leq 0.766 \ (\theta_{min} = 40^0) \tag{21b}$$

where η_{jet} is the pseudorapidity and θ_{ij} the angle between the 3-momenta of the jets i and j. We use $Q = \sqrt{\hat{s}}$, $\hat{s} = x_a x_b s$ and the structure-function parametrization EHLQ II [18] with $\Lambda_{\text{QCD}} = 0.29$GeV.

Since we are interested in enhancing the signal of the new interactions, we impose the supplementary cuts

$$M_{\text{njets}} \geq 6.4(12)\text{TeV} \tag{22a}$$

$$p_T \geq 0.4(1)\text{TeV} \tag{22b}$$

for $\sqrt{s} = 16(40)$TeV, where M_{njets} is the invariant mass of the produced jets [19] and p_T the transverse momentum. These cuts have the effect to suppress the QCD background, whereas the contact interaction contribution remains almost unaffected. Notice that the cuts (22a) and (22b) are necessary in the case $n = 3$, since a quark-quark contact interaction signal can be detectable only if we suppress the gg initial state contribution [19]. We focus our attention to the normalized χ distribution,

$$\frac{1}{\sigma} \frac{d\sigma}{d\chi}$$

where

$$\chi = \frac{1 + \cos\theta^*}{1 - \cos\theta^*} \tag{23}$$

[4]The details of the calculation will be given elsewhere

and θ^* is the c.m. angle of the beam and the produced jet momentum, in the 2-jet case, and the angle of the beam with the fastest jet, in the 3-jet case.

Figs.(1a) and (1b) show the 2-jet cross section for $\sqrt{s} = 16$ and 40 TeV respectively. As we can see, the contact interaction prefers to accumulate events at smaller values of χ (spherical events), whereas the QCD background is almost flat. If one assumes a statistical error

$$\frac{\delta\sigma}{\sigma} = \sqrt{\frac{1}{\sigma\mathcal{L}}} \tag{24}$$

where $\mathcal{L}$ is the luminosity , a χ^2 analysis gives that (at 95% C.L.):

$$\Lambda \geq 40\text{TeV}(\sqrt{s} = 16\text{TeV}) \tag{25a}$$

$$\Lambda \geq 50\text{TeV}(\sqrt{s} = 40\text{TeV}) \tag{25b}$$

where we have used $\mathcal{L} = 400\text{fb}^{-1}$ at LHC and $\mathcal{L} = 10\text{fb}^{-1}$ at SSC [20].

In figs.(2a) and (2b) we show the results for the three-jet cross section. The corresponding bounds are:

$$\Lambda \geq 15\text{TeV}(\sqrt{s} = 16\text{TeV}) \tag{26a}$$

$$\Lambda \geq 10\text{TeV}(\sqrt{s} = 40\text{TeV}) \tag{26b}$$

The bound for the SSC is smaller than for the LHC, due to the smaller luminosity of the SSC and to the fact that the 3-jet χ-distribution of QCD is not flat.

Although there are other quantities which are sensitive to contact interactions, like the p_T spectrum, the normalized χ distribution offers the very advantage of being relatively free of the uncertainties due to the small-x behaviour of the gluon distribution and the higher order QCD corrections (in particular, choice of the scale Q^2 and the jet-cone size) [8], which are expected not to be strongly dependent on χ.

Comparing the bounds in all cases, one can state, that the luminosity $\mathcal{L}$ is a crucial parameter in order to probe the contact interactions. Especially for the quark-quark contact interactions, LHC seems to be more sensitive than SSC.

V.4. Excited Quarks and Leptons

Contributors: U. Baur, M. Spira and P. Zerwas

Spin and isospin of the excited fermions will be set to 1/2 in order to restrict the number of parameters to be introduced in this study [3]. The assignment of left– and right–handed components to isodoublets, e.g. for the first generation

$$\begin{bmatrix} \nu_e \\ e^- \end{bmatrix}_L \quad \nu_{eR} \quad \begin{bmatrix} \nu_e^* \\ e^{*-} \end{bmatrix}_L \quad \begin{bmatrix} \nu_e^* \\ e^{*-} \end{bmatrix}_R \quad \text{and} \quad \begin{bmatrix} u \\ d \end{bmatrix}_L \quad u_R \quad \begin{bmatrix} u^* \\ d^* \end{bmatrix}_L \quad \begin{bmatrix} u^* \\ d^* \end{bmatrix}_R$$

allows for non-zero masses prior to $SU(2) \times U(1)$ symmetry breaking, and it protects $(g-2)_\ell$ quadratically in the mass ratio $(m_\ell/m^*)^2$. The coupling of excited fermion states to the chiral Standard Model particles consists of three interaction types:

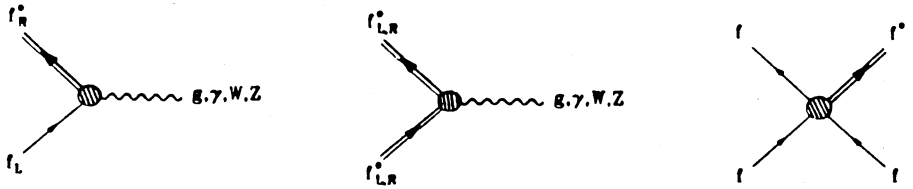

the first being the standard fermion–gauge boson interaction; the second being a gauge invariant magnetic type coupling between ground state and excited state; the third describing the strong excitation of fermions through contact interactions mediated, for instance, by preon interchange. Throughout this analysis we put $m^* = \Lambda$, for the sake of simplicity, and we neglect [minor] form factor effects.

Decay. Heavy excited fermions will decay into light fermions plus gauge bosons, but also, through preon–pair creation, into bunches of quarks and leptons

$$f^* \to f + V \qquad \text{and} \qquad f^* \to f + f'\bar{f}'$$

with $V = g,\ \gamma,\ Z,\ W$. Assuming $m^* \gg m_{W,Z}$ and neglecting light quark masses, the partial widths for the various gauge decay channels lead to the branching ratios listed in Table 3.

Table 3

	$\sum_V \Gamma(f^* \to fV)/m^*$ $[m^* = \Lambda]$
ν^*	$6.5 \cdot 10^{-3}$
e^*	$6.5 \cdot 10^{-3}$
u^*	$3.9 \cdot 10^{-2}$
d^*	$3.9 \cdot 10^{-2}$

e^*	B_G
$e\gamma$	0.28
eZ	0.11
νW	0.61

ν^*	B_G
νZ	0.39
eW	0.61

u^*	B_G
ug	0.85
$u\gamma$	0.02
uZ	0.03
dW	0.10

d^*	B_G
dg	0.85
$d\gamma$	0.005
dZ	0.05
uW	0.10

Contact interactions widen the excited states such that excited leptons and quarks would have comparable widths as expected from strong preon interactions. Results are shown in Table 4.

Table 4

	Γ_{tot}/m^*	Γ_G/Γ_{tot}	Γ_{CT}/Γ_{tot}	leptonic decays/all
ν^*	$8.9 \cdot 10^{-2}$	0.07	0.93	100%
e^*	$8.9 \cdot 10^{-2}$	0.07	0.93	100%
u^*	$1.2 \cdot 10^{-1}$	0.32	0.68	16.3%
d^*	$1.2 \cdot 10^{-1}$	0.32	0.68	16.3%

q^* production. Excited quarks can be produced in pp collisions through a variety of mechanisms. The dominant processes are the gluonic excitation of quarks $g + q \to q^*$ [3,21,22] and the excitation through contact interactions $qq \to qq^*$ [3,21].

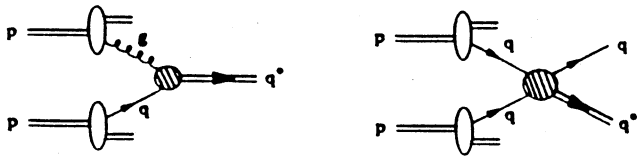

The cross section for the gluonic excitation of quarks, $qg \to q^*$, at pp colliders is shown in Fig. 3. Assuming gauge interactions to dominate over contact interactions, the signals for singly produced excited quarks are large transverse momentum jj, $j\gamma$, jZ or jW pairs with an invariant mass peaking at m^*. The jj mass distributions of the QCD background is integrated over twice the q^* width. The mass distributions for pp collisions at $\sqrt{s} = 16$ TeV are shown in Fig. 4 for various values of m^*. At LHC the q^* signal stands out clearly. Similar results are obtained for $j\gamma$, jW and jZ final states.

If contact interactions contribute significantly to the decay rate of excited quarks they may be a bubbling source for excited quarks q^* at hadron colliders. Excited quarks can be produced through contact interactions in qq collisions and $q\bar{q}$ annihilation together with an ordinary quark. Excited quark decays, mediated either by gauge or contact interactions lead to final states that consist of three or four jets, two jets and a photon, or two jets and a lepton pair. The qq^* production cross sections for LHC energies are shown in Fig. 5. The background to the qq^* signal, the q^* decaying into three jets via contact interactions, are four-jet final states. In addition to pure QCD processes the contact interactions are a second important source of four–jet background events. All these background cross sections however are significantly smaller than the signal, as demonstrated in Fig. 5. This is also the case for the background from diagrams involving both QCD and contact interactions, with gluons in either the initial or the final state. The combinatorial background arising from the wrong three-jet combination in the jjj mass distribution is of the same order as the signal.

ℓ^* production. The possibility to create leptons copiously through contact interactions in pp collisions is one of the most exciting phenomena expected in composite models in which quarks and leptons have common constituents [5]. In this case also excited leptons could be produced in large numbers either singly via $q\bar{q} \to \ell\bar{\ell}^*$, $\ell^*\bar{\ell}$, or pairwise via $q\bar{q} \to \ell^*\bar{\ell}^*$ ($\ell = e,\ \nu$), Fig. 6. Background reactions to these channels are very rare in the Standard Model, and purely leptonic decays would provide very clear signatures for the experimental identification of excited electrons.

Summary. Excited quarks and leptons are produced with large cross sections in pp collisions once the threshold energy has been reached. This observation can be condensed in a few numbers by deriving the maximum excited quark and lepton masses accessible at the pp collider. As the discovery criterion we require that at least 100 signal events be observed within cuts. The discovery limits are summarized in the following table. For the LHC we considered two options: an integrated luminosity of 10^4 pb^{-1} and a "high luminosity" option with $4 \cdot 10^5$ pb^{-1}.

pp colliders turn out to be well suited for the search of excited quarks. Single q^* production is expected to be much larger than $q^*\bar{q}^*$ production. Clean and simple experimental signatures with small background are predicted for excited quarks which are produced via qg fusion and which decay via gauge interactions. Contact interactions may substantially enhance the q^* production cross section. This is reflected by the discovery limits for the LHC summarized in the preceding table. If quarks and leptons share common subconstituents, even excited leptons could be produced copiously at this machine, producing spectacular lepton final states at very high rates.

Table 5

	LHC	LHC
$\int \mathcal{L} dt$	10^4 pb^{-1}	$4 \cdot 10^5$ pb^{-1}
q^* [G]	6.5 TeV	9.0 TeV
q^* [CT]	7.0 TeV	8.9 TeV
ℓ^* [CT]	4.0 TeV	5.6 TeV

Figure Captions

Fig. 1: Normalized χ-distributions for 2 jet cross sections at LHC (a) and SSC (b).

Fig. 2: Normalized χ-distributions for 3 jet cross sections at LHC (a) and SSC (b).

Fig. 3: Cross section for the production of excited quarks in quark-gluon fusion (solid line). The 2-jet QCD background is shown by the dashed line.

Fig. 4: Invariant mass distributions of excited quarks in the jj decay channel for various values of m* (dotted lines). The solid curve represents the QCD jj background.

Fig. 5: Cross section for the associated production of excited and ordinary quarks (solid line) with subsequent decay of the excited quark into three jets (contact interactions). The other curves show the four-jet background from QCD, contact interactions and diagrams involving both QCD and contact interactions.

Fig. 6: Cross sections for the associated production of ordinary and excited electrons (solid line) and e* pair production (dashed line).

References

[1] H. Harari, Proceedings of the 1984 Scottish Universities Summerschool, St. Andrews, Scotland.

[2] E. J. Eichten, K. D. Lane and M. I. Peskin, Phys. Rev. Lett. **50** (1983) 811.

[3] U. Baur, M. Spira and P. M. Zerwas, Phys. Rev. **D42** (1990) 815.

[4] P. Chiappetta and M. Perrottet, Preprint Marseille CPT-90/P.2440 (September 1990) to appear in Phys. Lett. B

[5] E. Eichten, I. Hinchliffe, K. Lane and C. Quigg, Rev. Mod. Phys. 56 (1984) 579.

[6] C. Bourrely, F.M. Renard, J. Soffer and P. Taxil, Phys. Rep. 177 (1989) 319.

[7] E.N. Argyres, C.G. Papadopoulos and S.D.P. Vlassopulos, Nucl. Phys. B324 (1989) 91.

[8] F. Aversa, P. Chiappetta, M. Greco and J.-Ph. Guillet, Phys. Rev. Lett. 65 (1990) 401; S.D. Ellis, Z. Kunszt and D.E. Soper, Phys. Rev. Lett. 64 (1990) 2121.

[9] M. Diemoz, F. Ferroni, E. Longo and G. Martinelli, Z. Phys. C39 (1988) 21.

[10] D.W. Duke and J.F. Owens, Phys. Rev. D30 (1984) 49.

[11] P. Méry, M. Perrottet and F.M. Renard, Z. Phys. C36 (1987) 249.

[12] P. Méry, S.E. Moubarik, M. Perrottet and F.M. Renard, Z. Phys. C46 (1990) 229.

[13] R. Rückl, in the Proceedings of the ECFA Workshop on LEP 200, CERN 87-08 (1987), Vol. II, p.453.

[14] P. Jenni, in the Proceedings of the ECFA Workshop on LEP 200, CERN 87-08 (1987), Vol. II, p.486.

[15] W.Buchmüller & D.Wyler, Nucl.Phys.**B268**(1986)621.

[16] E.N.Argyres & C.G.Papadopoulos: "Testing 3-boson couplings in the Standard Model via single W production at LEP", NCSR "Democritos" preprint, July 1990.

[17] R.Kleiss and W.J.Stirling, Nucl.Phys. **262**(1985)235.

[18] E.Eichten et *al.*, Rev.Mod.Phys.**56**(1984)579;**58**(1986)1065(E).

[19] E.N.Argyres, C.G.Papadopoulos & S.D.P. Vlassopulos, Nucl.Phys.**B324**(1989)91.

[20] U.Baur & E.W.N.Glover, Nucl. Phys. **B347**(1990) 12.

[21] R. Kleiss and P. Zerwas, Proceedings, Workshop *"Physics at Future Accelerators"*, La Thuile/CERN 1987.

[22] U. Baur, I. Hinchliffe and D. Zeppenfeld, Proceedings, Workshop *"From Colliders to Supercolliders"*, Madison (Wisconsin) 1987; Int. J. Mod. Phys. **A2** (1987) 1285.

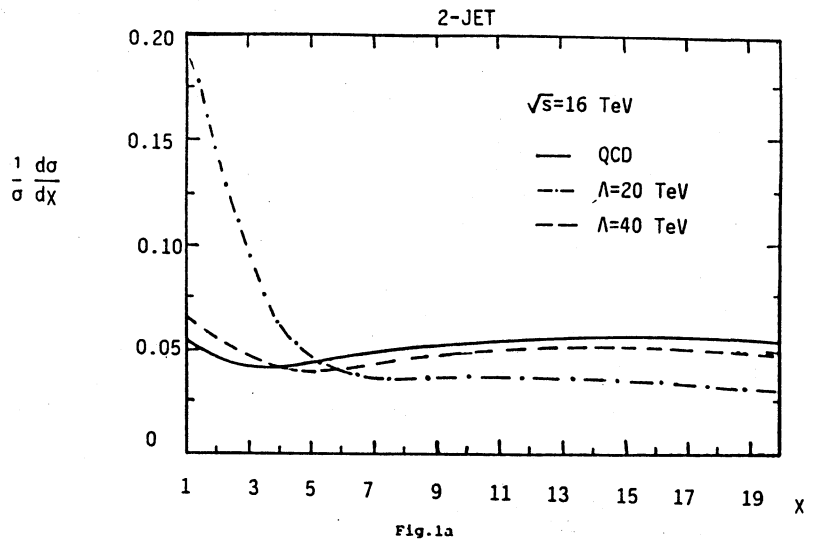

Fig.1a

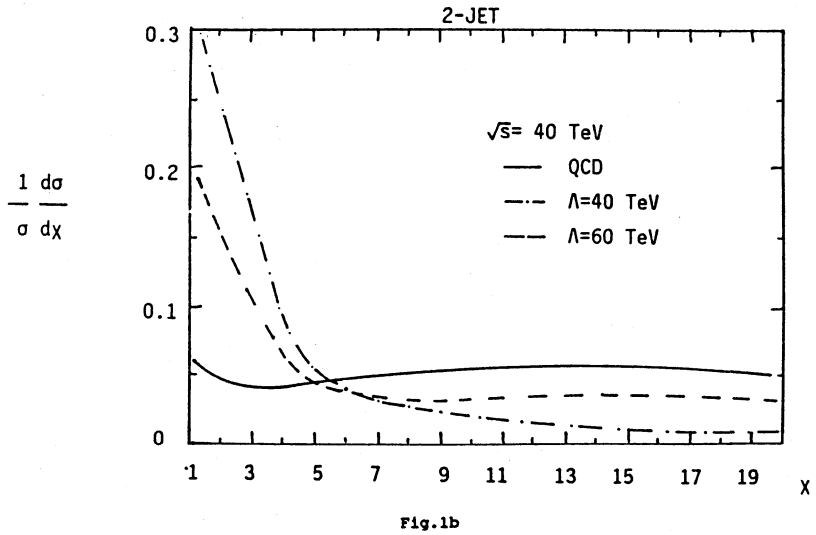

Fig.1b

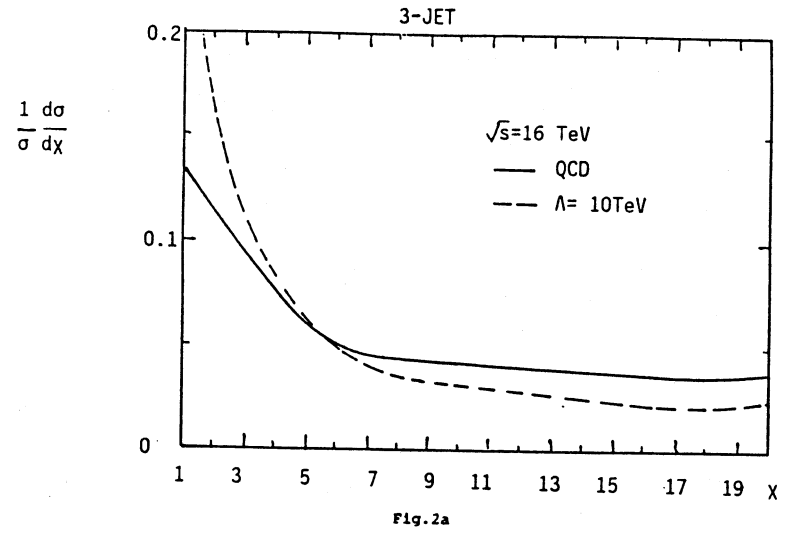

Fig.2a

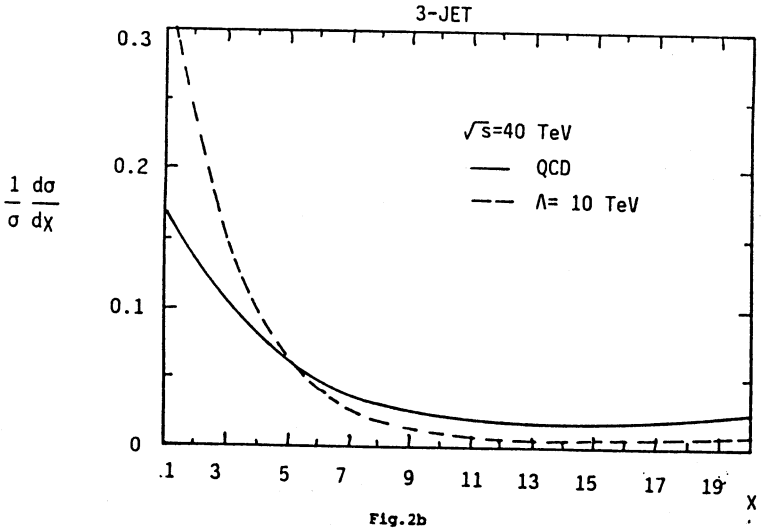

Fig.2b

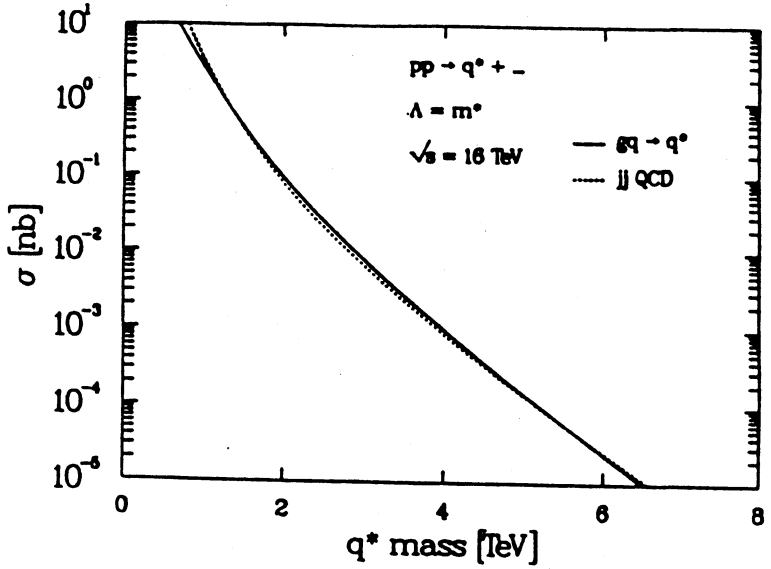

Fig. 3

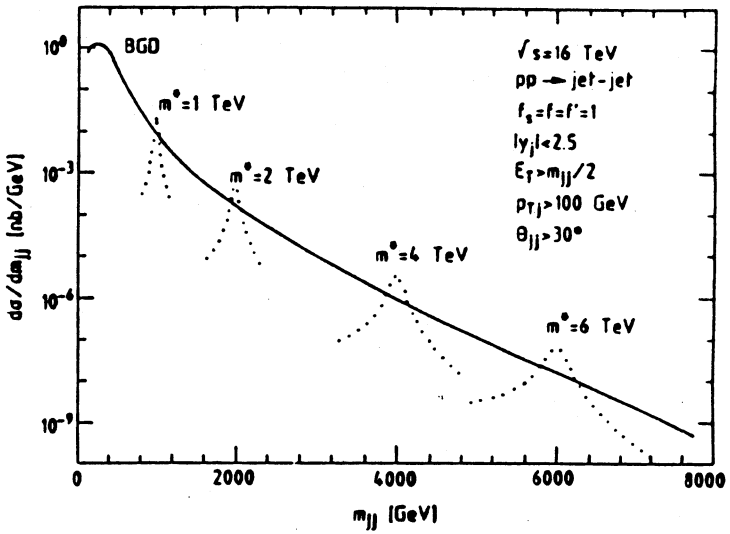

Fig. 4

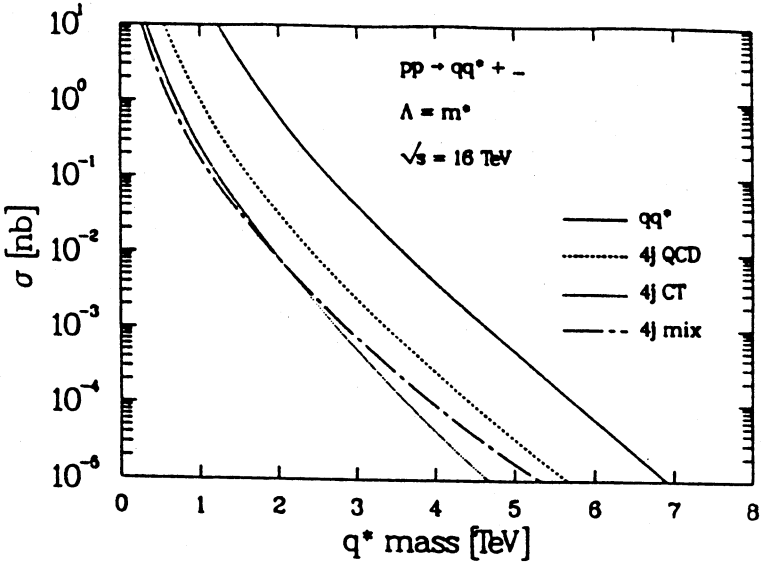

Fig. 5

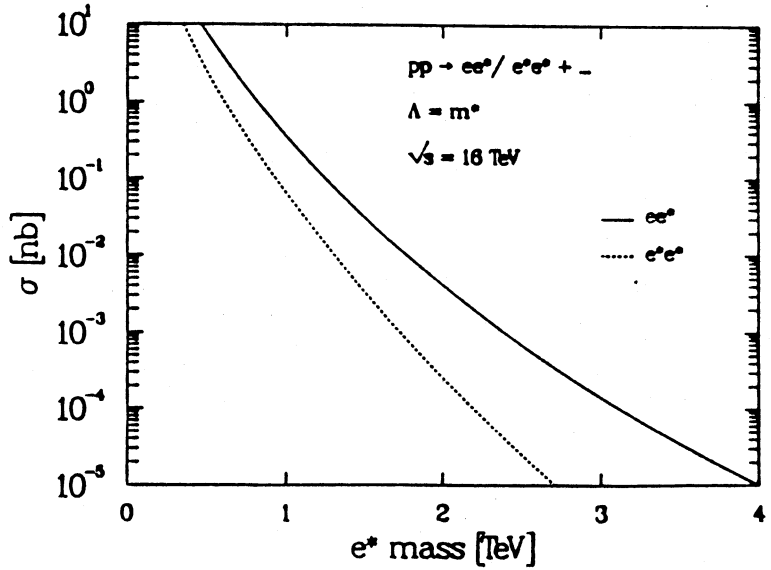

Fig. 6

VI. SIGNATURES FOR GEOMETRICAL FLAVOUR INTERACTIONS AND B+L VIOLATION AT THE LHC

Contributors: J. Ellis, V.A. Khoze, A. Ringwald, F. Schrempp, C. Wetterich

VI.1. Introduction

It has recently been suggested that there may be a large non-perturbative cross-section for electroweak interactions at high energies [1 – 4]. This suggestion originated from the observation that the s-wave cross-section for electroweak baryon (B) and lepton (L) number violating interactions [5] rises rapidly with energy [1, 2], and could become large at energies comparable to the sphaleron [6] energy $M_{sp} \simeq 10$ TeV. Instanton calculations suggest [1 – 3] a sharp threshold for strong flavour interactions at $E \sim M_{sp}$, with a high mean multiplicity of weakly-interacting particles $\overline{n}_w \simeq \pi/\alpha_w = \mathcal{O}(100)$, which would be produced quasi-isotropically close to threshold. At higher energies, the s-wave amplitude would then be bounded by unitarity and other partial waves as well as (B+L)-conserving amplitudes would become strong, inducing large forward-peaked cross-sections at asymptotic energies $E \gg M_{sp}$ [3].

There remain considerable theoretical uncertainties in these non-perturbative estimates, notably whether the rapidly-rising (B+L)-violating cross-section flattens out at some energy below M_{sp}, and whether it ever reaches a sizeable fraction of the unitarity limit. Nevertheless, there is by now a consensus that analogous (B+L)-violating effects are important in a hot plasma [7], and the consequences of large non-perturbative electroweak interactions are so far-reaching and dramatic[5], that we believe our experimental colleagues should include this contingency in their planning for the LHC.

There may even be deeper analogies between the electroweak interactions and QCD at very high energies, as both are non-Abelian gauge theories with similar infrared divergences [4] and topological features. These analogies refer not only to the scattering of a few particles at large angles, which is well described by (parton model) perturbation theory, but also to the large, logarithmically-rising, total inelastic cross-section, where perturbation theory presumably fails. In this note we adopt the following working hypotheses, motivated by the above considerations [3, 4, 8]:

1) At high parton cm energies $\sqrt{\hat{s}}$ the total weak inelastic cross-section becomes approximately energy-independent

$$\sigma_w = 4\pi c_w m_w^{-2} \approx 0.1 \text{ nb} \; - \; 10 \; \mu\text{b}, \tag{1}$$

where c_w is a logarithmically-varying coefficient;

2) the asymptotic behaviour sets in abruptly above a certain threshold energy of the order of a few TeV to about 20 TeV;

3) the mean constituent multiplicity is high, typically of order $1/\alpha_w \sim 30$;

4) there is a substantial contribution of (B+L)-violating events to the total weak cross-section;

[5] For a detailed discussion of the expected phenomenology see ref. [8].

5) the inclusive differential cross-sections decrease rapidly for transverse momenta exceeding a characteristic value of order m_w.

We call processes with these characteristics Geometric Flavour Interactions (GFI) [8].

VI.2. Cross-Sections and Production Rates

We start from the working hypothesis that the parton cross-section $\sigma_w(\hat{s})$ becomes almost constant above the threshold $E_w^{\rm crit}$, with a size of order $\sigma_w^0 \simeq 0.1$ nb $-$ 10 μb [4,8]. In particular, let us assume in this paper a relatively sudden onset of geometrical QFD cross-sections for $\sqrt{\hat{s}} \geq E_w^{\rm crit}$ and approximate $\sigma_w(\sqrt{\hat{s}}) = \sigma_w^0 \theta(\sqrt{\hat{s}} - E_w^{\rm crit})$. After folding σ_w with the parton distributions (no gluons) we obtain the event rate for the production of many weakly interacting particles in proton-proton collisions, see fig. 1. The limit of detectability should be around 100 events per year. We conclude that GFI events can be seen for $E_w^{\rm crit} < 11$ TeV for the LHC if σ_w^0 is around 1 nb.

VI.3. Critical Energy and Multiplicity

Weakly-interacting particles produced by geometrical flavour interactions at high energies comprise W and Z bosons, photons, Higgs bosons, leptons, and quarks. Quarks will appear as jets and we count jets as particles.

We explore the notion that GFI events set in abruptly once the energy is high enough to produce a critical number $n_w^{\rm crit}$ of weakly interacting particles. These phenomena are presumably related to the breakdown of perturbation theory for large particle numbers, namely when $n_w \alpha_w$ becomes large. We therefore, assume $n_w^{\rm crit} \alpha_w = \nu_w$ with ν_w some constant of order one. The threshold energy can then be roughly guessed by requiring that $\sqrt{\hat{s}}$ must be large enough to produce $n_w^{\rm crit}$ particles with mass m_w without a strong phase space suppression. We therefore parametrize

$$E_w^{\rm crit} = f_w n_w^{\rm crit} m_w = f_w \nu_w m_w / \alpha_w. \qquad (2)$$

Both, instanton estimates [1 – 3] as well as a comparison with QCD [4, 8] suggest values of $n_w^{\rm crit}$ and $E_w^{\rm crit}$ in the range $n_w^{\rm crit} \simeq 30 - 100$, $E_w^{\rm crit} \simeq (3.5 - 20)$ TeV. We use a conservative value $n_w = 30$ for the remainder of this paper: all results can be rescaled easily for the experimentally even more advantageous case of higher multiplicity.

VI.4. Transverse Momentum and Energy

At very high parton energies the characteristic transverse momentum of the weakly interacting particles produced in GFI events presumably corresponds to the geometrical size R_w of the cloud of gauge bosons and scalars around the quarks [3,8]. Exploiting the analogy to hadronic cross-sections, we take the (inclusive) distribution $d\sigma_w/dp_t \sim p_t \exp(-R_w\sqrt{m^2 + p_t^2})$, $R_w \simeq \sqrt{2}\cdot\pi/m_w$, for the transverse momentum of a "geometrically" produced particle with mass m [8]. This gives an average transverse momentum for a produced W, $\overline{p}_t \simeq 48$ GeV [6].

[6] Throughout this paper we denote by $\overline{A}$ the average of a quantity A for events with given parton kinematics, whereas $\langle A \rangle$ denotes averages in pp scattering with the (anti) quark distributions in the proton folded in. In particular one has $\langle p_t \rangle = \overline{p}_t$.

The W, Z bosons, Higgs scalars and top quarks will not be directly observable in the detectors of future pp colliders. They decay into jets and leptons. Let l_w denote the number of *light* quarks and leptons produced in GFI events, i.e. those particles with mass much smaller than $\langle p_t \rangle$, including the bottom quark. We expect $l_w/n_w \simeq 1.5 - 2$. Due to the decay of the heavy particles the average transverse momentum per light fermion will be somewhat smaller than the average transverse momentum of a produced W, namely $\overline{p}_t^{\,l} \simeq 36$ GeV [8]. The average total transverse energy per GFI event (for l_w between 45 and 60) is $\overline{E}_t^{\rm tot} = l_w \cdot \overline{p}_t^{\,l} \simeq (1.6 - 2.2)$ TeV.

VI.5. Event Topology

We estimate in fig. 2 the fraction $\langle l_{\rm centr.}/l_w \rangle$ of the number of light particles in a central range of pseudo-rapidities, $|\eta| < \eta_0 \simeq 2.5$, corresponding to $10^\circ < \vartheta < 170^\circ$, as a function of the dimensionless quantity $\sqrt{s}/\overline{E}_t^{\rm tot}$ for three values of $E_w^{\rm crit}/\sqrt{s}$. We assume for an individual light fermion an essentially constant rapidity distribution in the parton cms (for more details see ref. [8]). In order to provide an impression of the angular distribution of the light fermions in a GFI event, we plot in fig. 3 the relative number of particles in the angular region $\vartheta_0 < \vartheta < 180^\circ - \vartheta_0$ as a function of ϑ_0 for a fixed value $\overline{E}_t^{\rm tot} = 2$ TeV. We find that the average "centrality" of the events depends strongly on the parton threshold energy $E_w^{\rm crit}$. This effect arises since the average gets a large contribution from partons with "threshold kinematics" for which the "centrality" of the events essentially depends on f_w [8]. If f_w is near one, very little longitudinal momentum is available. In this case we expect important activity at scattering angles around or even above 35°.

VI.6. Charged Lepton Multiplicity

The cleanest signature of these events is probably the expected high number of isolated charged leptons in each event. We expect [8] $R_L \equiv \langle \#\text{ charged leptons}/n_w \rangle \simeq 1/8 - 1/3$, leading to a mean lepton multiplicity larger than $4 - 10$ for $n_w \geq 30$. Assuming that at least one third of the produced particles are gauge bosons and at most one fifth are scalars one finds (for $n_w = 30$) $R_L > 0.16$, $\langle \#\text{ charged leptons} \rangle > 5$. Similarly, one finds [8] $\langle N_{e,\mu}/l_w \rangle \simeq 1/20 - 1/25$, giving an average of 2.4 - 3 electrons and 2.4 - 3 muons for $l_w = 60$.

VI.7. Missing Transverse Momentum and Energy

The mean number of neutrinos is comparable to that of charged leptons. For $n_w = 30$ we thus expect around 5-9 neutrinos, each with an average transverse momentum $\sim 30 - 40$ GeV. We expect that the total missing transverse momentum and the total missing energy are given by $\langle \not{p}_t^{\rm tot} \rangle \simeq \sqrt{\langle N_\nu \rangle}\,\overline{p}_t^{\,l} \simeq 100$ GeV and $\langle \not{E}^{\rm tot} \rangle \simeq 1$ TeV, respectively.

VI.8. Jet Activity

We expect [8] $\langle \#jets/l_w \rangle \approx 3/4 - 5/6$. For $l_w = 60$, a typical event contains the enormous number of $45 - 50$ jets with a total charged hadron multiplicity ~ 500. These numbers are so high that it becomes hard to resolve all the jets individually if much of the activity is in the forward direction.

Within the range of the central detector ($\eta < 2.5$), however, there should be a good chance to resolve almost all jets. The number of jets in this region can be found from fig. 2, using # central jets = # jets $\langle l_{\text{centr.}}/l_w \rangle$. We see that more than 20 central jets are expected, yielding more than $\sim$ 200 charged hadrons in the central detector. If there are too many jets in the central region one may simply watch out for an impressive "jet-fireball topology" in the central region.

VI.9. Signal and Background

The main background [8] comes from the tails of strong interaction processes where leptons are produced from semi-leptonic decays of heavy quarks. Near the threshold of detectability, the effective cross section is only of order 10^{-2} pb. At the LHC, the QCD cross section for 6 widely separated jets ($\theta_{jj} > 50°$) with $p_t > 20$ GeV exceeds this value by seven orders of magnitude [9].

In order to reduce this huge QCD background we propose [8] to use criteria based on total transverse energy deposition and on the expected characteristics of GFI events in the central and forward/backward regions.

Typical cuts are in the total transverse energy ($E_t^{\text{tot}} > 700$ GeV) and the total missing transverse momentum ($\not{p}_t^{\text{tot}} > 50$ GeV). Another possible cut would select events containing more than two clearly isolated charged leptons with $p_t > 25$ GeV in the central region. One would also require 200 charged hadrons or more in the range $5° < \vartheta < 175°$.

These selection criteria reduce the background from strong interaction events considerably without affecting much the GFI event rate. Subsequently, the detailed leptonic and hadronic structure of the events has to be analyzed in the central region. This strategy should result in a clean distinction from QCD events, and we conclude that GFI events stand a very good chance to be seen, even if the rate is near the threshold of detectability.

VI.10. Violation of Baryon and Lepton Number

If B+L violation becomes strong in the TeV range $[1-3]$, the topology of the (B+L)-violating events will, presumably, resemble roughly the one corresponding to generic GFI events described above (for f_w not much bigger than one). It will be rather central close to the threshold energy and increasingly forward-oriented as the parton energy increases beyond the threshold. A search for B+L violation should therefore directly concentrate on quantum numbers [8] (see also ref. [10]). A (B+L)-violating interaction [5, 1] $q + q \Longrightarrow 7\bar{q} + 3\bar{l} + X$ produces on average more positrons and μ^+ than electrons and μ^-. Thus one should measure the average lepton charge asymmetries, $\langle N_{e^+(\mu^+)} - N_{e^-(\mu^-)} \rangle / \langle N_{e^+(\mu^+)} + N_{e^-(\mu^-)} \rangle$, for isolated electrons and muons (with $p_t > 20$ GeV) in the central region. The asymmetry vanishes, in principle, for L-conserving GFI events and gives, therefore, a direct measure of the relative strength of (B+L)-violating interactions. In addition, one expects the primary e^+'s and μ^+'s from a (B+L)-violating interaction to be more energetic than the decay products of the associated gauge bosons. This leads to an asymmetry in the mean energy of the fastest anti-lepton as compared to that of the fastest lepton. However, only L violation that is large compared to the (B+L)-conserving GFI background can be detected by a measurement of these asymmetries.

VI.11. Conclusions

We have discussed strategies to detect possible signals of geometrical flavour production (see points 1)-5) in the introduction) in the TeV regime. The corresponding events are characterized by the production of many $\mathcal{O}(\alpha_w^{-1}) \approx 30$ weakly-interacting particles. We have concentrated on light fermions of mass smaller than the transverse momentum, which may be produced both promptly and as decay products of W, Z bosons, etc. The associated jets and charged leptons are directly accessible experimentally.

We find the following characteristic features of "geometrical flavour interaction" (GFI) events (for $n_w = 30$):

1) For parton kinematics near the threshold ($\sqrt{\hat{s}} \approx E_w^{\text{crit}}$), the events look rather central, i.e. jets and charged leptons are distributed over the whole angular range. Only partons with energies much above E_w^{crit} produce more forward-oriented events. At the LHC most of the activity will be in the central detector ($10° < \vartheta < 170°$).

2) The average transverse momentum per light particle is estimated to be $\overline{p}_t^{\,l} \approx 35$ GeV, and the total transverse energy is large: $\langle E_t^{\text{tot}} \rangle \approx 1.6 - 2.2$ TeV.

3) We expect on average at least 3.5 "isolated" electrons or muons per event.

4) A similar number of neutrinos is responsible for an average missing transverse momentum $\langle \not{p}_t^{\text{tot}} \rangle \approx 100$ GeV.

5) More than 20 jets/event, corresponding to $\sim$ 200 charged hadrons, should be seen in the central detector.

6) In addition, we expect many events with a high charged hadron multiplicity ($n_h > 100$) in the forward and/or backward detectors ($|\eta| > 2.5$).

7) If B+L violation is relatively strong in comparison to the (B+L)-conserving GFI processes, it may be possible to observe the L violation by measuring average lepton charge asymmetries and/or $\langle E_{e^+,\mu^+} \rangle > \langle E_{e^-,\mu^-} \rangle$.

We conclude that there is essentially no background for these events. Even with a parton cross-section $\sigma_w^0 \approx 1$ nb they should be detected at the LHC if the threshold energy E_w^{crit} is below 11 GeV.

Acknowledgement: We thank W. Bartel, G. Schuler and J. Vermaseren for useful discussions.

Figure Captions

Fig. 1: Number of GFI events per second as a function of the (parton) threshold energy E_w^{crit} (taken from ref. [8]). We assume a constant cross section $\sigma_w^0 = 1$ nb for weakly interacting partons with energies above E_w^{crit} and a pp luminosity of $\mathcal{L} = 10^{33}$ cm^{-2}sec^{-1}.

Fig. 2: Fraction of the number of light particles in the angular region, $10° < \vartheta < 170°$, of a typical central detector, displayed versus $\sqrt{s}/E_t^{\text{tot}}$ for three representative values of $E_w^{\text{crit}}/\sqrt{s}$ [8]. The values for a fixed number of light fermions, $l_w = 60$, are marked by solid circles ($\sqrt{s} = 16$ TeV) and square ($\sqrt{s} = 40$ TeV).

Fig. 3: Relative number of light particles in the angular region $\theta_0 < \vartheta < 180^\circ - \theta_0$ versus θ_0 for fixed total transverse energy $\overline{E}_t^{tot} = 2$ TeV and the same values of E_w^{crit} and $\sqrt{s}$ as in fig. 2 [8].

References

[1] A. Ringwald, Nucl. Phys. B330 (1990) 1.

[2] O. Espinosa, Nucl. Phys. B343 (1990) 310.

[3] L. McLerran, A. Vainshtein and M. Voloshin, Phys. Rev. D42 (1990) 171.

[4] A. Ringwald and C. Wetterich, DESY 90-067.

[5] G. 't Hooft, Phys. Rev. D14 (1976) 3432.

[6] F. Klinkhamer and N. Manton, Phys. Rev. D30 (1984) 2212.

[7] V. Kuzmin, V. Rubakov and M. Shaposhnikov, Phys. Lett. 155B (1985) 36; P. Arnold and L. McLerran, Phys. Rev. D36 (1987) 581; A. Ringwald, Phys. Lett. 201B (1988) 510.

[8] A. Ringwald, F. Schrempp and C. Wetterich, DESY 90-127.

[9] Z. Kunszt, in Proc. "Physics at Future Accelerators", La Thuile, 1987, CERN 87-07, Vol 1.

[10] G. Farrar and R. Meng, DESY 90-099.

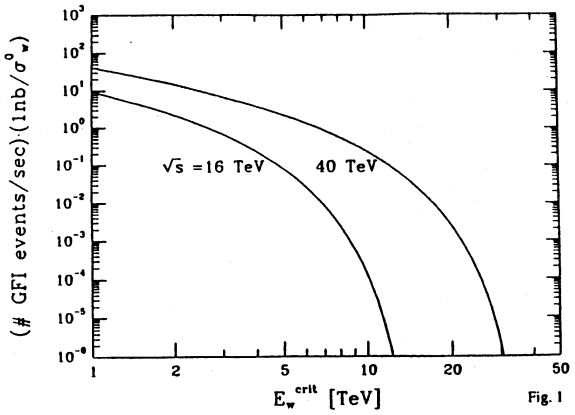

Fig. 1

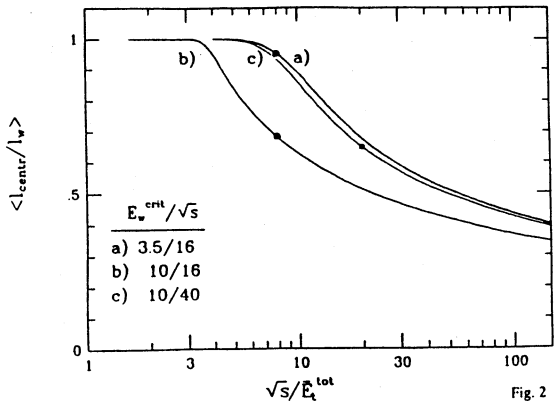

Fig. 2

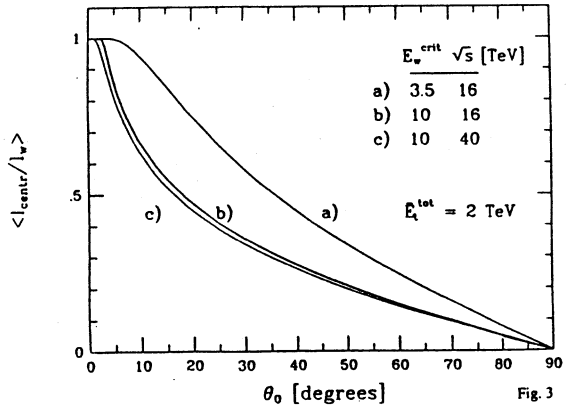

Fig. 3

VII. SUMMARY

In summary a main effort of this working group was to study how one can learn something about electroweak symmetry breaking at machines like LHC. The main result is that a ρ-like object as expected in QCD-like or Technicolor scenarios can be seen in the $W^{\pm}Z$ channel via leptonic decays if it has a mass up to $O(2\ TeV)$. The luminosity will determine the highest reachable mass. With $\mathcal{L} = 10^{34}\ cm^{-2}s^{-1}$ LHC should be able to detect such a state below $2\ TeV$ where good lepton detection capabilities are assumed. If this ρ-like object is however heavier then more luminosity will be essential. To surpass $2\ TeV$ and maybe even reach $2.5\ TeV$ the full luminosity of $4.0\ 10^{34} cm^{-2}s^{-1}$ is required. Both simulation methods (see section II and III) give comparable consistent results. The dominance of the contributions from qq' annihilation via mixing for masses $m_\rho < 2\ TeV$ particularly at LHC parameters was nicely emphasized by the BESS group and also included in the DHT approach.

The DHT approach allows to simulate more general dynamical cases such as Higgs-like dynamics for which the ZZ channel is most promising. The signal to background ratio is however not as good as in the QCD/Technicolor case. Correspondingly the limits on a Higgs like state will be weaker. For a Higgs particle a lower limit up to about $800\ GeV$ (see Higgs group) will arise. Since consistency requirements limit the Standard Model Higgs to values below this limit it will be possible to cover the full window of allowed masses of the Standard Model. If no Higgs is found then the normal (simplest) Higgs scenario is ruled out and alternatives must be sought. In this context it is important that the search for ρ-like objects will be possible up to 2 or $2.5\ TeV$ which is precisely the range where scaled QCD or Technicolor would predict it to be. Therefore the LHC can fully cover the two simplest scenarios of symmetry breaking. Note that the limits for a scalar or ρ-like object are a direct consequence of its mass and the underlying mass to width relations. Therefore any nonstandard width can make the corresponing signal more or less visible. If the widths are for whatever reason wider than normal then the limits get weaker.

Comparing the LHC and SSC one finds roughly the same physics potential. With the chosen parameters both machines are good at finding a ρ-like state in the $W^{\pm}Z$ channel up to masses $O(2\ TeV)$. The signal to background ratio is typically slightly better for the SSC but with a smaller number of events. The ability to reach the design parameters and to build such demanding detectors will therefore decide which machine is better.

The LHC will be able to put very strong limits on the scale of compositeness. Typically these limits are $\sim 20\ TeV$. Excited leptons and quarks can be limited to be heavier than $5 - 10\ TeV$.

Consequences of baryon number violating processes have been described in section VI. Some of the ingredients involved are still disputed and are hopefully fully clarified within the next years. If this mechanism is relevant and if the threshold energy is below $11\ TeV$ then this will be important at LHC any may be one out of many new things that could show up when we make such a big step forward towards higher energies.